



HAL
open science

Hydrodynamics and reaction characteristics of gas-liquid flow in circular microchannels

Tong Zhang

► **To cite this version:**

Tong Zhang. Hydrodynamics and reaction characteristics of gas-liquid flow in circular microchannels. Other. Université de Grenoble; Dalian Institute of Chemical Physics (Chine), 2012. English. NNT : 2012GRENA028 . tel-00804363

HAL Id: tel-00804363

<https://theses.hal.science/tel-00804363>

Submitted on 25 Mar 2013

HAL is a multi-disciplinary open access archive for the deposit and dissemination of scientific research documents, whether they are published or not. The documents may come from teaching and research institutions in France or abroad, or from public or private research centers.

L'archive ouverte pluridisciplinaire **HAL**, est destinée au dépôt et à la diffusion de documents scientifiques de niveau recherche, publiés ou non, émanant des établissements d'enseignement et de recherche français ou étrangers, des laboratoires publics ou privés.



UNIVERSITÉ DE
GRENOBLE

THÈSE

Pour obtenir le grade de

DOCTEUR DE L'UNIVERSITÉ DE GRENOBLE

préparée dans le cadre d'une cotutelle entre l'*Université de Grenoble* et le Dalian Institute of Chemical Physics

Spécialité **Energétique et Génie des procédés**

Arrêté ministériel : le 6 janvier 2005 -7 août 2006

Présentée par

Tong ZHANG

Thèse dirigée par **Shudong WANG**, **Yves GONTHIER** et **Lingai LUO**

préparée au sein des laboratoires : **LOCIE de l'université de Savoie** et le **Laboratory of Environmental Engineering du Dalian Institute of Chemical Physics**

dans les **Écoles Doctorales SISEO** et **Dalian Institute of Chemical Physics**

Hydrodynamique et étude des transferts de matière gaz-liquide avec réaction dans des microcanaux circulaires

Thèse soutenue publiquement le **31 octobre 2012**,
devant le jury composé de :

Madame Joelle AUBIN

Chargée de Recherche CNRS – Toulouse (Rapporteur)

Monsieur Xigang YUAN

Professeur, Tianjing University (Rapporteur)

Monsieur Xuehu MA

Professeur Dalian University of technology

Madame Lingai LUO

Professeur Université de Savoie

Monsieur Shudong WANG

Professeur Dalian Institute of Chemical Physics

Monsieur Yves GONTHIER

Professeur Université de Savoie



DEDICATION

À mes parents

À Xiaobo, Zhang bo et Hengheng

ACKNOWLEDGEMENTS

This dissertation could not be accomplished without the personal and practical support of numerous peoples. Thus, I would like to take this opportunity to express my sincere gratitude towards my parents, my friends, all my companions and superiors in LOCIE in France and DICP in China, for their love, support and patience over last several years.

Foremost, I am sincerely grateful to my supervisors Prof. Yves GONTHIER, Prof. Shudong WANG and Prof. Lingai LUO for giving me the chance to perform this thesis, and inspiring and encouraging me to accomplish it.

I wish to thank Dr. Yilin FAN and Dr. Bin CAO for instructive discussions and great help during the experiment in LOCIE and writing papers. I am also thankful to Mr. Yongjia XIAO, Mr. Deyi LI, Dr. Hongjiu SU, Dr. Defu LI, Mr. Qingdan KONG, Mr. Shengsheng ZHAO for their help with my experiment in DICP.

My particular thanks go to my French language teacher and also my Laoda Mr. Thierry GOLDIN for his help in developing and constructing test setup, for sharing a marvelous time at Aiguebelette and inviting my girl friend and me, and for all his help in France.

Sincere appreciation is acknowledged to members of my thesis committee, who agree to serve on my final defense. I wish to thank particularly Dr. Joelle AUBIN who attends my defense in Dalian from France. I also want to thank Prof. Xigang YUAN and Prof. Xuehu MA for their support and suggestions.

I would like to express my all my friends around me in France who have offered invaluable help through my research and in my life, including Dr. Qi ZHANG, Dr. Hua ZHANG and his wife Mme. Zhimao LIAO, Mr. Zhe FENG, Dr. Hui LIU, Dr. Yu BAI, Dr. Limin WANG. I am also thankful to all my friends in DICP for sharing a good time during my

study and for their help with my experiment in DICP, including Mme. Chunxi ZHANG, Dr. Ying LIU, Dr. Minghao WANG, Dr. Lei ZHANG, Dr. Xiaobo BAI, Dr. Guoquan ZHANG, Dr. Qiushi PAN, Dr. Xinyu REN, Dr. Min SU, Dr. Chundi YAN, Dr. Baolei DU, Dr. Weigang LIU, Dr. Jiangliang HU and so forth.

Financial supports from the French ANR (Agence National de la recherch , France) within the project MIGALI (ANR-09-BLAN-0381-1) and from National Nature Science Foundation of China (No. 20776138) are gratefully acknowledged.

RÉSUMÉ

Cette thèse traite principalement des connaissances fondamentales en hydrodynamique et des caractéristiques des réactions gaz-liquide dans des microréacteurs capillaires.

Dans une première partie, nous avons effectué des essais dans trois microcanaux circulaires en verre placés horizontalement. Les diamètres étudiés étaient de 302, 496 et 916 μm . Les arrivées de gaz et de liquide se font de manière symétrique et forme un angle de 120° entre elles. Une cartographie des écoulements diphasiques gaz-liquide a été systématiquement faite pour des vitesses du liquide comprises entre 0,1 et 2 m/s et des vitesses du gaz comprises entre 0,01 et 50 m/s. Ces essais mettent en évidence l'influence du diamètre des canaux, de la viscosité du liquide et de leur tension superficielle. Ces mesures ont été comparées avec les cartes décrivant les différents régimes d'écoulement (à bulles, en bouchons de Taylor, annulaires ou sous forme de mousse) et confrontés aux modèles de la littérature qui prédisent les transitions entre les différents régimes. Nous avons mis en évidence que ces derniers n'étaient pas totalement satisfaisant et en conséquence, un nouveau modèle de transition prenant en compte les effets de taille du canal, les propriétés physiques du liquide a été proposé.

Les pertes de charge engendrées par ces écoulements gaz-ont été étudiées. Nous avons constaté que la chute de pression est très dépendante du régime d'écoulement. Cependant pour décrire l'évolution de la perte de charge il est commode de la scinder en trois régions: une où les forces de tension superficielle sont le paramètre prépondérant et qui correspond aux faibles vitesses superficielle du gaz, une zone de transition et une dans laquelle les forces d'inertie sont dominantes et qui correspond aux grandes vitesses superficielles du gaz. La prédiction de cette chute de pression dans la troisième zone a été faite à partir d'un modèle de Lockhart-Martinelli. Ce modèle qui prend en compte les flux de chaque phase dépend d'un paramètre semi empirique C . Nous avons proposé de le corrélérer avec les nombres de Reynolds correspondant à chacune des deux phases en présence. Cette méthode permet de

bien rendre compte de nos mesures.

Les caractéristiques hydrodynamiques en écoulement de Taylor ont été examinées. Il a été montré que la formation des bulles dans un écoulement de Taylor est dominée par un mécanisme d'étranglement en entrée du capillaire. La taille des bulles dépend fortement de la viscosité du liquide et la tension superficielle. La chute de pression dans cette zone, lorsque le nombre capillaire est relativement faible, peut assez être bien décrite par le modèle de Kreutzer modifiée par Walsh et al.

Enfin dans une dernière partie, nous avons réalisé une réaction chimique en écoulement de Taylor.

L'oxydation du 2-hydrogène-ethyltetrahydroanthraquinone (THEAQH₂) pour former du peroxyde d'hydrogène a été expérimentalement étudiée dans un microcanal circulaire horizontal de 900 µm de diamètre et 30 cm de long. La présence d'une réaction chimique ne modifie que très peu les transitions entre les différents régimes d'écoulement ni l'évolution des pertes de charge. Les cinétiques de conversion du peroxyde d'hydrogène sont environ deux fois plus rapides celles obtenues dans les réacteurs gaz liquide utilisés habituellement.

Mots-clés: microcanal, écoulement diphasiques, écoulement de Taylor, pertes de charge, réaction gaz-liquide.

ABSTRACT

This dissertation mainly deals with the fundamental knowledge of hydrodynamics and reaction characteristics in gas-liquid microreactors. Extensive experimental investigations have been performed in horizontal circular microchannels with diameter from 302 μm to 916 μm .

Gas-liquid two-phase flow patterns in the microchannel have been systematic experimental investigated, in which the influence of channel diameters, liquid viscosities and surface tension were considered. Flow pattern regime maps in the present microchannels were developed, and the comparison with existing regime maps and flow pattern transition models in literature implied that transitions in present work could not be well predicted. As a result, a new transition model taking the effects of channel size, liquid physical properties into account was proposed.

The gas-liquid two-phase pressure drop characteristics in microchannels were studied. It has been found that the pressure drop was highly flow patterns dependent, and the main trend can be divided into three regions: surface tension-dominated region, transitional region and inertia-dominated region. The pressure drop characteristics in surface tension-dominated and inertia-dominated region were discussed respectively. A modified Lockhart-Martinelli separated flow model in which the effects of channel diameter and liquid properties on the C-value are taken into account was proposed, and it showed a good agreement with respect to our experimental data and others' reported in literature.

Hydrodynamics characteristics of Taylor flow have been examined. It was shown that the formation of Taylor flow was dominated by squeezing mechanism, on which the effects of liquid viscosity and surface tension were dramatically. The two-phase pressure drop of Taylor flow could be well predicted with the Kreutzer's model modified by Walsh et al., when capillary number was relatively low.

Oxidation of hydrogenated 2-ethyltetrahydroanthraquinone (THEAQH₂) in a horizontal circular microchannel have been experimental investigated. Results of visualization study on oxygen-anthraquinone working solution two-phase flow in microchannel showed that the

flow pattern transition model and pressure drop model for inertia-dominated region proposed in this dissertation had good predicting accuracy. It was indicated that the gas-liquid interfacial area and space-time yield of hydrogen peroxide in the microchannel are at least one to two orders of magnitude higher than those in the conventional gas-liquid reactors.

Keywords: microchannel, two-phase flow pattern, pressure drop, gas-liquid reaction, Taylor flow.

TABLE OF CONTENTS

DEDICATION	I
ACKNOWLEDGEMENTS.....	II
RÉSUMÉ.....	IV
ABSTRACT	VI
TABLE OF CONTENTS	VIII
NOMENCLATURE	XI
CHAPTER 1: LITERATURE REVIEW	2
1.1 General introduction.....	2
1.2 Hydrodynamics of two-phase flow in microchannels	5
1.2.1 Microchannel definition	5
1.2.2 Two-phase flow patterns	9
1.2.3 Two-phase flow regime maps.....	13
1.2.4 Effects of channel diameters and liquid properties on two-phase flow patterns	17
1.2.5 Two-phase pressure drop in microchannels.....	21
1.3. Two-phase mass transfer and reaction in microreactors.....	24
1.3.1 Two-phase mass transfer in microreactors.....	23
1.3.2 Gas-liquid reaction in microreactors	26
1.4 Conclusions.....	28
References	31
CHAPTER 2: GAS-LIQUID FLOW PATTERNS IN CIRCULAR MICROCHANNELS	40
2.1 Experimental set-up.....	41
2.1.1 Test rig	41
2.1.2 Test section	42
2.1.3 Working fluids.....	44
2.1.4 Parameters measurement and uncertainty analysis	45
2.2 Flow patterns and flow regime maps in horizontal circular microchannel with a Y junction	48
2.2.1 Nitrogen-water flow – Influence of channel size	48
2.2.2 Nitrogen-CMC solution horizontal flow in circular microchannel – influence of viscosity.....	53

2.2.3 Nitrogen-SDS solution and Nitrogen-ethanol horizontal flow in circular microchannel – influence of surface tension.....	55
2.3 Comparison with existing flow regime maps and available transition criteria.....	59
2.3.1 Comparison with existing flow regime maps.....	59
2.3.2 Comparison with available transition criteria	61
2.4 Transition criteria based on the present experimental data.....	65
2.5 Conclusions.....	68
References	70
CHAPTER 3: TWO-PHASE PRESSURE DROP MODEL FOR INERTIA-DOMINATED REGION ...	72
3.1 Introduction.....	73
3.2 Experimental condition and data reduction.....	80
3.3 Dependence of pressure drop on the flow regimes.....	81
3.4 Two-phase pressure drop in circular horizontal microchannel in inertia-dominated region	85
3.4.1 The comparison of experimental results with existing homogeneous-flow model correlations..	85
3.4.2 The comparison of experimental results with existing Lockhart-Martinelli model correlations	88
3.5 New correlation for modified Lockhart-Martinelli model	92
3.5.1 The influence of channel diameter.....	92
3.5.2 The influence of liquid viscosity and surface tension	93
3.5.3 The proposal of new C correlation	96
3.5.4 Verification of the modified Lockhart-Martinelli model using presently proposed C correlation.....	101
3.6 Conclusions.....	102
References	104
CHAPTER 4: HYDRODYNAMIC CHARACTERISTICS OF TAYLOR FLOW IN CIRCULAR MICROCHANNELS	108
4.1 Introduction.....	109
4.2 Results and discussion.....	110
4.2.1 Taylor bubble velocity and void fraction	110
4.2.2 Formation mechanism of Taylor bubbles	114

4.2.3 Pressure drop characteristics	116
4.3 Conclusions	122
References	124
CHAPTER 5: OXIDATION OF HYDROGENATE 2-ETHYLTETRAHYDROANTHRAQUINONE IN CIRCULAR MICROCHANNEL	126
5.1 Introduction	127
5.2 Experiments	127
5.2.1 Set up	127
5.2.2 Working solution and analytical method	129
5.3 Oxygen-anthraquinone working solution two-phase flow in circular microchannel.....	130
5.3.1 Two-phase flow patterns	129
5.3.2 Pressure drop.....	130
5.4 Oxidation of THEAQH ₂ in circular microchannel	134
5.4.1 Gas-liquid specific interfacial area	134
5.4.2 Effects of temperature on oxidation.....	135
5.4.3 Effects of operating pressure	137
5.4.4 Effects of liquid velocities on the oxidation.....	138
5.5 Conclusions	139
References	141
CONCLUDING REMARKS.....	142
1 Thesis summary.....	142
2 Future work perspectives.....	143
LIST OF FIGURES.....	146
LIST OF TABLES	150
BIOGRAPHY	151

NOMENCLATURE

Notes: Symbols that appear infrequently are explained in the text.

Latin symbols:

a_i	Specific interfacial area, m^2/m^3
A	Aspect ratio, depth/width, dimensionless
$c_0 - c_8$	Correlation constants, dimensionless
C	Chisholm's parameter, dimensionless
C_{oxy}	Production concentration of hydrogen peroxide, g/L
C_{Total}	Total concentration of hydrogen peroxide, g/L
d_b	Diameter of Taylor bubble, m
d_{c1}	Critical diameter, m
d_{c2}	Critical diameter, m
d_H	Hydraulic diameter, m
d_i	Inner diameter of circular microchannel, m
E_m	Mean relative deviation, dimensionless
F	Darcy friction factor, dimensionless
g	Acceleration of gravity, m/s^2
G	Mass flux, $\text{kg}/(\text{m}^2 \cdot \text{s})$
k	Correlation constant, dimensionless
k_L	Liquid side mass transfer coefficient, m/s
k_S	Roughness of channel wall, m
La	Laplace length: $\sqrt{\frac{\sigma}{g(\rho_L - \rho_G)}}$, m
L_B	Length of bubble, m
L_S	Length of liquid slug, m

n	Correlation constant, dimensionless
$P_{30\%}$	Percentage of points falling within the relative deviation of 30%, dimensionless
ΔP	Pressure drop, Pa
ΔP_{acc}	Acceleration pressure drop, Pa
ΔP_{fri}	Frictional pressure drop, Pa
ΔP_{gra}	Gravitational pressure drop, Pa
Q	Volumetric flow rate, m ³ /s
r_{AS}	Gas-liquid volumetric ratio, dimensionless
r_0	Radii of the channel, m
R	Gas constant, dimensionless
S_B	Interfacial area between gas and liquid phase, m ²
T	Temperature, °C
T_f	Thickness of liquid film, m
U	Velocity, m/s
V_{Bubble}	Volume of Taylor bubble, m ³
x_e	Gas mass fraction, dimensionless
X	Lockhart-Martinelli parameter, dimensionless
Z	Channel length, m

Greek symbols:

α	Fitting parameter, dimensionless
β	Gas phase volumetric fraction, dimensionless
δ	Relatively roughness of channel wall, dimensionless
ε_G	Void fraction, dimensionless
ϕ	Two-phase frictional multiplier, dimensionless

$\dot{\gamma}$	Shear rate, s^{-1}
η	Oxidation conversion, dimensionless
μ	Dynamic viscosity, Pa·s
μ_{eff}	Dynamic viscosity of non-Newtonian liquid, Pa·s
θ	Channel angle of inclination with respect to the gravity force, dimensionless
ρ	Density, kg/m ³
σ	Surface tension, N/m
τ	Shear stress, N/m ²
ξ	Additional function to the frictional factor f , dimensionless

Dimensionless number :

Bo	Bond number: $d_H^2 g(\rho_L - \rho_G) / \sigma$
Ca	Capillary number: $\mu_L U_{LS} / \sigma$
Kn	Knudsen number: $\frac{\mu \sqrt{\pi}}{\rho \sqrt{2RT}} / d_H$
Lo^*	Dimensionless Laplace constant: $\sqrt{\frac{\sigma}{g(\rho_L - \rho_G)}} / d_H$
λ	Dimensionless number in C correlation of Lee et Lee (2001) and Lee et Lee (2008): $\mu_L^2 / \rho_L \sigma d_H$
ψ	Dimensionless number in C correlation of Lee et Lee (2001) and Lee et Lee (2008), which equal to Ca : $\mu_L U_{LS} / \sigma$
N_{conf}	Confinement number: $\sqrt{\frac{\sigma}{g(\rho_L - \rho_G)}} / d_H$
Re	Reynolds number: $\rho U d_H / \mu$

Su	Su number: $\sigma d_H \rho_L / \mu_L^2$
We	Weber number: $\rho U^2 d_H / \sigma$

Subscripts

B	Bubble
Exp	Experimental measured
fri	Frictional
G	Gas
GS	Gas superficial
hom	Homogeneous-flow model
H	Hydraulic
L	Liquid
$Liquid$	Liquid slug
LS	Liquid superficial
$meas$	Measured
pre	Predicted
sep	Separated-flow model
$Taylor$	Taylor flow
tp	Two-phase mixture
TP	Two-phase total
TS	Liquid slug in Taylor flow
TUC	Taylor unit cell

CHAPTER 1: LITERATURE REVIEW

1.1 General introduction

In the last decade, to satisfy both the market requirement and the social and environmental constraints of industry processes, chemical industry has been undergoing reformation rapidly. The evolution of chemical engineering is vitally necessary to survive in the globalization of world trade and competition, which require the future chemical processes to be environment-friendly, highly efficient, defect-free and perfectly safe. Microreaction technology has provided a possibility to confront the challenges, for it is generally considered to have many advantages for chemical processes, i.e. heat and mass transfer enhancement, improved reaction performance, perfect safety, easily-controlled process, continuous operation mode and well-defined flow property, and attracted an increasing worldwide academic interest and growing attention from industry. Microreaction technology represents microstructured devices integrated into a variety of operation units, which are composed of small size channels having dimensions with the order of tens or hundreds of microns. After twenty years development, microreaction technology is no longer in its infancy, and its practical applications in many processes of chemical industry have been emerging, which tabulated in Table 1-1. However, the application of gas-liquid multiphase microreaction technology in practice is rarely reported. There are two main reasons considered to be responsible for this phenomenon. On one hand, it is more complicate that the hydrodynamic and reaction characteristics of gas-liquid multiphase microreactors than that of others microreactors, due to the predominance of surface forces induced by the miniaturization of channel dimensions. On the other hand, the fundamental knowledge of gas-liquid microreactors is found to be significantly different from that of their macro scale counterpart, hence the theory founded for the common size reactor are no longer applicable and the general understanding about the fundamental knowledge, i.e. hydrodynamics, mass transfer

and reaction, of gas-liquid microreactors are still lacking. At the same time, the successful application reported in others chemical processes incited a growing interest to introduce microreaction technology to gas-liquid reactions, and the studies undertaken have indeed showed that the excellent performance of gas-liquid reaction could be achieved in microreactors. Consequently, to fundamentally understand and well-designed gas-liquid microreactor is now of great interest. It is agreed that the gas-liquid two-phase hydrodynamics play a primary role regarding the microreactor design, as well as characteristics of the specific reaction. Thus, this work will be concentrated on the gas-liquid two-phase flow in microchannels, and attempt to perform and investigate a gas-liquid reaction in microchannel.

In this chapter, a short review of gas-liquid two-phase flow in microchannels in literature is given, as well as the current research status of gas-liquid reaction.

Table 1-1: Examples of microchemical engineering applications in practice. t/y: tons per year

Scale level	Company	Process	Micro-system type	Scale t/y
Small-scale	Heatric (Seris et al., 2005)	Hydrogen production	Gas phase microreactor	8
	Merck (O'Driscoll, 2004)	Specialty intermediate production	Liquid phase microreactor	15
	Lonza (Roberge et al., 2005)	Fine chemical/pharmaceutical campaign	Liquid phase microreactor	44
	Clariant (Dietrich, 2009)	Synthesis of red, yellow azo pigments	Liquid phase microreactor	130
	Xi'an Huain /IMM (Dietrich, 2009)	Nitroglycerin plant operational	Liquid phase microreactor	130
	Chart (wood, 2005)	Hydrogen production for refueling station	Gas phase microreactor	160
Large-scale	Heatric (Banister and Rumbold, 2005)	Methanol production	Gas phase microreactor	12 000 to 60 000
	DSM/Karlsruhe (Dietrich, 2009)	Liquid chemical products	Liquid phase microreactor	15 000
	Velocys (Jarosch et al., 2006)	Production of transportation fuels	Gas phase microreactor	16 000
	IMM (Dietrich, 2009)	Star-laminator mixer	Liquid-liquid micromixer	26 000
	Velocys (Tonkovicha et al., 2004)	Hydrogen production	Gas phase microreactor	30 000
	Degussa/UDH (Albrecht et al., 2006)	Vinyl acetate synthesis	Gas phase microreactor	150 000
	UOP/IMM (Hessel et al., 2005)	Direct synthesis of hydrogen peroxide	Liquid phase microreactor	162 000
Mega-scale	Velocys (Mazanec, 2006)	Ethylene production	Gas phase microreactor	1 million
	Velocys (Wang et al., 2005)	Fischer-Tropsch synthesis	Gas phase microreactor	1.4 million

1.2 Hydrodynamics of two-phase flow in microchannels

Gas-liquid two-phase flow in capillaries or microchannels have attracted increased attention in the last decades, caused by the miniaturization of devices in many engineering fields, i.e. chemical and space industries, hydrogen and nuclear power, material processing, thin film deposition technology and biotechnology. There are three major distinctions of two-phase flow hydrodynamics in microchannels compared to macro-systems. To begin with, the relative importance of surface tension, inertia, and viscosity over buoyancy, in another word, gravity, increases. Moreover, the flow is usually characterized by small Reynolds numbers, and laminar flow is occurred. Finally, there are significant effects of the roughness, wettability of the channel wall, and wall confinement on the two-phase flow in microchannels (Akbar et al., 2003; Rebrov, 2010; Shao et al., 2009). In view of these differences, the existing prediction correlations for large size tubes cannot be applicable to predict hydrodynamics characteristics of two-phase flow in microchannels, such as two-phase flow patterns, pressure drop, etc. Accordingly, extensive works have been conducted with aim at characterizing gas-liquid two-phase flow in microchannels, and we will give a review on the current research status on it in detail in this section.

1.2.1 Microchannel definition

In the microchannels, gas-liquid two-phase flow is so different, due to dominant position of surface forces, while two-phase flow is dominated by gravity in normal size tubes. However, the classification between normal, small and microchannel, has not been well defined yet. The transition of channel scale to surface tension dominated, which is also considered as the transition from normal scale to microchannel, has been intensively discussed based on experimental data. Engineers used to consider tubes with diameters larger than one centimeter and in order of millimetre as normal and small-scale, respectively. But it is now generally accepted that the transition criterion should be determined by the correlation of channel size, operating conditions and fluid properties rather than only by the channel diameter (Brauner and Maron, 1992; Kew and Cornwell, 1997; Shao et al., 2009; Suo, 1963).

The criterion for the microchannel has been proposed in various ways by researchers based on different dimensionless numbers, among which Laplace length La and Eötvös number $Eö$ or named Bond number Bo are usually involved, described as:

$$La = \sqrt{\frac{\sigma}{g(\rho_L - \rho_G)}} \quad (1.1)$$

$$Bo = \frac{d_H^2 g(\rho_L - \rho_G)}{\sigma} \quad (1.2)$$

As early as in 1961, Bretherton (1961) found that the free rise of a long bubble in a vertical sealed tube would be completely inhibited if $Bo/4 < 0.842$, due to effects of gravity suppressed by that of surface forces. Based on the experimental results and discussion, Suo and Griffith (1964) gave a criterion for negligible gravity effects on two-phase flow in a horizontal capillary as follow:

$$\sqrt{\frac{\sigma}{g(\rho_L - \rho_G)}} / d_H \geq 3.3 \quad (1.3)$$

Which could be rewritten as:

$$La/d_H \geq 3.3 \quad (1.4)$$

Here, it could be derived that 2.7 mm for the air-water two-phase flow at 0.1MPa from Eq. (1.3) was the critical diameter for microchannel.

According to the linear stability analysis and well-posedness of the unidirectional momentum and continuity equations of the stratified two-phase flow, Brauner and Moalem-Maron (1992) suggested following criterion for the dominance of surface forces in two-phase flow:

$$Eö = \frac{d_H^2 g(\rho_L - \rho_G)}{\sigma} = Bo < (2\pi)^2 \quad (1.5)$$

Kew and Cornwell (1997) investigated two-phase flow and heat transfer characteristics in small-diameter tubes, and found that when confinement number, $N_{conf} = \sqrt{\frac{\sigma}{g(\rho_L - \rho_G)}} / d_H$, which also called as dimensionless Laplace number, was greater than 0.5, typical flow regime

for microchannels, i.e. confined bubble flow would be formed.

The critical channel diameters derived from correlations of Bretherton (1961), Suo and Griffith (1964), Brauner and Moalem-Maron (1992) and Kew and Cornwell (1997), should be 4.97 mm, 0.82 mm, 17.1 mm and 5.4 mm, respectively, for air-water two-phase flow under absolute pressure of 0.1 MPa and temperature of 25 °C.

Meanwhile, other methods also have been used to classify the channels. Kandlikar and Grande (2003) proposed the channel classification based on the evolution of flow in small channels and on the discussion of gas Knudsen number ($Kn = \frac{\mu_G \sqrt{\pi}}{\rho_G \sqrt{2RT}} / d_H$, where R is the gas constant, μ_G is gas viscosity, ρ_G is the gas density, T is the absolute temperature in K), as follows:

Conventional channels: $d_H > 3$ mm

Minichannels: 3 mm $\geq d_H \geq 200$ μ m

Microchannels: 200 μ m $\geq d_H \geq 10$ μ m

Transitional channels: 10 μ m $\geq d_H \geq 0.1$ μ m

Transitional Microchannels: 10 μ m $\geq d_H \geq 1$ μ m

Transitional Nanochannels: 1 μ m $\geq d_H \geq 0.1$ μ m

Nanochannels: 0.1 μ m $\geq d_H$

Li and Wang (2003) analyzed two-phase flow regimes during vapor flow condensation in horizontal mini/microchannels, and considered that the major two-phase flow patterns could be classified into three categories: symmetrical, semi-symmetrical and asymmetrical flow. They gave two correlations to determine the critical diameters as follows:

$$d_{c1} = 0.224 \left[\frac{\sigma}{(\rho_L - \rho_G)g} \right]^{1/2} \quad (1.6)$$

$$d_{c2} = 1.75 \left[\frac{\sigma}{(\rho_L - \rho_G)g} \right]^{1/2} \quad (1.7)$$

When $d_H \geq d_{c2}$, the flow regimes were similar to those in common size tubes. And when $d_H \leq d_{c1}$, the effects of gravity on the flow regime were negligible, so that the channel

could be regarded as microchannel. According to Eq. (1.6) and (1.7), Li and Wang (2003) calculated the critical channel diameters for several liquids under different temperatures, tabulated in Table 1-2.

Table 1-2: Critical channel diameters for liquid-vapor two-phase flow based on the correlation of Li and Wang (2003)

Liquid	Temperature K	Surface tension N/m	d_{c1} μm	d_{c2} μm
Water	300	0.0717	600	4680
	350	0.0632	560	4374
	400	0.0536	534	4170
	450	0.0429	490	3827
Glycol	300	0.0478	464	3624
	330	0.0451	454	3546
	360	0.0425	444	3468
	373	0.0413	442	3452
R22	283	0.0104	206	1609
	303	0.0076	183	1429
	323	0.0047	153	1195
	333	0.0034	136	1062
R134a	283	0.0103	207	1617
	303	0.0075	183	1429
	323	0.0050	156	1218
	333	0.0038	140	1093

Many researchers experimentally investigated two-phase flow in capillaries or small size channels, and the critical diameters for microchannel could be derived by observing the two-phase flow patterns. Triplett et al. (1999) conducted experiments on the air-water two-phase flow in circular channels with diameter of 1.10 and 1.45 mm, and in semi-triangular channels with hydraulic diameter of 1.09 and 1.49 mm. Typical flow patterns for microchannels were obtained, i.e. slug flow, churn flow, annular flow and slug-annular flow, etc., which indicated the transition of channel diameters to surface forces dominated regime at $1 \text{ mm} < d_H < 2 \text{ mm}$. Chen et al. (2006) studied the effects of tube size on two-phase flow regimes in vertical small tubes. The results indicated that when channel diameter less than 2.01 mm, the two-phase flow became different from that of normal size tubes, and when the channel diameter decreased to 1.10 mm, typical flow pattern of microchannel, such as confined bubble flow would occur, for which surface forces was dominant. Likewise, Venkatesan et al. (2010) also found that typical flow patterns of microchannels would form

when channel diameters less than 2 mm. Therefore, the channel diameter of about 1 mm may be considered as the upper boundary of microchannels (Rebrov, 2010; Shao et al., 2009).

1.2.2 Two-phase flow patterns

In gas-liquid processes in microchannels, the *two-phase flow pattern* is of primary importance because other characteristics such as the pressure drop, heat and mass transfer and reaction all depend on it (Cheng et al., 2008; Rebrov, 2010; Tsoligkas et al., 2006). Therefore, rather extensive researches have been dedicated to the study of flow patterns and the construction of flow pattern maps based on superficial gas and liquid velocities (U_{GS} , U_{LS}) in microchannels having circular, rectangular or triangular cross-section.

However, the uniformity in the terminology of two-phase flow patterns in microchannel is still lacking, which now become a major problem in this subject. For example, slug flow is usually called Taylor flow, segmented flow, elongated bubble flow (Shao et al., 2009), even sometimes bubble-train flow (Thulasidas et al., 1997). In addition, the same name is sometimes used to describe different flow patterns. Take the slug flow as an example, it also refer to wavy-annular flow in some report (Yang and Shieh, 2001). Two main reasons are responsible for this problem. One is that transitional flow patterns are difficulty to categorize. The other one is that some researchers have observed more detail about some flow patterns using advanced camera, based on which some typical flow patterns can be divided into two or more types. In this work, a classic classification will be adopted, in which six main typical flow patterns are included, i.e. bubbly flow, Taylor flow (slug flow), Taylor-annular flow (Taylor-annular flow), annular flow, churn flow and dispersed flow. And these flow patterns can be depicted respectively in a flow regimes map with gas and liquid superficial velocities (U_{GS} and U_{LS}) as coordinates according to the flow conditions, as shown in Figure 1-1 (Shao et al., 2009).

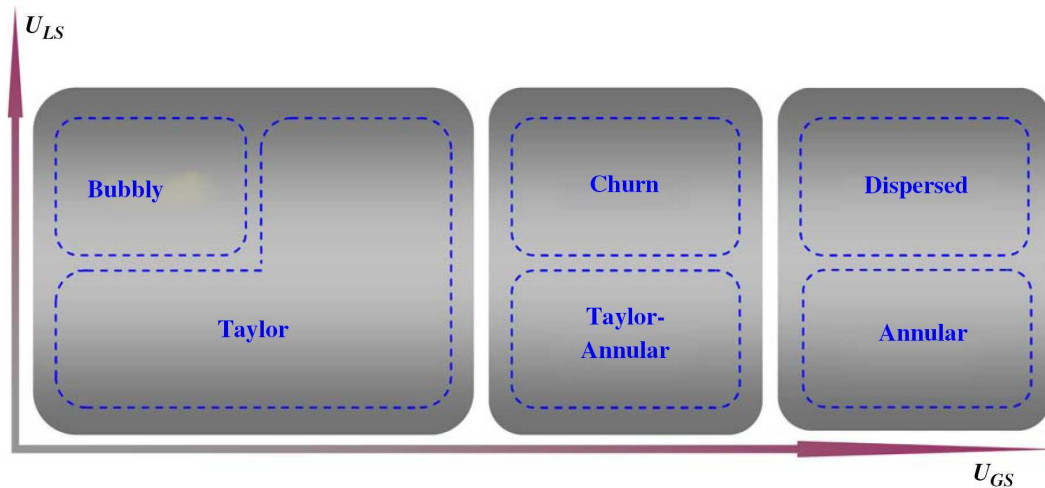


Figure 1-1: General classification of two-phase flow patterns in microchannel (Shao et al., 2009)

Main two-phase flow patterns in microchannels have been reported by many researchers. For instance, Triplett et al. (1999) investigated air-water two-phase flow in circular and semi-triangular microchannels, and several typical two-phase flow patterns were observed, as shown in the Figure 1-2.

Bubbly flow occurs at high U_{LS} and low U_{GS} , with discrete and irregular bubbles dispersed in bulk liquid with bubble diameters smaller than channel size.

Slug flow (Taylor flow) is a quasi-regular flow pattern forming within a rather large range of intermediate U_{LS} and U_{GS} . The length of elongated gas bubbles in slug flow is larger than channel diameter. Gas bubbles are separated by the liquid slugs in the axial direction, and a liquid film also form separating the bubbles from channel wall. Usually, the lengths of gas slug and liquid slug are constant in slug flow.

Slug-annular flow (Taylor-annular flow) is characterized by the liquid slugs in slug flow just broken through by the gas flow, in which gas bubbles are elongated and finally merge into a continuous gas core flow surrounded by a liquid film where large-amplitude waves appear.

Annular flow appears when the gas superficial velocity is excessively high and relatively low U_{LS} . Annular flow is morphologically similar to slug-annular flow, except that the liquid film is ring-like along the channel wall and no large-amplitude waves appear.

Churn flow is usually considered as a flow patterns developed from slug flow with increasing of U_{LS} and U_{GS} , which is characterized by the disruption in trailing ends of gas

bubbles and dispersion of tiny gas bubbles into the liquid phase as shown in the Figure 1-2 (c) or by the liquid film disturbed at high U_{GS} and small liquid drops appearing in the gas core as shown in the Figure 1-2 (d).

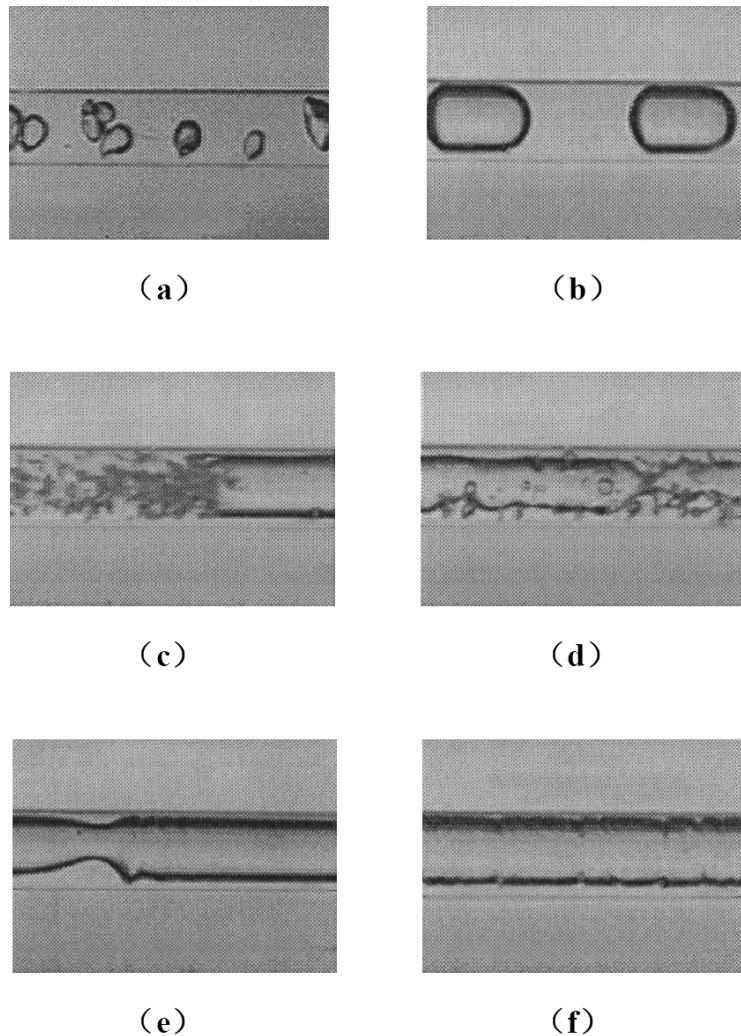


Figure 1-2: Two phase flow pattern in microchannel: (a) bubbly flow; (b) slug or Taylor flow; (c) and (d) churn flow; (e) slug-annular or Taylor-annular flow; (f) annular flow

Another main two-phase flow pattern did not appear in Triplett's investigation, which is **dispersed flow**. Due to extremely high U_{LS} and U_{GS} , the clear photo of dispersed flow is rarely reported. The Figure 1-3 is only a picture which conveys basic meaning of dispersed flow, of which the major characteristic is that most of the liquid phase entrained into gas

phase as small droplets, and sometimes named as mist flow (Chen et al., 2006).

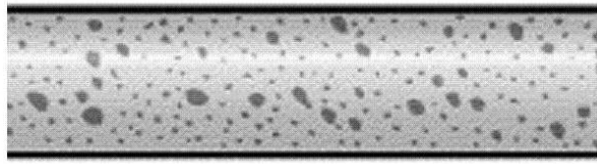


Figure 1-3: Dispersed flow in microchannels

Besides these main flow patterns, there are transitional patterns, i.e. bubble-train slug flow (Chen et al., 2002; Yue et al., 2008), slug bubbly flow (Liu and Wang, 2008a), slug-churn flow, unstable slug flow (Yue et al., 2008), slug-annular-churn flow (Simmons et al., 2003) etc. Bubble-train slug flow is also regarded as one type of unstable flow, developed from slug flow by increasing gas superficial velocity. In this flow pattern, gas bubbles are elongated and the some liquid slugs between bubbles become thin liquid film, even broken, then bubble-train formed. But there are still liquid slugs separate bubble-trains. With increasing of U_{GS} in the bubble-train slug flow, slug-annular flow will occur. In a word, between main two-phase flow patterns, there always are transitional flow patterns, which can be easily understood according to the characteristics of main flow patterns.

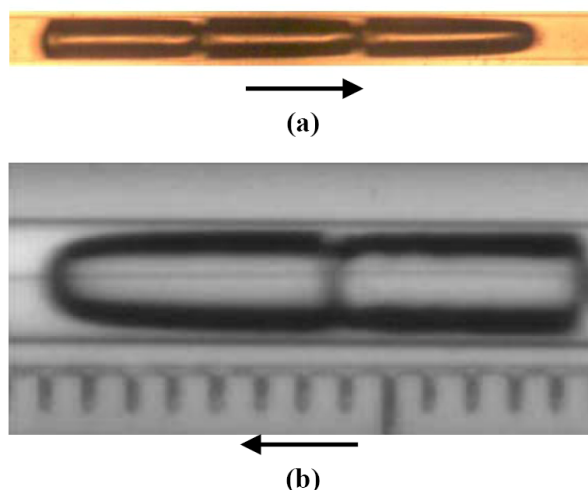


Figure 1-4: The images of bubble-train slug flow in microchannels: (a) Two-phase flow in a square microchannel with hydraulic diameter of 0.4 mm of Yue et al. (2008); (b) Two-phase flow in a circular microchannel with diameter of 1 mm of Chen et al. (2002)

1.2.3 Two-phase flow regime maps

Two dimensional flow patterns maps are usually introduced to represent two-phase flow regimes and the transitional boundary between them with some appropriate hydrodynamic parameters as coordinates. The superiority of flow regime maps is that various flow patterns regions and the transition lines between them can be easily determined, and the effects of hydrodynamic parameters and physical properties can be expressed by using various coordinates.

The most popular coordinates are U_{LS} and U_{GS} . Barajas and Panton (1993) and Triplett et al. (1999) exhibited flow regime maps based on their experiments using U_{LS} and U_{GS} as coordinates, as shown in Figure 1-5, from which it can be noted obviously that the transition lines shift with the variation of channel size, channel section shape and wettability of channel wall.

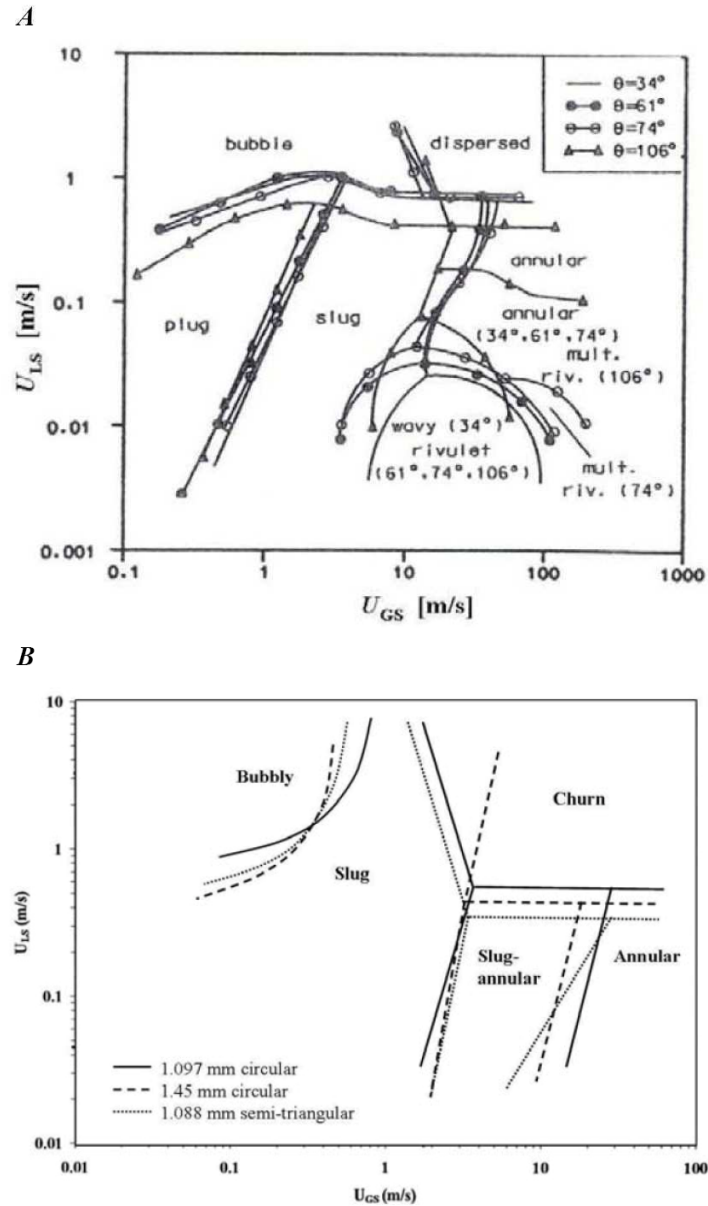


Figure 1-5: The two-phase flow pattern regime maps in microchannels: (A) for the experiments of Barajas and Panton (1993); (B) for the experiments of Triplett et al. (1999)

A regime map using U_{LS} and U_{GS} as coordinates was also reported by Hassan et al. (2005). They studied air-water two-phase flow patterns in horizontal small channels with diameters of 3.0, 1.0 and 0.8 mm, and then summarized extensive existing experimental data, finally established a universal regime maps as depicted in Figure 1-6, in which the difference of terminology was eliminated and appropriate deviation was acceptable.

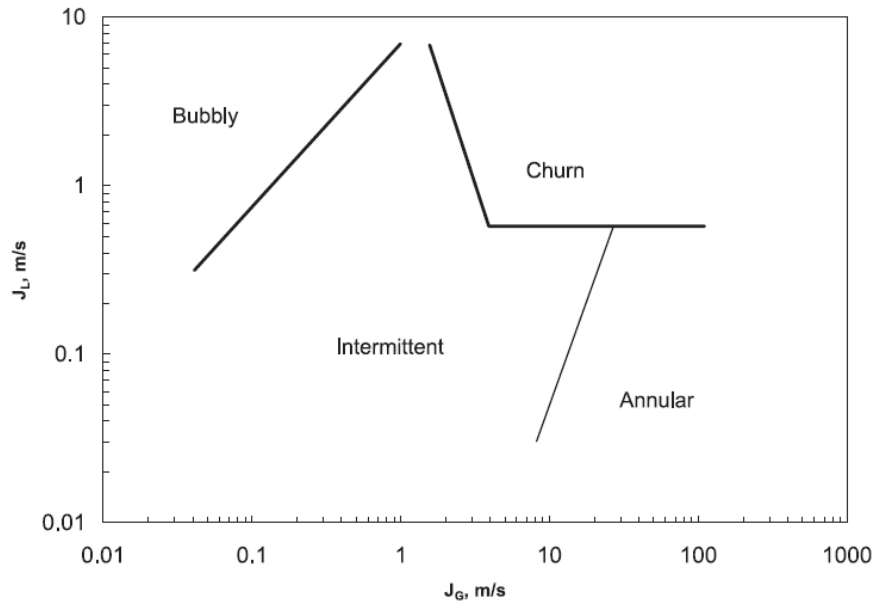


Figure 1-6: Universal two-phase flow regime map for horizontal microchannel proposed by Hassan et al. (2005) (J_L and J_G represent U_{LS} and U_{GS})

Other dimensionless numbers were also employed as coordinates to draw two-phase flow regime maps, with the aim to obtain a universal flow regime map. For instance, Su number ($\sigma d_H \rho_L / \mu_L^2$) and Re_{GS}/Re_{LS} were used by Jayawardena et al. (1997) as coordinates, We_{GS} and We_{LS} by Zhao and Rezkallah (1993) and Akbar et al. (2003), We_G and We_L by Rezkallah (1996), $10^7 Re_{LS}^{0.2} We_{LS}^{0.4} (k_s / d_H)$ and $Re_{GS}^{0.2} We_{GS}^{0.4}$ by Waelchli and Rudolf von Rohr (2006) (k / d_H is the relative roughness of microchannel), as well as void fraction used by Zhao and Rezkallah (1993), Bousman et al. (1996) and Cubaud and Ho, (2004).

The flow regime map proposed by Akbar et al. (2003), which was exhibited in Figure 1-7, is noteworthy for that it have given some reasonable physical explanation. In a flow regime map using Weber numbers as coordinates inspired by the maps of Zhao and Rezkallah (1993) and Rezkallah (1996) for two-phase flow under microgravity, Akbar et al. (2003) summarized flow regime transitions in literature and considered that Weber numbers were more appropriate coordinates than U_{LS} and U_{GS} . They divided the flow regime map into four regions: the surface tension-dominated region (large and elongated bubble flow or so-called slug flow), the inertia-dominated region 1 (annular flow and wavy-annular flow or

slug-annular flow), the inertia-dominated region 2 (dispersed flow) and the transition region. The proposed flow regime map could predict well the experimental data obtained by some researchers using air-water two-phase flow in horizontal channels with diameters about 1 mm, not only circular, but also non-circular.

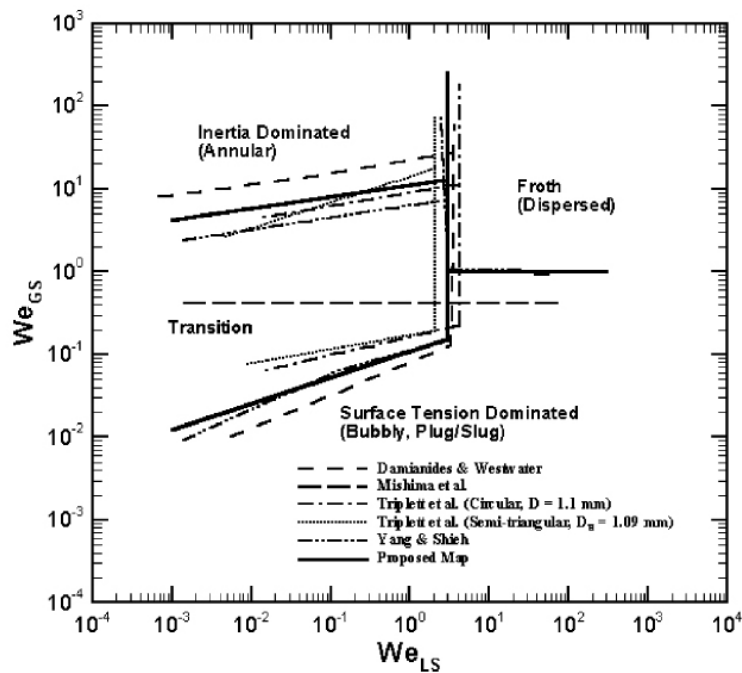


Figure 1-7: Two-phase flow regime map with Weber number as coordinates and transition lines proposed by Akbar et al. (2003)

However, in spite of so many flow regime maps were proposed, no one could represent all parameters influencing gas-liquid flow in microchannel. Moreover, Shao et al. (2009) found that the universal flow regime maps using U_{LS} and U_{GS} as coordinates had good prediction accuracy with experimental data examined from comparison with several universal flow regime maps in their study. They also pointed out that effects of other important parameters, i.e. channel diameter, surface tension, liquid viscosity, wettability of channel wall, were not reflected on the transition lines by using U_{LS} and U_{GS} as coordinates. Such parameters were included when using dimensionless numbers as coordinates, but that led to obvious deviation, because effects of such parameters on each transition lines were various. For example, the effects of surface tension on the flow patterns in surface tension-dominated

region are greater than that of inertia-dominated region. Therefore, more experimental work should be conducted and more reasonable flow regime maps are still needed to develop for universal prediction of two-phase flow patterns in microchannels.

1.2.4 Effects of channel diameters and liquid properties on two-phase flow patterns

Channel size is considered as the most influencing factor on gas-liquid flow patterns in microchannels. Coleman and Garimella (1999) conducted experiments in capillaries with diameters from 1.3 mm to 5.5 mm to investigate the effect of capillary diameter on air-water flow patterns. They found that with decreasing capillary diameter the transitions from slug to bubbly, from slug to slug-annular and from slug-annular to dispersed flow shifted to higher U_{GS} and U_{LS} , whereas the transition from slug-annular to annular and from annular to dispersed flow seemed to be independent on capillary size. Zhao and Bi (2001) investigated air-water flow in triangular channels with hydraulic diameter of 0.866, 1.443 and 2.886 mm. They observed that when channel size decreased the region of slug flow extended, i.e. the transition from slug to churn and to dispersed-bubbly flow shifted to higher U_{GS} and U_{LS} . Meanwhile, the dispersed bubbly flow region shrank, even unobservable in 0.866 mm channel. Flow patterns in circular microchannels were also investigated by Chung and Kawaji (2004). They found that the flow regimes in smaller channels ($d_i = 100$ and $50 \mu\text{m}$) were very different with respect to those in larger ones ($d_i = 530$ and $250 \mu\text{m}$), and special flow patterns such as slug-ring, ring-slug and semi-annular flow were observed. Chen et al. (2006) found that the transition boundaries from slug to churn and from churn to annular flow depend strongly on tube diameter. The Weber number ($\rho U^2 d_H / \sigma$), which is generally used to measure the relative importance of the fluid's inertia compared to its surface tension, might be the appropriate parameter to reveal the size effect. Yue et al. (2008) investigated CO₂-water flow in rectangular channels ($d_H = 0.2, 0.4, 0.667$ mm) and reported the extension of slug flow to higher U_{GS} velocities with decreasing channel size. However, other transition boundaries seemed not to follow certain trend. There are a lot of other researches on this subject but a general agreement of how the channel size exactly affects the two-phase flow patterns is still lacking.

Besides the channel size, liquid physical properties such as density, liquid viscosity and surface tension may also have significant influences on two-phase flow patterns in microchannels (Akbar et al., 2003; Rebrov, 2010; Shao et al., 2009). Many researchers attempted to implement experiments using various liquids as working fluid to investigate this subject. To list some, Suo (1963) and Suo and Griffith (1964) proposed to use dimensionless numbers such as Reynolds number and Weber number to identify the transition boundary from slug flow to bubbly flow. Yang and Shieh (2001) found that the surface tension played an important role for the transitions from slug to bubbly flow and from slug to annular flow. Similar tendency was also reported by Haverkamp et al. (2006). Waelchli and Rudolf von Rohr (2006) proposed a dimensionless group ($Re^{0.2} We^{0.4}$) to identify the flow pattern transitions. Good agreement was found with their experimental data. However, detail and exact effect of each influencing factor has not been discussed. Pohorecki et al. (2008) investigated the effects of contact angle and liquid surface tension. The transition from slug flow to annular flow shifted to lower U_{GS} at high values of contact angle and surface tension. Yang et al. (2010) observed that the rheological properties of non-Newtonian fluid significantly influenced the two-phase flow patterns. Noteworthy that Cubaud et al. (2006) observed uncommon flow patterns, i.e. *foam flow* when surfactant was used to modify the surface properties of water. Detail characteristics of these studies are tabulated in Table 1-3.

Based on the literature, we may conclude that for almost all the existing experiments, the effects of viscosity, surface tension and density were mixed. Effective comparisons are lacking so that how each factor exactly influences the two-phase flow patterns can not be clearly revealed. Moreover, as pointed out in the reviews of Akbar et al. (2003), Rebrov (2010) and Shao et al. (2009), the available experiments data on the effects of liquid physical properties and common understanding are still rare. Systematic and well-designed experiments are still in need to explain fundamental gas-liquid transport mechanisms.

Table 1-3: Selected literature on the effects of liquid physical properties on gas-liquid flow regimes

Authors	Gas-liquid	Test section*	Flow patterns observed	Key findings
Suo and Griffith (1964)	Air-water, N ₂ -water, He-heptane, N ₂ -heptane	H, circular, $d_i = 1.024$ and 1.590 mm	Bubbly slug, slug and annular flow	Re , We , λ used to describe the transition correlation.
Yang and Shieh (2001)	Air-water, air-R134a	H, circular, Pyrex glass, $d_i = 1.0$ to 3.0 mm	Bubbly, dispersed, plug, slug, slug-annular, annular and wavy flow	Transitions from intermittent to bubbly and from slug to annular flow occur at lower U_{GS} due to larger surface tension.
Liu et al. (2005)	Air-water, air-ethanol, air-oil mixture	V, circular ($d_i = 0.91$, 2.00 , 3.02 mm), square ($d_H = 0.99$, 2.89 mm)	Bubbly, slug-bubbly, slug, churn, annular flow	The hydrodynamics of Taylor flow (slug flow) and the influence of liquid properties on the Taylor bubble rise velocity were investigated.
Waelchli and Rudolf von Rohr (2006)	N ₂ -water, N ₂ -ethanol, N ₂ -glycerol (10%), N ₂ -glycerol (20%),	H, rectangular silicon, $d_H = 0.188$ and 0.218 mm	Bubbly, intermittent and annular flow	$10^7 Re_{LS}^{0.2} We_{LS}^{0.4} (k_s/d_H)^5$ and $Re_{GS}^{0.2} We_{GS}^{0.4}$ proposed as coordinates in flow maps
Haverkamp et al. (2006)	N ₂ -water and N ₂ -isopropanol	H, rectangular, $d_H = 0.0667$, 0.150 and 0.294 mm	Bubbly, slug, slug-annular, annular, annular-spray, spray flow	All the transitions shift to higher U_{GS} due to smaller surface tension; Smaller bubbles and larger specific interfacial surface areas are formed.
Cubaud et al. (2006)	Air-water, air-water with surfactant	H, square glass, $d_H = 0.525$ mm	Bubbly, slug, annular, dry foam and wet foam flow	Significant influences of wall properties and liquid surface properties on two-phase flow in microchannel revealed.
Pohorecki et al. (2008)	N ₂ -water, N ₂ -ethanol	H, rectangular PMMA, $d_H = 0.293$ mm	Bubbly, slug, slug-annular, annular flow	Observable influences of the contact angle and surface tension. For higher these values the transition from slug to annular flow shifts to lower U_{GS} .
Lee and Lee (2008)	Air-water, air-methanol	H, circular channels, $d_i = 1.46$, 1.8 mm glass; $d_i = 1.59$ mm Teflon; $d_i = 2.0$ mm polyurethane	Bubbly, dispersed, plug, slug, annular, wavy, rivulet flow	Effect of surface wettability: wet flow: $U_{LS} = 1$ m/s, $\theta < 50^\circ$; dry flow: $U_{LS} = 1$ m/s, $\theta > 90^\circ$.

Table 1-3(Continued)

Authors	Gas-liquid	Test section*	Flow patterns observed	Key findings
Niu et al. (2009)	Gas: CO ₂ and N ₂ mixture liquid: polyethylene glycol dimethyl ether	H, circular, $d_i = 1.0$ mm	Bubbly, slug, churn, slug-annular flow	Absorption and liquid physical properties considered.
Weinmueller et al. (2009)	CO ₂ -water, CO ₂ -1M methanol aqueous, CO ₂ -methanol	H, rectangular, $d_H = 0.2$ mm	Bubbly, slug(wedging), annular, stratified flow	Significant influences of nozzle, channel geometries and fluid properties; Easy formation of smaller bubbles at lower surface tension
Zhang and Fu (2009)	Vapor- liquid N ₂	V, circular, $d_i = 0.531$ and 1.042 mm	Bubbly, confined bubbly, slug, churn, annular, mist flow	The transition from slug to churn and from churn to annular move to lower U_{GS} while the transition from bubbly to slug moves to higher U_{GS} with decreasing surface tension.
Pamitran et al. (2010)	Vapor-R22, vapor-R134a, vapor-R410A, vapor-R290, vapor-R744	H, circular stainless steel, $d_i = 0.5, 1.5$ and 3.0 mm	Intermittent, annular, stratified, stratified wavy, dry out, mist	Significant influences of liquid density, viscosity and surface tension on the flow pattern and pressure drop.
Yang et al. (2010)	N ₂ -CMC aqueous (0.4%), PAM aqueous (0.2%), XG aqueous (0.2%)	V, triangular ($d_H = 0.866$ and 2.886 mm), square ($d_H = 2.5$ mm)	Bubbly, dispersed bubbly, slug, churn, annular, chained bubble-slug flow	Significant influences of rheological properties of the non-Newtonian fluids.
Ong and Thome (2011)	Vapor-R134a, Vapor-R236fa, vapor-R245fa	H, circular, $d_i = 1.03, 2.20$ and 3.04 mm	Bubbly, coalescing bubbly, slug, annular flow	The transitions from bubbly to coalescing bubbly and coalescing bubbly to annular shift to lower U_{GS} with increasing surface tension, density and liquid viscosity; Transition criteria based on Re , We , Bo , Co , viscosity and density ratios proposed.

* H: Horizontal; V: Vertical.

1.2.5 Two-phase pressure drop in microchannels

Two-phase pressure drop is one of the most important hydrodynamic aspects of gas-liquid flow not only in common tubes, but also in mini/micro channels, which is an essential element for design of gas-liquid two-phase reactors and other processes in chemical industry, as well as others gas-liquid systems, such as boiling and condensation in pipes. Generally, two main methods are used to predict the pressure drop of gas-liquid two-phase flow in common tubes, i.e. homogeneous mixture model and separated flow model (Collier and Thome, 1994) (more detailed introduction about these two type models will be given in Chapter 3). However, in the mini/micro size channels, due to the reduction of the channel size, the effects of surface tension, confinement of channel wall and two-phase interaction on the two-phase pressure drop increase (Choi et al., 2011; English and Kandlikar, 2006), leading to the inapplicability of the traditional pressure drop prediction models. The homogeneous mixture model have been proved to be not appropriate prediction model for gas-liquid pressure drop in mini/micro channels by many researchers (Niu et al., 2009; Su et al., 2010; Yue et al., 2004), because interaction between gas and liquid flow is not considered. Recently, many researchers found that separated flow model could predict well the two-phase pressure drop in their experiments after modification, and various modified separated flow models were proposed (Chen et al., 2007; Choi et al., 2008; English and Kandlikar, 2006; Hwang and Kim, 2006; Kawahara et al., 2009; Mishima and Hibiki, 1996; Lee et al., 2010; Lee and Lee, 2001; Li and Wu, 2010; Ma et al., 2010; Niu et al., 2009; Qu and Mudawar, 2003; Saisorn and Wongwises, 2010; Su et al., 2010; Yue et al., 2004; Yue and Mudawar, 2005; Zhang et al., 2010). But up to now, general agreement on this issue is still lacking, much more experimental work is required to give a more reasonable and universally applicable prediction model. Actually, it is known that separated flow model is based on the assumption that gas and liquid phase flow separately in the tube with each phase flowing continuous and occupying a sector of the pipe cross section. Therefore, separated flow model should be more suitable to predict the two-phase pressure drop in mini/micro channels under some flow patterns, i.e. churn flow, slug-annular and annular flow, but not bubbly or Taylor flow, because that the gas phase is obviously discontinuous and the motion of liquid film vary from that of liquid slug in bubbly or Taylor flow.

On the other hand, Taylor flow can be regarded as a steady process due to it consists of several or a lot of unit cells (one bubble, the liquid film surrounding the bubble and one slug) which are almost identical. Therefore, it is possible to build accurate physical model to calculate the two-phase pressure drop of the Taylor flow. As early as 1961, Bretherton theoretically studied the motion of gas bubbles at small Reynolds number in small size tubes using a lubrication analysis, forming a contribution to the issue predicting the profile of the gas bubbles and the rise rate of gas bubbles in vertical capillaries. Based on the assumptions that surface tension was well-defined and no tangential stress on the gas-liquid interfacial, inertia forces was negligible, and tube wall was perfect wettable with sufficiently thin liquid film surround the gas bubbles, he found that the pressure drop over the bubble caps in the circular capillaries could be expressed as:

$$\Delta P_{cap,TUC} = 7.16(3Ca)^{2/3} \frac{\sigma}{d_i} \quad (1.8)$$

And for the whole bubble, the pressure drop could be expressed as:

$$\Delta P_{TUC} = 9.04(3Ca)^{2/3} \frac{\sigma}{d_i} \quad (1.9)$$

Computer simulation was another method used to study the Taylor flow in the microchannels. Kreutzer et al. (2005a, 2005b) used CFD (Computational Fluid Dynamics) to calculate the two-phase pressure drop of Taylor flow in circular capillaries. They considered that the contribution of bubbles could be calculated as a part of the total frictional pressure drop of Taylor flow across the channel, based on the assumption that for the infinitely long liquid slugs, the pressure drop was equal to the frictional pressure drop of liquid single phase flow which could be calculated by the Hagen-Poiseuille equation:

$$\Delta P_{liquid,TUC} = \frac{64}{\text{Re}_{liquid,TUC}} \frac{L_S \rho_L U_{liquid}^2}{2d_i} = \frac{16}{\text{Re}_{liquid,TUC}} \left(\frac{1}{2} \rho_L U_{liquid}^2 \right) \frac{4L_S}{d_i} \quad (1.10)$$

The contribution of gas bubble to pressure drop could be represented by an additional factor ξ within the friction factor f :

$$f = \frac{64}{\text{Re}_{liquid}} (1 + \xi) \quad (1.11)$$

In which, ξ was given as:

$$\xi = a \left(\frac{d_i}{L_s} \left(\frac{\text{Re}_{liquid}}{Ca} \right)^b \right) \quad (1.12)$$

By assuming inertia was negligible ($Ca \ll 1$ and $We \ll 1$).

According to the experimental measurements using air as gas phase and three various liquid (water, decane and tetradecane) as liquid phase, Kreutzer et al. (2005a, 2005b) found that $a = 0.33$, $b = 0.07$ for $Re > 50$ and $b = 0.17$ for $Re \leq 50$ ($0.002 < Ca < 0.04$, $8 < L_s / d_i < 12$), respectively. Walsh et al. (2009) performed experimental study on the pressure drop of Taylor flow in mini scale capillaries, employing water, FC 40, dodecane, AR 20 Si oil and n-Hexane as liquid phase ($1.58 < Re < 1024$, $0.0023 < Ca < 0.2$), and found that prediction of the model proposed by Kreutzer et al. (2005a, 2005b) with the fitting parameter $b = 0.12$ corresponded well with their experimental data. However, Yue et al. (2009) carried out experiments on gas-liquid two-phase flow in rectangular microchannels (d_H : 200 and 400 μm), and noted that when the liquid slugs were very short, the frictional pressure drop of Taylor flow in microchannels was significantly higher than the predictions of Kreutzer's correlation, caused by the inadequacy of the model to describe the excess pressure drop of the inner circulation in liquid slugs. They modified appropriately Kreutzer's correlation to improve its applicability in microchannels, to add a new item $5.5 \times 10^{-5} \left(\frac{L_s}{d_h \text{Re}_{slug}} \right)^{-1.6}$ to the frictional factor which was adopted in the analysis on the apparent frictional factor for the hydrodynamically developing flow in non-circular ducts (Muzychka and Yovanovich, 1998; Shah and London, 1978) to ξ . Besides two-phase pressure drop, the effects of inlet on Taylor bubble formation (Shao et al., 2008), Taylor flow formation mechanism (Santos and Kawaji, 2010), Taylor bubble size and shape, liquid film thickness and velocity field (Liu and Wang, 2008b) also could be simulated and calculated by using CFD. But the thorough understanding of fundamental knowledge of Taylor flow is still lacking, for instance, the exact mechanism of two-phase pressure drop and others important parameters of Taylor flow are still not clear, and more theoretical study, numerical simulation and well-designed experimental measurements are deadly required.

1.3 Two-phase mass transfer and reaction in microreactors

1.3.1 Two-phase mass transfer in microreactors

For gas-liquid absorption or reaction process, especially for fast and highly exothermic reactions, the absorption or reaction rate is usually limited by the gas-liquid mass transfer. Heat and mass transfer enhancement is one of the most important advantages of microreactors. Due to the reduction of the channels size to the order of tens or hundreds micron meter, the specific interfacial area of the microreactors is significantly larger than that of common reactors, which not more than $200 \text{ m}^2/\text{m}^3$ (Ehrfeld et al., 2004), generally. Yue et al. (2007) measured two-phase specific interfacial area of rectangular microchannels (d_H : 200 and 400 μm) during the absorption of CO_2 in the water, NaOH and $\text{Na}_2\text{CO}_3/\text{NaHCO}_3$ solutions, and found that the specific interfacial area reached as high as $9000 \text{ m}^2/\text{m}^3$. In addition, the liquid side volumetric mass transfer coefficient ($k_L a_i$) could achieve 21 s^{-1} , more than one hundred times larger than that of traditional gas-liquid contactors. Yeong et al. (2004) experimentally investigated the nitrobenzene hydrogenation in a gas-liquid falling film microreactor (64 straight parallel channels with width of 300 μm , height of 100 μm and length of 78 mm). The specific interfacial area was $9000\text{-}15000 \text{ m}^2/\text{m}^3$ and $k_L a_i$ was $3\text{-}8 \text{ s}^{-1}$, significantly higher than that of common reactors. The absorption of H_2S in MDEA (methyldiethanolamine solution) was performed in circular microchannels (d_i : 0.56, 1.00 and 1.80 mm) by Su et al. (2010), during which the specific interfacial area could be larger than $11100 \text{ m}^2/\text{m}^3$. Niu et al. (2009b) implemented the experiments to study the absorption of CO_2 in the MDEA in a circular microchannel (d_i : 1.00 mm). The $k_L a_i$ was found extremely high and increasing with gas flow velocity and liquid flow velocity, and could achieve 3.34 s^{-1} . Losey et al. (2001) reported that the $k_L a_i$ would achieve $5\text{-}15 \text{ s}^{-1}$ when the hydrogenation of cyclohexene in their micro packed-bed gas-liquid reactor with ten reactor chambers (width: 625 μm ; depth: 300 μm ; length: 2 cm) packed by catalytic particles as shown in Figure 1.8, hundreds times magnitude larger than standard laboratory-scale reactors.

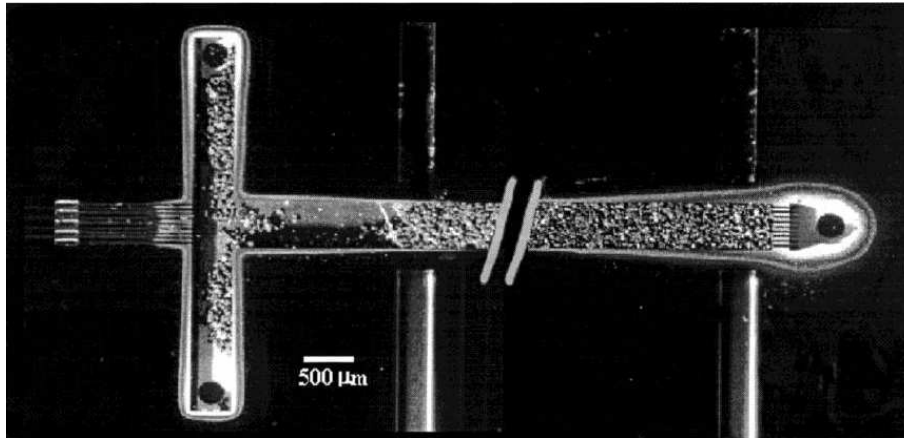


Figure 1-8: Single-reactor chamber of micro packed-bed gas-liquid reactors (Losey et al., 2001)

The flow patterns were considered to affect the mass transfer in gas-liquid microreactors. Hessel et al. (2000) carried out experimental study on this issue in a rectangular microchannel with a width of 300 μm and a height of 100 μm . They measured the specific interfacial area by using the absorption of CO_2 in the sodium hydroxide solution, and the example values are tabulated in Table 1-4, which also can be found in Völkel's thesis.

Table 1-4: Specific interfacial area measured by Hessel et al. (2000) under various flow patterns

Flow regime	bubbly	slug	annular
$a_i \text{ m}^2/\text{m}^3$	5100	18700	25300

It can be noted in the Table 1-4, the largest specific interfacial area of the microchannel would reach in the annular flow.

On the other hand, many researchers believed that slug flow or named Taylor flow was the most interesting condition for gas-liquid mass transfer, due to the enhancement of molecular transport between gas-liquid interface and liquid bulk led by the recirculation motion in the liquid slug, which had been confirmed by simulation (using CFD; Liu and Wang, 2008b) and visual studies using particle image velocimetry (PIV; Günther et al., 2004; Günther et al., 2005; Günther et al., 2006; Thulasidas et al., 1997; Trachsel et al., 2005; Waelchli and von Rohr, 2006). The mass transfer of Taylor flow in microchannels was numerically and experimentally studied (Liu et al., 2009; Liu and Wang, 2011; Van Baten and Krishna, 2004; Vandu et al.,

2005). It was considered that the k_{La_i} was significantly affected by the detailed parameters of Taylor flow, i.e. bubble length, bubble velocity, liquid slug length, and liquid film thickness, with which the prediction of two-phase mass transfer should be possible.

1.3.2 Gas-liquid reaction in microreactors

Due to the superior advantage in gas-liquid mass transfer and reaction, gas-liquid microreaction technology has attracted increasing academic interest, and extensive exploratory work has been implemented to perform gas-liquid reactions in microreactors.

Jähnisch et al. (2000) experimentally investigated the direct fluorination of toluene in falling film micro reactor (Figure 1-9) and micro bubble column reactor (Figure 1-10) using elemental fluorine, and compared the results with that of a common laboratory bubble column, as shown in Figure 1-11. Extremely large specific interfacial area was obtained, as large as $14800 \text{ m}^2/\text{m}^3$ for a micro bubble column reactor and $27000 \text{ m}^2/\text{m}^3$ for a falling film micro reactor. The superior heat transfer performance ensured the safety during the fluorination. It could be seen from Figure 1-11 that conversion, selectivity and space-time yield of microreactors were obviously higher than that of common laboratory bubble column. Such great performance of microreactors in direct fluorination also has been reported by de Mas et al. (2005).

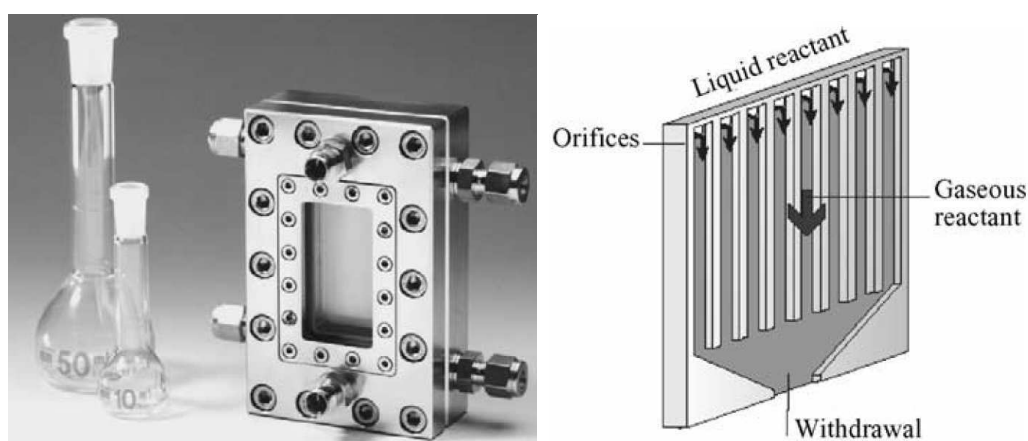


Figure 1-9: Falling film micro reactor and the principle of contacting liquid and gas reactants

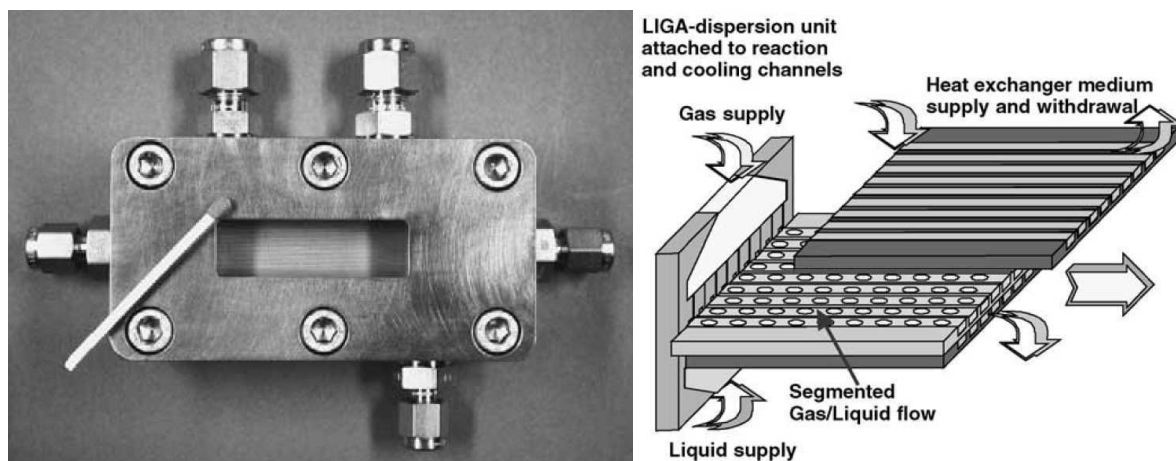


Figure 1-10: Micro bubble column reactor and the schematic illustration of contacting liquid and gas reactants

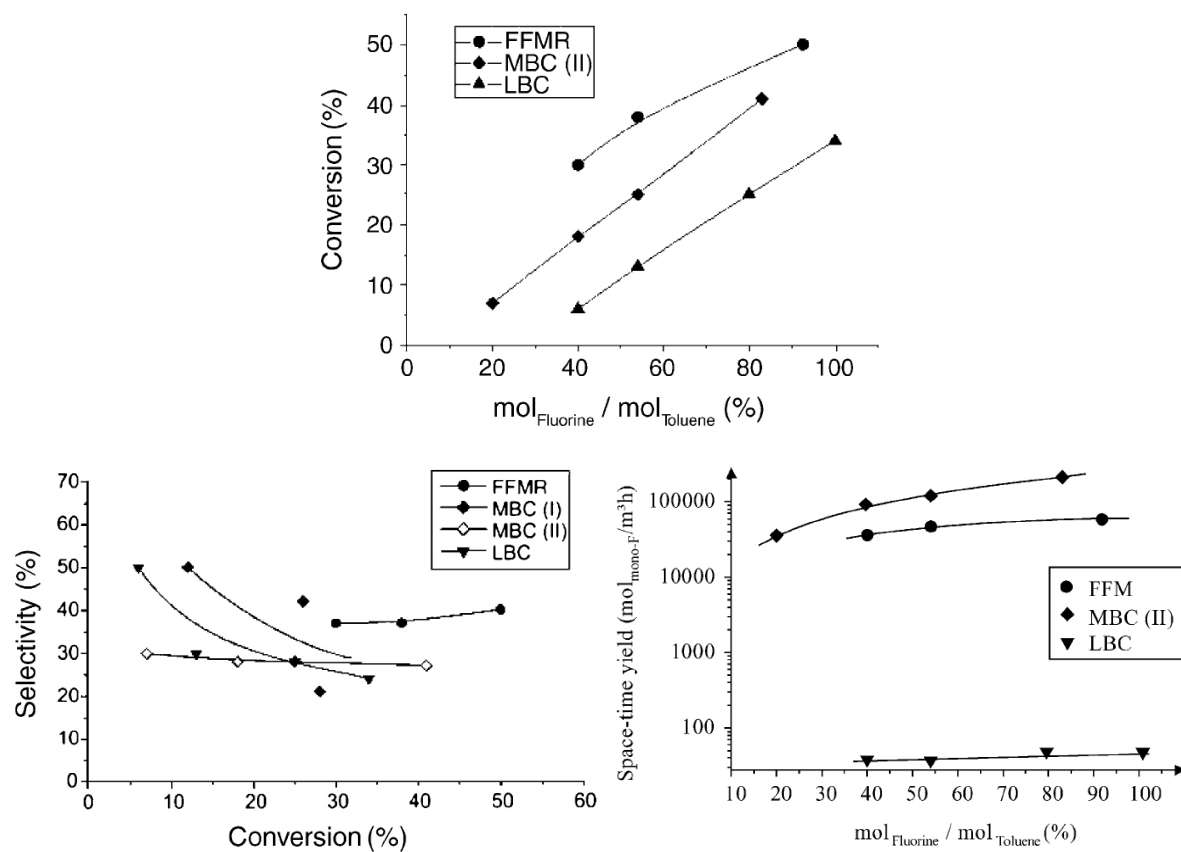


Figure 1-11: The comparison of conversion, selectivity, and space-time yield of direct fluorination of toluene between in microreactors and in laboratory bubble column (LBC): FFMR, falling film microreactor; MBC, micro bubble column reactor

Chambers et al. (1999, 2001, 2005a, 2005b, 2005c) studied the direct fluorination of

various organic compounds in microchannels using elemental fluorine, rather high conversion and selectivity was obtained. For example, for the direct fluorination of para-nitrotoluene, very high conversion (44-77%) was obtained, corresponding to the maximum space-time yield of 78%.

Halder and Lawal (2007) performed the hydrogenation of anthraquinone derivative in microchannel reactor, which was generally considered as a reaction limited by mass transfer. The space-time yield reached $1100 \text{ g}_{\text{H}_2\text{O}_2} \cdot \text{g}_{\text{Pd}}^{-1} \cdot \text{h}^{-1}$ due to the enhancement of mass transfer in microchannels, tens times magnitude higher than conventional reactors.

Inoue et al. (2007, 2009, 2010a, 2010b) implemented the investigation of direct synthesis of hydrogen peroxide from hydrogen and oxygen in microreactors, using H_2/D_2 and O_2/N_2 as gas phase, and mixture of sulfuric acid, phosphoric acid and sodium bromide solution as liquid phase. By using Pd/C hydrogenation catalyst, the space-time yield could achieve $5.78 \text{ g}_{\text{H}_2\text{O}_2} \cdot \text{g}_{\text{Pd}}^{-1} \cdot \text{h}^{-1}$, similar with that of anthraquinone process, but with more simple production process.

Beside the reaction mentioned above, there were also others various reactions investigated in microreactors, i.e. nitrobenzene hydrogenation (Yeong et al., 2004), chlorination and bromination of organic compounds (Löb et al., 2004), photochemical chlorination of alkyl aromatics (Ehrich et al., 2002), catalytic asymmetric hydrogenation (Abdallah et al., 2004, 2006). In all the previous researches, microreaction technology has showed a great potential in gas-liquid reaction, and will certainly be introduced in the gas-liquid industrial processes in the near future.

1.4 Conclusions

From the above review, it is revealed that the hydrodynamics characteristics of gas-liquid two-phase flow, such as flow patterns, pressure drop and mass transfer, in microchannels with inner diameter less than 1 mm vary from that of conventional gas-liquid contactors. Moreover, the potential of microreactors in gas-liquid chemical process have been demonstrated, for its superior advantages in mass transfer and reaction performance. Although extensive dedicated work have been implemented, general agreements on the fundamental knowledge of

gas-liquid microreaction system are still lacking, and systematically researches are urgently required to provide theoretical guidance for the design of gas-liquid microreaction system. Some important issues need to uncover and can be identified as follows:

(1) *Gas-liquid two-phase flow in microchannels*. It mainly include the formation mechanism of two-phase flow patterns and the transition between them, as well as the influence of channel size, liquid physical properties, channel surface properties, etc., on two-phase flow patterns.

(2) *Two-phase pressure drop in microchannels*. Two-phase pressure drop in microchannels is rather different from that of larger tubes, reasonable theoretical mechanism and prediction model need to be founded. It was reported that the two-phase pressure drop was highly depended on flow patterns, which also need deeply studied.

(3) *Gas-liquid reaction in microchannels*. Although many exploratory work have been conducted to investigate gas-liquid reaction in microreactors, more various gas-liquid reaction system need to be performed in microchannels to provide empirical guidance for practical application of microreaction technology in gas-liquid reaction process.

Consequently, the following chapters of this thesis will focus on the gas-liquid two-phase hydrodynamics and reaction characteristics in microchannels. The microchannels employed in the present thesis is on the order of hundreds microns with circular cross-section. This thesis consists of following main parts. To begin with, we give a short overview on the current research status of gas-liquid microreaction technology in Chapter 1. Then, in Chapter 2 gas-liquid two-phase flow pattern will be systematically investigated, special emphasis will be put on the influence of channel size and liquid properties. The existing transition model will be examined and a new model will be proposed. Moreover, Chapter 3 will concentrate on two-phase pressure drop in microchannels. In which, the dependence of two-phase pressure drop on gas-liquid flow patterns will be discussed and the pressure drop in inertia-dominated region will be deeply studied. Furthermore, Chapter 4 is concerned with Taylor flow in microchannels. The detailed characteristics of Taylor flow, i.e. Taylor bubble length and void fraction will be analyzed, as well as the formation mechanism of the Taylor bubble. The pressure drop of Taylor flow will also be discussed. In Chapter 5, gas-liquid reaction will be

experimentally investigated using the oxidation of hydrogenated 2-ethyltetrahydroanthraquinone (THEAQH₂) as model reaction. Finally, the key finding achieved in the present thesis will be summarized at the end of the present thesis, as well as the perspectives about the future work.

References

- Abdallah, R., Meille, V., Shaw, J., Wenn, D., de Bellefon, C., 2004. Gas-liquid and gas-liquid-solid catalysis in a mesh microreactor. *Chemical Communications* 4, 372-373.
- Abdallah, R., Magnico, P., Fumey, B., de Bellefon, C., 2006. CFD and kinetic methods for mass transfer determination in a mesh microreactor. *AICHE Journal* 52, 2230-2237.
- Akbar, M.K., Plummer, D.A., Ghiaasiaan, S.M., 2003. On gas-liquid two-phase flow regimes in microchannels. *International Journal of Multiphase Flow* 29, 855-865.
- Albrecht, J., Becht, S., Geisselmann, A., Hahn, H., Caspary, K.J., Schirmermeister, S., 2006. Degussa and Uhde develop a production scale microstructured reactor for use in commercial chemical plants. *Elements (Degussa Science Newsletter)* 15, 18-31.
- Barajas, A.M., Panton, R.L., 1993. The effects of contact-angle on 2-phase flow in capillary tubes. *International Journal of Multiphase Flow* 19, 337-346.
- Banister, J., and Rumbold, S., 2005. A compact gas-to-methanol process and its application to improved oil recovery. Paper presented at the gas processors association Europe annual conference, Warsaw, Poland, September.
- Bousman, W.S., Mcquillen, J.B., Witte, L.C., 1996. Gas liquid flow pattern in microgravity: effect of tube diameter, liquid viscosity and surface tension. *International Journal of Multiphase Flow* 22, 1.35-1053.
- Brauner, N., Maron, D.M., 1992. Identification of the range of small diameters conduits, regarding 2-phase flow pattern transitions. *International Communications in Heat and Mass Transfer* 19, 29-39.
- Bretherton, F.P., 1961. The motion of long bubbles in tubes. *J. Fluid. Mech.* 10, 166-188.
- Chambers, R.D., Fox, M.A., Holling, D., Nakano, T., Okazoeb, T., Sandford, G., 2005a. Elemental fluorine Part 16. Versatile thin-film gas-liquid multi-channel microreactors for effective scale-out. *Lab on a Chip* 5, 191-198.
- Chambers, R.D., Fox, M.A., Sandford, G., 2005b. Elemental fluorine Part 18. Selective direct fluorination of 1,3-ketoesters and 1,3-diketones using gas/liquid microreactor technology. *Lab on a Chip* 5, 1132-1139.
- Chambers, R.D., Fox, M.A., Holling, D., Nakano, T., Okazoe, T., Sandford, G., 2005c. Versatile gas/liquid microreactors for industry. *Chemical Engineering and Technology* 28, 344-352.
- Chambers, R.D., Holling, D., Spink, R.C.H., Sandford, G., 2001. Elemental fluorine Part 13. Gas-liquid thin film

- microreactors for selective direct fluorination. *Lab on a Chip* 1, 132-137.
- Chambers, R.D., Spink, R.C.H., 1999. Microreactors for elemental fluorine. *Chemical Communications* 10, 883-884.
- Chen, I.Y., Chen, Y.M., Liaw, J.S., Wang, C.C., 2007. Two-phase frictional pressure drop in small rectangular channels. *Experimental Thermal and Fluid Science* 32, 60-66.
- Chen, L., Tian, Y.S., Karayiannis, T.G., 2006. The effect of tube diameter on vertical two-phase flow regimes in small tubes. *International Journal of Heat and Mass Transfer* 49, 4220-4230.
- Chen, W.L., Twu, M.C., Pan, C., 2002. Gas-liquid two-phase flow in micro-channels. *International Journal of Multiphase Flow* 28, 1235-1247.
- Cheng, L.X., Ribatski, G., Thome, J.R., 2008. Two-phase flow patterns and flow-pattern maps: Fundamentals and applications. *Applied Mechanics Reviews* 61, 050802-1-050802-28.
- Choi, K.I., Pamitran, A.S., Oh, C.Y., Oh, J.T., 2008. Two-phase pressure drop of R-410A in horizontal smooth minichannels. *International Journal of Refrigeration* 31, 119-129.
- Choi, C.W., Yu, D.I., Kim, M.H., 2011. Adiabatic two-phase flow in rectangular microchannels with different aspect ratios: Part I - Flow pattern, pressure drop and void fraction. *International Journal of Heat and Mass Transfer* 54, 616-624.
- Chung, P.M.Y., Kawaji, M., 2004. The effect of channel diameter on adiabatic two-phase flow characteristics in microchannels. *International Journal of Multiphase Flow* 30, 735-761.
- Coleman, J.W., Garimella, S., 1999. Characterization of two-phase flow patterns in small diameter round and rectangular tubes. *International Journal of Heat and Mass Transfer* 42, 2869-2881.
- Collier, J.G., Thome, J.R., 1994. *Convective boiling and condensation*. New York, USA: Oxford University Press.
- Cubaud, T., Ulmanella, U., Ho, C.M., 2006. Two-phase flow in microchannels with surface modifications. *Fluid Dynamics Research* 38, 772-786.
- de Mas, N., Günther, A., Kraus, T., Schmidt, M. A., Jensen, K. F., 2005. Scale-out multilayer gas-liquid microreactor with integrated velocimetry sensors. *Industrial and Engineering Chemistry Research* 44, 8997-9013.
- Dietrich, T.R., 2009. *Microchemical engineering in practice*. Hoboken, New Jersey: John Wiley & Sons, Inc.
- Ehrfeld, W., Hessel, V., Löwe, H., 2004. *Microreactors: new technology for modern chemistry*. Weinheim, Germany: Wiley-VCH.

- Ehrich, H., Linke, D., Morgenschweis, K., Baerns, M., Jähnisch, K., 2002. Application of microstructured reactor technology for the photochemical chlorination of alkylaromatics. *Chimia* 56, 647-653.
- English, N.J., Kandlikar, S.G., 2006. An experimental investigation into the effect of surfactants on air-water two-phase flow in minichannels. *Heat Transfer Engineering* 27, 99-109.
- Günther, A., Khan, S.A., Thalmann, M., Trachsel, F., Jensen, K.F., 2004. Transport and reaction in Microscale segmented gas-liquid flow. *Lab on a Chip* 4, 278-286.
- Günther, A., Jhunjhuwala, M., Thalmann, M., Schmidt, M.A., Jensen, K.F., 2005. Micromixing of Miscible liquids in segmented gas-liquid flow. *Langmuir* 21, 1547-1555.
- Günther, A., Jensen, K.F., 2006. Multiphase microfluidics: from flow characteristics to chemical and materials synthesis. *Lab on a Chip* 6, 1487-1503.
- Halder, R., Lawal, A., 2007. Experimental studies on hydrogenation of anthraquinone derivative in a microreactor. *Catalysis Today* 125, 48-55.
- Hassan, I., Vaillancourt, M., Pehlivan, K., 2005. Two-phase flow regime transitions in microchannels: A comparative experimental study. *Microscale Thermophysical Engineering* 9, 165-182.
- Haverkamp, V., Hessel, V., Lowe, H., Menges, G., Warnier, M.J.F., Rebrov, E.V., de Croon, M., Schouten, J.C., Liauw, M.A., 2006. Hydrodynamics and mixer-induced bubble formation in micro bubble columns with single and multiple-channels. *Chemical Engineering & Technology* 29, 1015-1026.
- Hessel, V., Ehrfeld, W., Herweck, T., Haverkamp, V., Löwe, H., Schiewe, J., Wille, C., Kern, T., Lutz, N., 2000. Gas/liquid microreactors: hydrodynamics and mass transfer. *IMRET 4: Proceedings of the 4th International Conference on Microreaction Technology*, 174.
- Hessel, V., Lowe, H., Muller, A., Kolb, G., 2005. *Chemical micro process engineering: processing and plants*. Weinheim, Germany: Wiley-VCH.
- Hwang, Y.W., Kim, M.S., 2006. The pressure drop in microtubes and the correlation development. *International Journal of Heat and Mass Transfer* 49, 1804-1812.
- Inoue, T., Kikutani, Y., Hamakawa, S., Mawatari, K., Hibara, A., Mizukami, F., Kitamori, T., 2010a. Reactor design optimization for direct synthesis of hydrogen peroxide. *Chemical Engineering Journal* 160, 909-914.
- Inoue, T., Ohtaki, K., Kikutani, Y., Sato, K., Nishioka, M., Hamakawa, S., Mawatari, K., Mizukami, F., Kitamori, T., 2009. The direct synthesis of hydrogen peroxide (ca. 5 wt%) from hydrogen and oxygen by microreactor technology. *Chemistry Letters* 38, 820-821.
- Inoue, T., Ohtaki, K., Kikutani, Y., Sato, K., Nishioka, M., Hamakawa, S., Mawatari, K., Hibara, A., Mizukami,

- F., Kitamori, T., 2010b. Direct synthesis of hydrogen peroxide based on microreactor technology. Abstracts of Papers of the American Chemical Society 240.
- Inoue, T., Schmidt, M.A., Jensen, K.F., 2007. Microfabricated multiphase reactors for the direct synthesis of hydrogen peroxide from hydrogen and oxygen. *Industrial & Engineering Chemistry Research* 46, 1153-1160.
- Jähnisch, K., Baerns, M., Hessel, V., Ehrfeld, W., Haverkamp, V., Löwe, H., Wille, Ch., Guber, A., 2000. Direct fluorination of toluene using elemental fluorine in gas/liquid microreactors. *Journal of Fluorine Chemistry* 105, 117-128.
- Jarosch, K., Mazanec, T., McDaniel, J., Tonkovich, A. L., and Fitzgerald, S., 2006. Compact mobile synthetic fuel unit. Paper presented at the American Institute of Chemical Engineers Spring National Meeting, Orlando, FL, April 23-27.
- Jayawardena, S.S., Balakotaiah, V., Witte, L.C., 1997. Flow pattern transition maps for microgravity two-phase flow. *AICHE J.* 43, 1637-1640.
- Kandlikar, S.G., Grande, W.J., 2003. Evolution of microchannel flow passages-thermo hydraulic performance and fabrication technology. *Heat transfer engineering* 24, 3-17.
- Kawahara, A., Sadatomi, M., Nei, K., Matsuo, H., 2009. Experimental study on bubble velocity, void fraction and pressure drop for gas-liquid two-phase flow in a circular microchannel. *International Journal of Heat and Fluid Flow* 30, 831-841.
- Kew, P.A., Cornwell, K., 1997. Correlations for the prediction of boiling heat transfer in small-diameter channels. *Applied Thermal Engineering* 17, 705-715.
- Kreutzer, M.T., Kapteijn, F., Moulijn, J.A., Heiszwolf, J.J., 2005a. Multiphase monolith reactors: Chemical reaction engineering of segmented flow in microchannels. *Chemical Engineering Science* 60, 5895-5916.
- Kreutzer, M.T., Kapteijn, F., Moulijn, J.A., Kleijn, C.R., Heiszwolf, J., 2005b. Inertial and interfacial effects on pressure drop of Taylor flow in capillaries. *AICHE Journal* 51, 2428-2440.
- Lee, C.Y., Lee, S.Y., 2008. Influence of surface wettability on transition of two-phase flow pattern in round mini-channels. *International Journal of Multiphase Flow* 34, 706-711.
- Lee, H.J., Lee, S.Y., 2001. Pressure drop correlations for two-phase flow within horizontal rectangular channels with small heights. *International Journal of Multiphase Flow* 27, 783-796.
- Lee, H.J., Liu, D.Y., Alyousef, Y., Yao, S.C., 2010. Generalized two-phase pressure drop and heat transfer correlations in evaporative micro/minichannels. *Journal of Heat Transfer-Transactions of the ASME* 132.

- Lee, J., Mudawar, I., 2005. Two-phase flow in high-heat-flux micro-channel heat sink for refrigeration cooling applications: Part I--pressure drop characteristics. *International Journal of Heat and Mass Transfer* 48, 928-940.
- Li, J.M., Wang, B.X., 2003. Size effect on two-phase regime for condensation in micro/mini tubes. *Heat Transfer—Asian Research* 32, 65-71.
- Li, W., Wu, Z., 2010. A general correlation for adiabatic two-phase pressure drop in micro/mini-channels. *International Journal of Heat and Mass Transfer* 53, 2732-2739.
- Liu, D., Wang, S., 2008a. Flow pattern and pressure drop of upward two-phase flow in vertical capillaries. *Industrial and Engineering Chemistry Research* 47, 243-255.
- Liu, D., Wang, S., 2008b. Hydrodynamics of Taylor flow in noncircular capillaries. *Chemical Engineering and Processing* 47, 2098-2106.
- Liu, D., Wang, S., 2011. Gas-liquid mass transfer in Taylor flow through circular capillaries. *Industrial & Engineering Chemistry Research* 50, 2323-2330.
- Liu, H., Vandu, C.O., Krishna, R., 2005. Hydrodynamics of taylor flow in vertical capillaries: flow regimes, bubble rise velocity, liquid slug length, and pressure drop. *Industrial & Engineering Chemistry Research* 44, 4884-4897.
- Liu, D., Zhang, J., Li, D., Kong, Q., Zhang, T., Wang, S., 2009. Hydrogenation of 2-ethylanthraquinone under Taylor flow in single square channel monolith reactors. *AICHE Journal* 55, 726-736.
- Löb, P., Lowe, H., Hessel, V., 2004. Fluorinations, chlorinations and brominations of organic compounds in micro reactors. *Journal of Fluorine Chemistry* 125, 1677-1694.
- Losey, M.W., Schmidt, M.A., Jensen, K.F., 2001. Microfabricated multiphase packed-bed reactors: characterization of mass transfer and reactions. *Industrial and Engineering Chemistry Research* 40, 2555-2562.
- Ma, Y., Ji, X., Wang, D., Fu, T., Zhu, C., 2010. Measurement and correlation of pressure drop for gas-liquid two-phase flow in rectangular microchannels. *Chinese Journal of Chemical Engineering* 18, 940-947.
- Mazanec, T., 2006. Catalytic selective oxidation in microchannel reactor. Paper presented at the ACS Fall Symposium, San Francisco, CA, September 12.
- Mishima, K., Hibiki, T., 1996. Some characteristics of air-water two-phase flow in small diameter vertical tubes. *International Journal of Multiphase Flow* 22, 703-712.

- Muzychka, Y.S., Yovanovich, M.M., 1998. Modeling friction factors in non-circular ducts for developing laminar flow. In: Proceeding of the Second AIAA Theoretical Fluid Mechanics Meeting, AIAA Paper 98-2492, Albuquerque, NM, 15-18 June 1998.
- Niu, H.N., Pan, L.W., Su, H.J., Wang, S.D., 2009a. Effects of design and operating parameters on CO₂ absorption in microchannel contactors. *Industrial & Engineering Chemistry Research* 48, 8629-8634.
- Niu, H.N., Pan, L.W., Su, H.J., Wang, S.D., 2009b. Flow pattern, pressure drop, and mass transfer in a gas-liquid concurrent two-phase flow microchannel reactor. *Industrial & Engineering Chemistry Research* 48, 1621-1628.
- O'Driscoll, C., 2004. Small is bountiful. *Chemistry World* 1, 1.
- Ong, C.L., Thome, J.R., 2011. Macro-to-microchannel transition in two-phase flow: Part 1 - Two-phase flow patterns and film thickness measurements. *Experimental Thermal and Fluid Science* 35, 37-47.
- Pamitran, A.S., Choi, K.I., Oh, J.T., Hrnjak, P., 2010. Characteristics of two-phase flow pattern transitions and pressure drop of five refrigerants in horizontal circular small tubes. *International Journal of Refrigeration* 33, 578-588.
- Pohorecki, R., Sobieszuk, P., Kula, K., Moniuk, W., Zielinski, M., Cyganski, P., Gawinski, P., 2008. Hydrodynamic regimes of gas-liquid flow in a microreactor channel. *Chemical Engineering Journal* 135, S185-S190.
- Qu, W., Mudawar, I., 2003. Measurement and prediction of pressure drop in two-phase micro-channel heat sinks. *International Journal of Heat and Mass Transfer* 46, 2737-2753.
- Rebrov, E.V., 2010. Two-phase flow regimes in microchannels. *Theoretical Foundations of Chemical Engineering* 44, 355-367.
- Rezkallah, K.S., 1996. Weber number based flow-pattern maps for liquid-gas flows at microgravity. *International Journal of Multiphase Flow* 22, 1265-1270.
- Roberge, D., Ducry, L., Bieler, N., Cretton, P., and Zimmermann, B., 2005. Microreactor technology: A revolution for the fine chemical and pharmaceutical industries? *Chemical Engineering Technology* 28, 318-323.
- Saisorn, S., Wongwises, S., 2010. The effects of channel diameter on flow pattern, void fraction and pressure drop of two-phase air-water flow in circular micro-channels. *Experimental Thermal and Fluid Science* 34, 454-462.
- Santos, R.M., Kawaji M., 2010. Numerical modeling and experimental investigation of gas-liquid slug formation in a microchannel T-junction. *International Journal of Multiphase Flow* 36, 314-323.

- Seris, E., Abroamowitz, G., Johnston, A., and Haynes, B., 2005. Demonstration plant for distributed production of hydrogen from steam reforming of methane. *Chemical engineering Research and Design* 86, 619-625.
- Shah, R.K., London, A.L., 1978. *Laminar Flow Forced Convection in Ducts*. Academic Press, New York.
- Shao, N., Gavriilidis, A., Angeli, P., 2009. Flow regimes for adiabatic gas-liquid flow in microchannels. *Chemical Engineering Science* 64, 2749-2761.
- Shao, N., Salman, W., Gavriilidis, A., Angeli, P., 2008. CFD simulation of the effect of inlet conditions on Taylor flow formation. *International Journal of Heat and Fluid Flow* 29, 1603-1611.
- Simmons, M.J., Wong, D.C.Y., Travers, P.J., Rothwell, J.S., 2003. Bubble behavior in three-phase capillary microreactors. *International Journal of Chemical Reactor Engineering* 1, A30.
- Su, H.J., Niu, H.N., Pan, L.W., Wang, S.D., Wang, A.J., Hu, Y.K., 2010. The characteristics of pressure drop in microchannels. *Industrial & Engineering Chemistry Research* 49, 3830-3839.
- Su, H., Wang, S., Niu, H., Pan, L., Wang, A., Hu, Y., 2010. Mass transfer characteristics of H₂S absorption from gaseous mixture into methyldiethanolamine solution in a T-junction microchannel. *Separation and Purification Technology* 72, 326-334.
- Suo, M., 1963. Two phase in capillary tubes. PhD. Thesis. Mechanical Engineering Department Massachusetts Institute of Technology.
- Suo, M., Griffith, P., 1964. Two-phase flow in capillary tubes. *Journal of Basic Engineering* 86, 576-582.
- Thulasidas, T.C., Abraham, M.A., Cerro, R.L., 1997. Flow patterns in liquid slugs during bubble-train flow inside capillaries. *Chemical Engineering Science* 52, 2947-2962.
- Tonkovicha, A.Y., Perrya, S., Wangb, Y., Qiua, D., LaPlantea, T., Rogersa, W.A., 2004. Microchannel process technology for compact methane steam reforming. *Chemical Engineering Science* 59, 4819-4824.
- Trachsel, F., Gunther, A., Khan, S., Jensen, K. F., 2005. Measurement of residence time distribution in microfluidic systems. *Chemical Engineering Science* 60, 5729-5737.
- Triplett, K.A., Ghiaasiaan, S.M., Abdel-Khalik, S.I., Sadowski, D.L., 1999. Gas-liquid two-phase flow in microchannels - Part I: two-phase flow patterns. *International Journal of Multiphase Flow* 25, 377-394.
- Tsoligkas, A.N., Simmons, M.J.H., Wood, J., 2006. Two phase gas-liquid reaction studies in a circular capillary. *Chemical Engineering Science* 62, 5397-5401.
- van Baten, J.M., Krishna, R., 2004. CFD simulation of mass transfer from Taylor bubbles rising in circular capillaries. *Chemical Engineering Science* 59, 2535-2545.
- Vandu, C.O., Liu, H., Krishna, R., 2005. Mass transfer from Taylor bubbles rising in single capillaries. *Chemical*

- Engineering Science 60, 6430-6437.
- Venkatesan, M., Das, S.K., Balakrishnan, A.R., 2010. Effects of tube diameter on two-phase flow patterns in mini tubes. *The Canadian Journal of Chemical Engineering* 88, 936-944.
- Völkel, N., 2009. Design and characterization of gas-liquid microreactors. PhD. Thesis, University of Toulouse, France.
- Waelchli, S., Rudolf von Rohr, P., 2006. Two-phase flow characteristics in gas-liquid microreactors. *International Journal of Multiphase Flow* 32, 791-806.
- Walsh, E., Muzychka, Y., Walsh, P., Egan, V., Punch, J., 2009. Pressure drop in two phase slug/bubble flows in mini scale capillaries. *International Journal of Multiphase flow* 25, 879-884.
- Wang, Y., Jun, J., Cao, C. and Mazanec, T. J., 2005. Microprocess technology for Fischer-Tropsch gas-to-liquids. *American Chemical Society Division of Petroleum Chemistry* 50, 69-70.
- Weinmueller, C., Hotz, N., Mueller, A., Poulikakos, D., 2009. On two-phase flow patterns and transition criteria in aqueous methanol and CO₂ mixtures in adiabatic, rectangular microchannels. *International Journal of Multiphase Flow* 35, 760-772.
- Wood, M., 2005. Compact reactor technology for gas processing. Paper presented at the microchannel heat exchangers work shop, Houston, TX, December 7.
- Yang, C.Y., Shieh, C.C., 2001. Flow pattern of air-water and two-phase R-134a in small circular tubes. *International Journal of Multiphase Flow* 27, 1163-1177.
- Yang, Z.C., Bi, Q.C., Liu, B., Huang, K.X., 2010. Nitrogen/non-Newtonian fluid two-phase upward flow in non-circular microchannels. *International Journal of Multiphase Flow* 36, 60-70.
- Yeong, K.K., Gavriilidis, A., Zapf, R., Hessel, V., 2004. Experimental studies of nitrobenzene hydrogenation in a microstructured falling film reactor. *Chemical Engineering Science* 59, 3491-3494.
- Yue, J., Chen, G., Yuan, Q., 2004. Pressure drops of single and two-phase flows through T-type microchannel mixers. *Chemical Engineering Journal* 102, 11-24.
- Yue, J., Chen, G., Yuan, Q., Luo, L., Gonthier, Y., 2007. Hydrodynamics and mass transfer characteristics in gas-liquid flow through a rectangular microchannel. *Chemical Engineering Science* 62, 2096-2108.
- Yue, J., Luo, L., Gonthier, Y., Chen, G., Yuan, Q., 2008. An experimental investigation of gas-liquid two-phase flow in single microchannel contactors. *Chemical Engineering Science* 63, 4189-4202.
- Yue, J., Luo, L., Gonthier, Y., Chen, G., Yuan, Q., 2009. An experimental study of air-water Taylor flow and mass transfer inside square microchannels. *Chemical Engineering Science* 64, 3697-3708.

Zhang, P., Fu, X., 2009. Two-phase flow characteristics of liquid nitrogen in vertically upward 0.5 and 1.0 mm micro-tubes: Visualization studies. *Cryogenics* 49, 565-575.

Zhang, W., Hibiki, T., Mishima, K., 2010. Correlations of two-phase frictional pressure drop and void fraction in mini-channel. *International Journal of Heat and Mass Transfer* 53, 453-465.

Zhao, T.S., Bi, Q.C., 2001. Co-current air-water two-phase flow patterns in vertical triangular microchannels. *International Journal of Multiphase Flow* 27, 765-782.

Zhao, L., Rezkallah, K.S., 1993. Gas-liquid flow patterns at microgravity conditions. *International Journal of Multiphase Flow* 19, 751-763.

CHAPTER 2: GAS-LIQUID FLOW PATTERNS IN CIRCULAR MICROCHANNELS

This chapter is mainly concerned with gas-liquid two phase flow patterns in horizontal circular microchannels. In this chapter, Nitrogen-water two-phase flow in three horizontal circular microchannels ($d_i = 302 \mu\text{m}$, $496 \mu\text{m}$ and $916 \mu\text{m}$, respectively) have been experimentally investigated. The flow patterns and flow pattern maps will be exhibited and compared to investigate the effects of channel size on the flow patterns and their transition. In addition, the influences of liquid physical properties, i.e. surface tension and viscosity on gas-liquid flow patterns in circular microchannel ($d_i = 496 \mu\text{m}$) will also be discussed. The results obtained will be compared to appropriate transition models in literature. Finally, transition criteria based on the present experimental data will be proposed with the aim of attaining fundamental understanding of the transport phenomena of gas-liquid processes.

2.1 Experimental set-up

2.1.1 Test rig

As shown in Figure 2-1, the experimental setup constructed for this study is composed of a test section, gas and liquid circuits and the data acquisition system. Precise pumps were used to control the liquid flow in the microchannel. The pulse of the pump was maximally reduced by installation of a back-pressure regulator and two buffer tanks, so that constant flow rate and steady flow in the microchannel could be achieved. The temperature of liquid was maintained constant at 25°C for all the tests by using a water bath. Flow rate of gas was controlled and adjusted by mass flow controllers. A Y type junction connected with the downstream microchannel was prepared for the pre-contact of gas and liquid. To visualize and record the two-phase flow patterns in the microchannels, a high speed camera was installed at a side of the test channel, with background illumination provided by two homemade LED lamps installed at the opposite side.

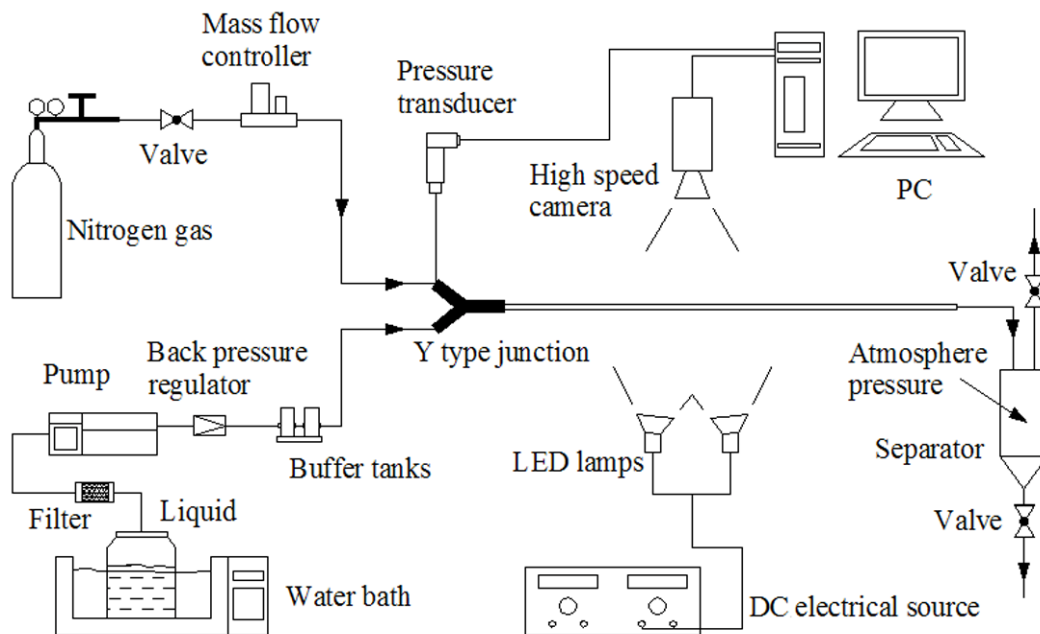


Figure 2-1: Schematic representation of the experimental setup

2.1.2 Test section

Three microchannels with different diameters (302 μm , 496 μm , and 916 μm) have been used, all of them having circular cross-section and the same length (10 cm). For convenience of visualization, these microchannels were made of quartz glass, and fabricated through precise hot-stretching by “Verre et Séparation Technologies S.A.”, Lyon, France. The Y junction through which gas and liquid were fed to the main microchannel was made of Plexiglas. The microchannel was glued carefully with the Y junction to ensure the smooth connection between them, as shown in Figure 2-2.

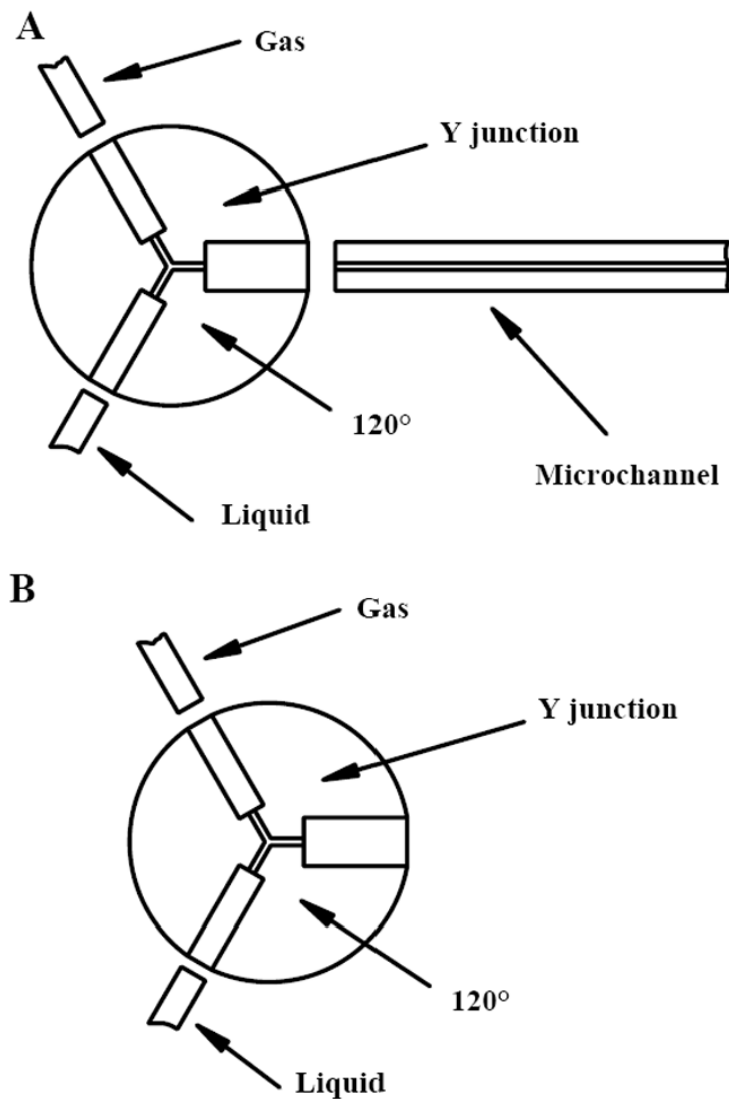


Figure 2-2: Detail of the test section. (A) TC I; (B) TC II

Table 2-1: The physical properties of working fluids and rheological parameters of the CMC solutions

Fluids	Molecular formula	Molecular weight	Concentration (wt%)	Density (kg/m ³) _{25°C}	Viscosity (mPa·s) _{25°C}	Surface tension (mN/m) _{25°C}	Rheological parameter	
							<i>k</i>	<i>n</i>
Nitrogen	N ₂	28	-	1.25	0.018	-	0.018	1
Demineralized Water	H ₂ O	18	-	997	0.89	72.0	0.89	1
Ethanol	C ₂ H ₅ OH	46	-	789	1.11	21.5	1.11	1
Aqueous solution of SDS	NaC ₁₂ H ₂₅ SO ₄	288	0.0608	998	0.89	49.8	0.89	1
			0.2610	1000	0.90	39.6	0.90	1
Aqueous solution of CMC	(NaC ₈ H ₁₁ O ₇) _m	90000	0.0464	998	1.27- 1.76	72.0	0.0025	0.93
			0.1262	998	2.02 – 2.88	72.1	0.0042	0.92
			0.2446	1000	2.61 – 3.87	72.2	0.0059	0.91

2.1.3 Working fluids

One of the objectives of the present study is to investigate the effects of the liquid physical properties on the gas-liquid flow patterns in microchannel. Therefore, demineralized water, ethanol and a series of aqueous solution of CMC (Sodium carboxymethyl cellulose) and SDS (Sodium dodecyl sulfate) were employed in the tests. Nitrogen was selected as gas phase in all the tests for its good stability. The physical properties of liquids used and the rheological parameters of the CMC solutions are listed in Table 2-1.

CMC was selected as thickener, for that low CMC concentration would change the liquid viscosity significantly, keeping other physical properties almost constant. SDS was chosen as surfactant to vary the surface tension of the liquid phase, while keeping other physical properties constant at very low concentration. Three CMC solutions (0.0464%, 0.1262%, and 0.2446% CMC) and two SDS solutions (0.0608% and 0.2610% SDS) have thus been employed as liquid flow phase, whereas demineralized water and ethanol of which the surface tension is just one third of water's, were also used as reference case.

In fact, the aqueous solution of CMC is a type of non-Newtonian liquid, of which the viscosity changes with the shear rate. The rheological characteristics can be described in the form of power-law equation (Barnes, 2000; Yang et al., 2010):

$$\tau = k(\dot{\gamma})^n \quad \text{and} \quad \mu = k(\dot{\gamma})^{n-1} \quad (2.1)$$

where τ is the shear stress, μ the viscosity, $\dot{\gamma}$ the shear rate. k and n are the consistency coefficient and the power-law index, respectively. In the present work, the effective viscosity values were obtained by measuring the pressure drop of non-Newtonian fluids single flow according to the velocity in the circular microchannel (Barnes, 2000), which can be expressed as:

$$\Delta P = \frac{2kL}{r_0} \left(Q \cdot \frac{3 + \frac{1}{n}}{\pi r_0^3} \right)^n \quad (2.2)$$

In which, Q is the volumetric flow-rate, r_0 the radii and L the length of the microchannel.

The liquid velocity is defined as

$$U_L = \frac{Q}{\pi r_0^2} \quad (2.3)$$

For certain non-Newtonian fluid whose k and n are constant when temperature is invariable, we defined the parameter k' as:

$$k' = \frac{2kL}{r_0^{n+1}} \cdot \left(3 + \frac{1}{n}\right)^n = \frac{4kL}{d_i^{n+1}} \cdot \left(6 + \frac{2}{n}\right)^n \quad (2.4)$$

Combining Eqs. 2.2-2.4, we obtain:

$$\Delta P = k' U_L^n \quad (2.5)$$

In this work, k' and n could be obtained through a least square regression of the experimental data, and then the k was obtained from Eq. 2.4.

2.1.4 Parameters measurement and uncertainty analysis

The flow-rates of gas and liquid and absolute pressure at the inlet of gas flow were measured. Gas flow-rate was controlled by a mass flow controller (AALBORG GFC17 or BROOKS SLA5850S1). The experimental range is 0.3 - 500 mL/min, corresponding to a U_{GS} from 0.028 to 74.5 m/s. Liquid flow-rate was controlled by a precise pump (ELDEX 2HM or SHIMADZU LC-20AD). The experimental range is 0.1 – 32.6 mL/min, corresponding to a U_{LS} from 0.008 to 2.77 m/s. The ranges of U_{GS} and U_{LS} were as large as possible to observe more flow pattern transitions and to give more information about the hydrodynamic characteristics in microchannel.

To measure the pressure drop in the microchannel, a pressure transducer (KELLER PR 21s) was installed on the gas flow side at the inlet of Y type junction. The pressure at the outlet of the microchannel was atmosphere pressure. To eliminate the effects of inlet and outlet, experiments were also implemented in the TC II(Figure 2-2B) under the same experimental conditions. The data redaction of pressure drop followed the method described in detail in references (Yue et al., 2008, 2009).

Gas-liquid flow patterns were visualized and recorded by a fast camera (Fastcam, PCI

R2). The camera lens used in the experiments was PENTAX 25mm F/1.4 coupled with a 10 mm extension loop. The CCD camera was operated at a frame rate of 500 fps and a shutter speed of 1/70000s, and it was connected to a personal computer via a special software interface (Photron FASTCAM Viewer) for storing image information. Details about the instruments and their ranges and precisions are presented in Table 2-2.

Table 2-2: Range and precision of experimental instruments

Parameter	Device	Range	Unit	Precision
Liquid flow rate	ELDEX 2HM pump	0-40	mL/min	1%
	SHIMADZU LC-20AD pump	0-10		1%
	AALBORG GFC17 mass flow controller	0-10		0.5% full scale
Gas flow rate	BROOKS SLA5850S1 mass flow controller	0-500	mL/min	0.2% full scale
Pressure transducer	KELLER PR 21s pressure transducer	0-500	kPa	0.5% full scale
Viscosity	PROLABO-PARIS falling ball viscometer	-	-	1%
Surface tension	PROLABO-PARIS LECOMTE du NOUY Tensiometer	0-140	mN/m	1% full scale
Camera	Fastcam, PCI R2 high speed camera	-	-	-

For convenience of comparison, all the tests were carried out at 25 °C to avoid the variation of fluid physical properties with temperature. For each measurement, it took about 10 to 20 minutes for the stabilization of two-phase flow. Good reproductivity was observed (less than $\pm 5\%$ variation). Table 2-3 gives the working conditions of the present study.

In the present work, the measurement errors have been analyzed following the method proposed by Wahlin et al. (2005). The calculated parameters may be expressed by:

$$U_{G,L} = \frac{4Q_{G,L}}{\pi d_i^2} \quad (2.6)$$

$$\text{Re}_{G,L} = \frac{4Q_{G,L}\rho_{G,L}}{\mu_{G,L}\pi d_i} \quad (2.7)$$

$$\text{We}_{G,L} = \frac{16Q_{G,L}^2\rho_{G,L}}{\pi^2 d_i^3 \sigma} \quad (2.8)$$

Therefore, the relative uncertainties of the gas and liquid superficial velocities, Re numbers and We numbers may be estimated by following expressions:

$$\frac{\Delta U_{G,L}}{U_{G,L}} = \sqrt{\left(\frac{\Delta Q_{G,L}}{Q_{G,L}}\right)^2 + \left(2\frac{\Delta d_i}{d_i}\right)^2} \quad (2.9)$$

$$\frac{\Delta \text{Re}_{G,L}}{\text{Re}_{G,L}} = \sqrt{\left(\frac{\Delta Q_{G,L}}{Q_{G,L}}\right)^2 + \left(\frac{\Delta d_i}{d_i}\right)^2 + \left(\frac{\Delta \rho_{G,L}}{\rho_{G,L}}\right)^2 + \left(\frac{\Delta \mu_{G,L}}{\mu_{G,L}}\right)^2} \quad (2.10)$$

$$\frac{\Delta \text{We}_{G,L}}{\text{We}_{G,L}} = \sqrt{\left(2\frac{\Delta Q_{G,L}}{Q_{G,L}}\right)^2 + \left(3\frac{\Delta d_i}{d_i}\right)^2 + \left(\frac{\Delta \rho_{G,L}}{\rho_{G,L}}\right)^2 + \left(\frac{\Delta \sigma}{\sigma}\right)^2} \quad (2.11)$$

The calculation indicates the uncertainty of 1.7% for the flow velocity, 1.9% for Reynolds number and 3.2% for the Weber number. 2.21% for Capillary number can be also obtained following this method. It should be claimed that the uncertainty of liquid properties depends on the measured accuracy of temperature; the correlations to describe them and the uncertainty of channel diameter depend on the measuring method. Here, the uncertainty of gas and liquid physical properties was assumed to be 1%, and 2 μm for Δd_i in this paper in acceptable extent.

Table 2-3: Experimental conditions

Parameters	Ranges
	302
Channel inner diameter, d_i (μm)	496 916
Temperature, ($^{\circ}\text{C}$)	25
Pressure drop (kPa)	1 – 399
Liquid superficial velocity, U_{LS} (m/s)	0.008 - 2.8
Gas superficial velocity, U_{GS} (m/s)	0.028 – 74.5
Liquid Reynolds number, Re_L	0.84 - 1558
Gas Reynolds number, Re_G	0.98 - 1510
Liquid Weber number, We_L	3.1×10^{-4} - 50.5
Gas Weber number, We_G	5.4×10^{-6} - 33.6

2.2 Flow patterns and flow regime maps in horizontal circular microchannel with a Y junction

2.2.1 Nitrogen-water flow – Influence of channel size

The hydrodynamic characteristics of Nitrogen-water flow have been investigated in three circular microchannels. The typical gas-liquid flow patterns which were generally reported in the existing literature, i.e. bubbly flow, slug flow, churn flow and annular flow, were also observed, as shown in Figures 2-3A-C.

In microchannel, *bubbly flow* is characterized by shell bubbles dispersed in the continuous liquid phase, of which the shape is often distorted spherical because of high liquid velocity, and the axial length is generally smaller than the channel diameter (Shao et al., 2009; Triplett et al., 1999). As shown in Figures 2-3A(a), B(a), C(a), bubbly flow occurs at relatively high U_{LS} and very low U_{GS} . Dispersed bubbly flow, which characterized by the gas phase dispersed in cluster of bubbles scattering in continuous liquid phase and the bubbles size is much smaller than the channel diameter (Yang et al., 2010), was not observed, due to relatively small channel size and U_{LS} . When the ratio U_{GS}/U_{LS} increases, the bubble size grows up and reaches the channel diameter, and the axial length extend gradually. Eventually slug flow develops.

Slug flow is also known as Taylor flow, plug, segmented, intermittent, bubble-train or elongated flow (Shao et al., 2009). It is characterized by elongated gas bubbles (gas slug) with axial length larger than the channel diameter and separated by the liquid slugs in the axial direction, and usually the lengths of gas slug and liquid slug are constant. When the U_{LS} is relatively low, the gas slugs have regular shapes including smooth body and near-spherical nose and tail (Figs 2-3A(b), B(b)). When U_{LS} and U_{GS} increase, the shape of gas slugs deforms like bullet with flattened tail and projecting nose (Figure 2-3B(c), C(b)).

With increasing U_{GS} at relatively low U_{LS} , the gas slugs are elongated and merge due to the increasing mixture volumetric flux, and *slug-annular flow* (Figure 2-3A(c), B(e), C(e)) is established, also called Taylor-annular flow (Shao et al., 2009) or wavy-annular flow

(Coleman and Garimella, 1999). In this flow pattern, gas core is surrounded by a liquid film in which large-amplitude solitary waves appear frequently. Slug-annular flow looks like that the gas flow just break through the liquid slug or the waves do not grow sufficiently to block the channel. With further increasing U_{GS} , the large-amplitude solitary waves gradually disappear and annular flow is formed.

Generally, *annular flow* occurs at excessively high U_{GS} and relatively low U_{LS} . Continuous gas flowing through the channel center is surrounded by continuous ring shape liquid film along the channel wall (Figure 2-3A(d), B(f)) (Triplett et al., 1999). In non-circular channels, the liquid phase is concentrated at the corners (Shao et al., 2009; Zhao and Bi, 2001).

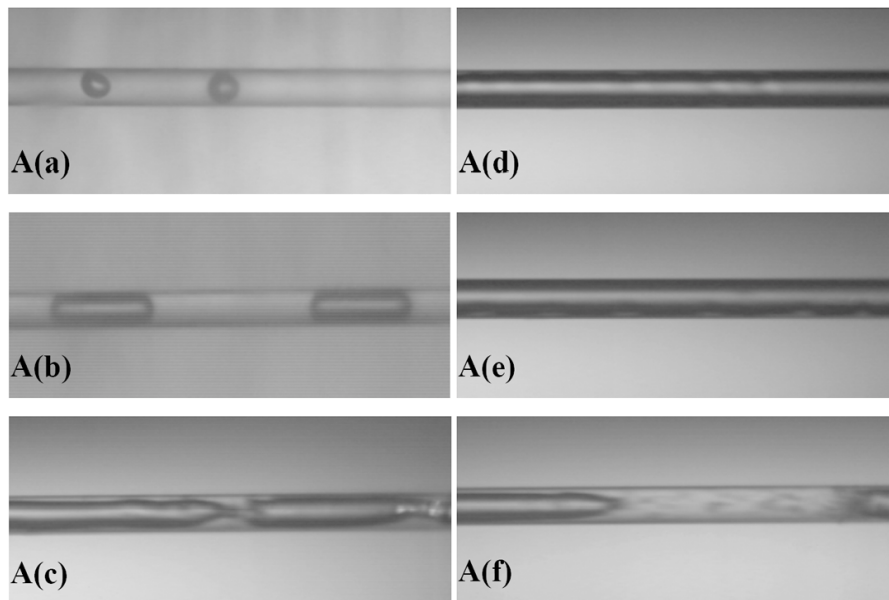
At high U_{GS} and U_{LS} , *churn flow* is formed in the channel, which is generally considered as a transitional flow pattern between slug flow and inertia dominated dispersed flow (Shao et al., 2009). This flow pattern is generally in two forms, with very chaotic structure. One form is unstable gas slugs leading to the disruption in their trailing ends and dispersion of tiny gas bubbles into the liquid phase (Figure 2-3A(f), B(h)). The other is that liquid film is disturbed at high U_{GS} and small liquid drops appear in the gas core (Figure 2-3C(h)).


Under our experimental conditions, *dispersed flow* characterized by small liquid droplets dispersed in gas core and liquid film lost the contact with channel wall, was not observed in these channels. Indeed, it is reported that dispersed flow is rarely observed in microchannels with hydraulic diameter smaller than 1 mm (Shao et al., 2009).

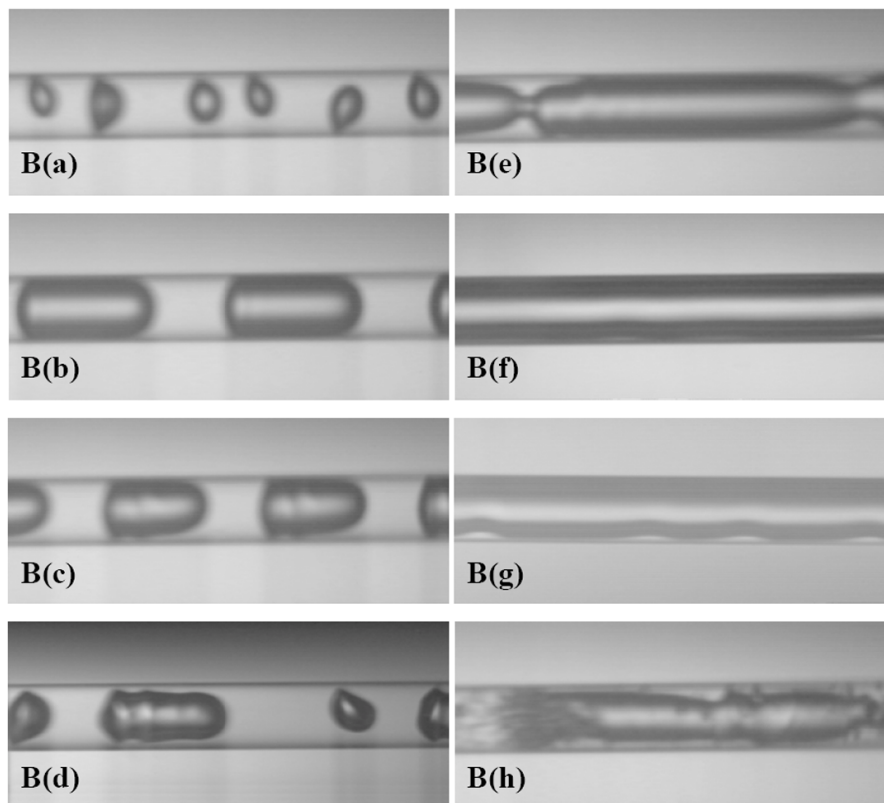
Meanwhile, two transitional flow patterns, namely *slug-bubbly flow* and *unstable slug flow* were observed. Slug-bubbly flow characterized by most of gas slugs followed by one or more gas bubbles is considered as a transitional pattern from bubbly flow to slug or to unstable slug flow with increasing U_{GS} at relatively high U_{LS} , as shown in Figures 2-3B(d) and C(c). The unstable slug flow characterized by variable gas and liquid slug length, even sometimes two or more gas bubbles merge to form bubble-train slug (Chen et al., 2002) or even with a segment of slug-annular flow, is considered as a transitional flow pattern between slug and slug-annular flow or churn flow, as shown is Figure 2-3C(d).


Another flow pattern rarely reported, namely the *wavy flow*, was also observed. Instead of a continuous liquid film, the liquid exits just in one side of the channel, and form unstable

wavy at gas-liquid interface due to very high U_{GS} , as shown in Figures 2-3A(e) and B(g). Barajas and Panton (1993) considered that this flow pattern is related to the wetting properties or contact angle between the liquid and channel wall, channel contamination and amount of liquid in presence.



Flow direction: 



Flow direction: 

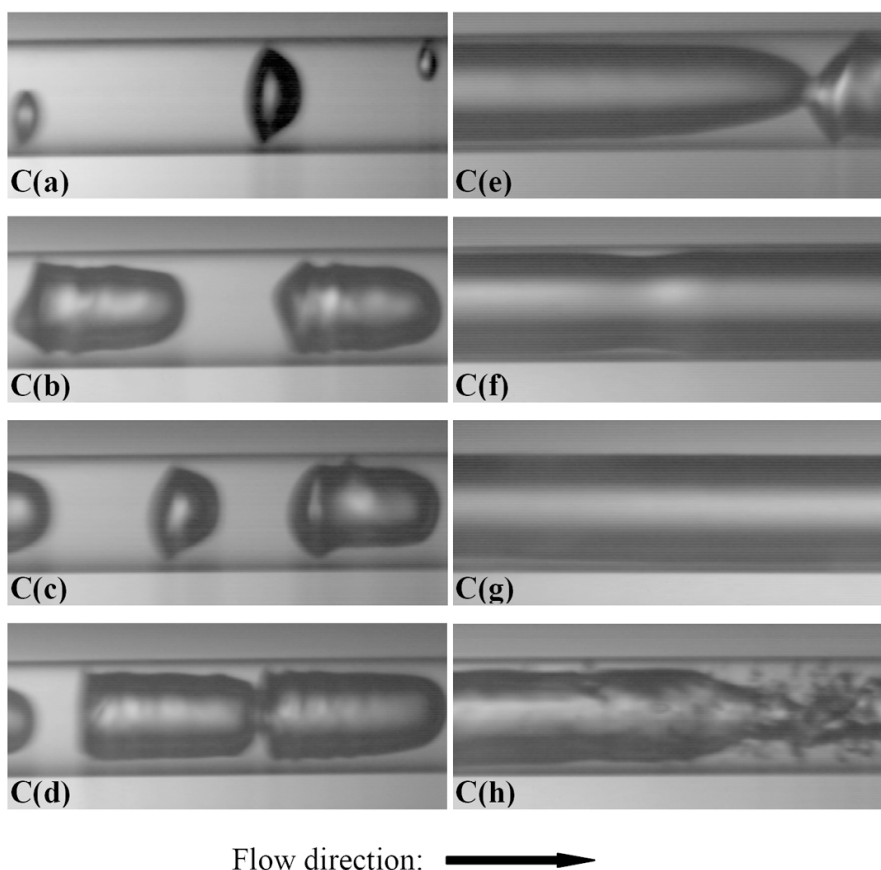


Figure 2-3: Representative flow patterns of Nitrogen-water horizontal flow in the circular microchannels. (A): $d_i = 302 \mu\text{m}$; (a) bubbly flow ($U_{LS} = 1.973 \text{ m/s}$, $U_{GS} = 0.076 \text{ m/s}$); (b) slug flow ($U_{LS} = 0.212 \text{ m/s}$, $U_{GS} = 0.127 \text{ m/s}$); (c) slug-annular flow ($U_{LS} = 0.212 \text{ m/s}$, $U_{GS} = 15.99 \text{ m/s}$); (d) annular flow ($U_{LS} = 0.069 \text{ m/s}$, $U_{GS} = 74.45 \text{ m/s}$); (e) wavy flow ($U_{LS} = 0.023 \text{ m/s}$, $U_{GS} = 74.48 \text{ m/s}$); (f) churn flow ($U_{LS} = 1.152 \text{ m/s}$, $U_{GS} = 21.32 \text{ m/s}$). (B): $d_i = 496 \mu\text{m}$; (a) bubbly flow ($U_{LS} = 2.024 \text{ m/s}$, $U_{GS} = 0.028 \text{ m/s}$); (b) smooth slug ($U_{LS} = 0.065 \text{ m/s}$, $U_{GS} = 0.094 \text{ m/s}$); (c) slug flow ($U_{LS} = 0.698 \text{ m/s}$, $U_{GS} = 1.042 \text{ m/s}$); (d) slug-bubbly flow ($U_{LS} = 0.951 \text{ m/s}$, $U_{GS} = 0.659 \text{ m/s}$); (e) slug-annular flow ($U_{LS} = 0.065 \text{ m/s}$, $U_{GS} = 5.176 \text{ m/s}$); (f) annular flow ($U_{LS} = 0.048 \text{ m/s}$, $U_{GS} = 46.95 \text{ m/s}$); (g) wavy flow ($U_{LS} = 0.026 \text{ m/s}$, $U_{GS} = 46.92 \text{ m/s}$); (h) churn flow ($U_{LS} = 2.024 \text{ m/s}$, $U_{GS} = 9.401 \text{ m/s}$). (C) $d_i = 916 \mu\text{m}$; (a) bubbly flow ($U_{LS} = 1.101 \text{ m/s}$, $U_{GS} = 0.028 \text{ m/s}$); (b) slug flow ($U_{LS} = 0.555 \text{ m/s}$, $U_{GS} = 0.553 \text{ m/s}$); (c) slug-bubbly flow ($U_{LS} = 1.101 \text{ m/s}$, $U_{GS} = 0.444 \text{ m/s}$); (d) unstable slug flow ($U_{LS} = 1.201 \text{ m/s}$, $U_{GS} = 1.103 \text{ m/s}$); (e) slug-annular flow ($U_{LS} = 0.050 \text{ m/s}$, $U_{GS} = 3.311 \text{ m/s}$); (f) annular flow ($U_{LS} = 0.020 \text{ m/s}$, $U_{GS} = 13.76 \text{ m/s}$); (g) wavy flow ($U_{LS} = 0.005 \text{ m/s}$, $U_{GS} = 3.310 \text{ m/s}$); (h) churn flow ($U_{LS} = 1.101 \text{ m/s}$, $U_{GS} = 11.02 \text{ m/s}$)

Figure 2-4 indicates the influence of channel size on the two-phase flow regime maps in microchannel. It can be observed that the regions of slug and unstable slug flow become wider when channel size decreases. Later transitions occur from slug to churn, to slug-annular and to bubbly flow. This trend may be explained in three aspects. Firstly, the smaller the channel size is, the more difficult to form bubbly flow due to more energy needed to disperse the gas phase in gas bubbles with smaller volume. Secondly, the liquid slug is more difficult to break through due to the high surface tension, which is dominant in smaller channels. Thirdly, churn flow is generally considered as a chaotic flow, which appears under higher Reynolds number conditions. Therefore, the smaller the channel is, the higher values of gas and liquid velocities are required for the transition from slug flow to churn flow. This tendency is also reported by Akbar et al. (2003), who divided two-phase flow regime into four parts, i.e. surface tension-dominated region (bubbly, slug flow), inertia-dominated region 1 (slug-annular and annular flow), inertia-dominated region 2 (dispersed flow) and transition zone. The effect of surface tension on two phase flow increases with the decreasing of channel size, and that leads to the larger region of surface tension-dominated flow.

Wavy flow is observed for all three channels, and its region becomes wider with increasing channel size. In our tests, the liquid film in the horizontal microchannel was asymmetry due to the gravity effect, i.e. the liquid film near the upside of the channel was thinner than that of downside. this asymmetry increases with increasing channel size (Li and Wang, 2003).

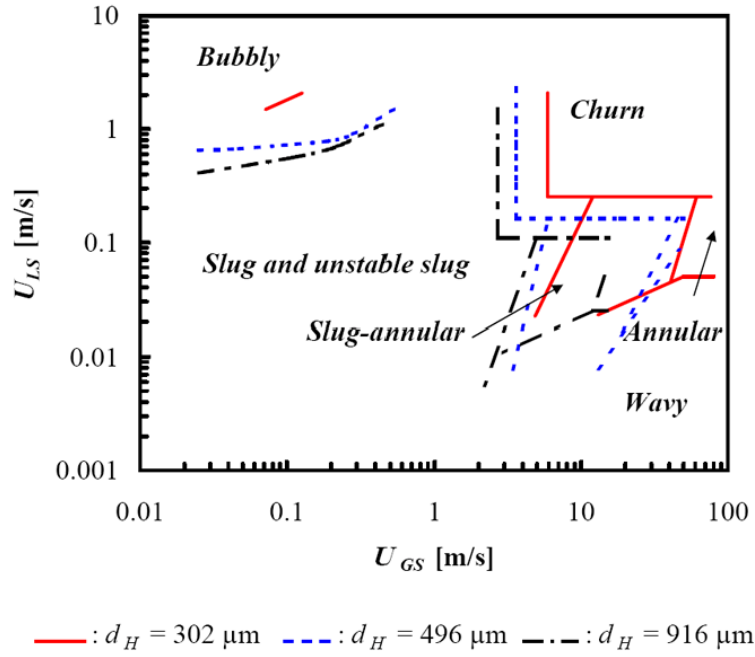


Figure 2-4: Comparison of flow regime maps of Nitrogen-water horizontal flow in circular microchannels with different diameters

2.2.2 Nitrogen-CMC solution horizontal flow in circular microchannel – influence of viscosity

Three solutions with different CMC concentrations (0.0464%, 0.1262%, and 0.2446%) were employed to study the influence of liquid viscosity on the gas-liquid flow patterns in microchannel with diameter of 496 μm .

According to Spisak (1986), the effective viscosity of non-Newtonian liquid flow can be described in a laminar flow as follow:

$$\mu_{\text{eff}} = k \left(\frac{8U_{LS}}{d_H} \right)^{n-1} \quad (2.12)$$

Where k and n are the rheological parameters listed in the Table 2-1. Therefore the effective viscosity values of working liquid can be obtained, as indicated in Figure 2-5.

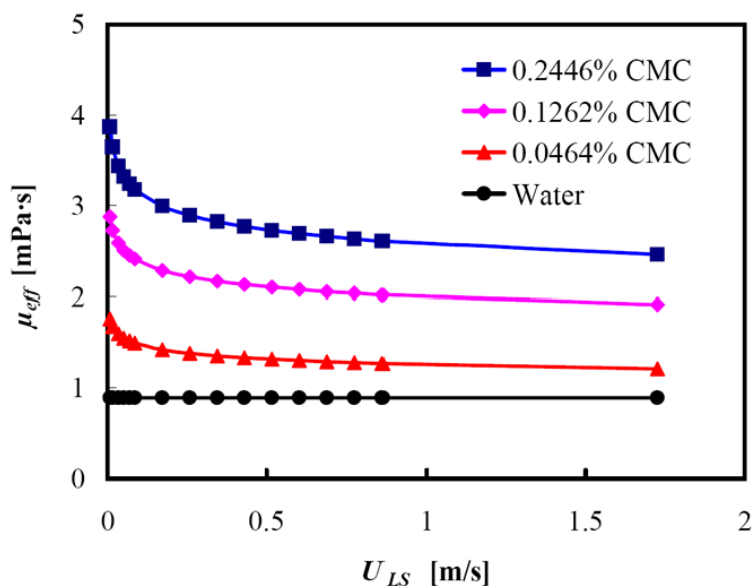


Figure 2-5: The effective viscosity of CMC solution and water as a function of liquid superficial velocity

Typical flow patterns, i.e. bubbly flow, slug flow, slug-annular flow, annular flow and churn flow, were observed whereas slug-bubbly flow, capillary bubbly flow and dispersed flow did not appear. In particular, wavy flow has not been observed for 0.2446% CMC solution. It was also found that some detail characteristics are different with respect to Nitrogen-water system in the same microchannel. For example, with increasing CMC concentration, the thickness of liquid film of slug-annular flow increases. This is due to the higher liquid viscosity, for that when gas flow breaks through the liquid slug, more driving force is needed and thicker liquid film will be formed at the same U_{GS} .

Figure 2-6 shows the influence of the liquid viscosity on the gas-liquid flow regime maps. For all these working liquids, the transition from slug to bubbly flow occurs at almost the same U_{GS} and U_{LS} , implying that the liquid viscosity does not have much influence on this transition.

It should be noted that the increasing liquid viscosity leads to lower value of Re_L , which in turn causes the transitions from slug-annular or annular to churn flow occurring at higher U_{LS} . One may also observe the later transitions from slug to slug-annular or to churn flow at higher U_{LS} , because that higher U_{GS} lead to the increase of actual U_L in the microchannel.

In the present work, with increasing liquid viscosity, the region of wavy flow reduces or even disappears under high liquid viscosity condition (0.2446% CMC solution). It is the wavy flow, with high U_{GS} and very little amount of liquid in presence, occurs when the thickness of liquid film decreases below a certain limit. And the thickness of liquid film is considered to increase with the liquid viscosity and to decrease with surface tension under the same U_{LS} and U_{GS} (Bretherton, 1961). Therefore, the higher the liquid viscosity is, the smaller the wavy flow region becomes.

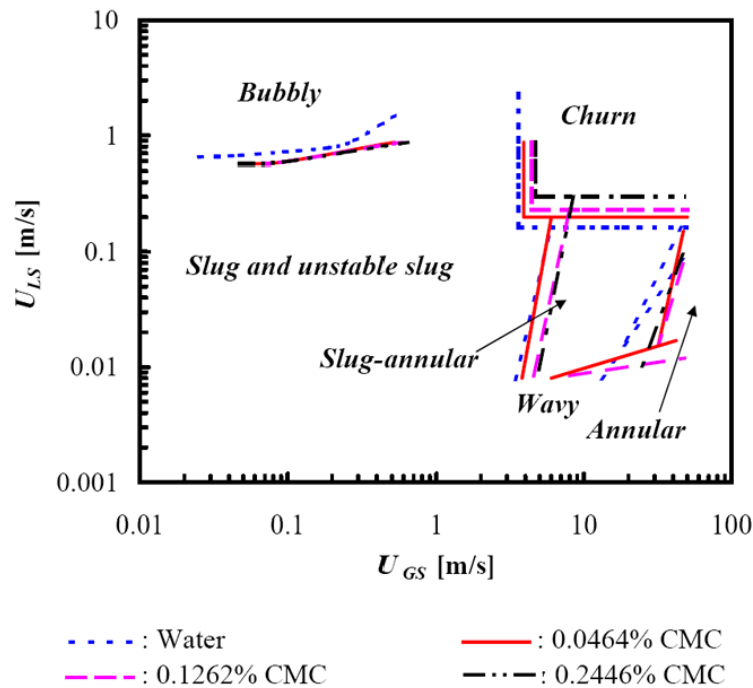


Figure 2-6: Comparison of two-phase horizontal flow regime maps in circular microchannels ($d_i = 496 \mu\text{m}$) with different liquid viscosity

2.2.3 Nitrogen-SDS solution and Nitrogen-ethanol horizontal flow in circular microchannel – influence of surface tension

Two SDS solutions with different concentrations and ethanol were used as working liquid in this study. For the Nitrogen-SDS solution flow, typical flow patterns such as bubbly flow, slug flow, wavy flow and churn flow could be identified. In addition, some distinct flow patterns that were not observed in other two-phase systems, i.e. *foam-slug* (Figure 2-7(a)), *foam-slug-annular* (Figure 2-7(b)) and *foam annular* (Figure 2-7(c)) were observed.

Foam-slug flow is similar to slug flow, but contains foams in both liquid and gas slugs. Similarly, foams occur in liquid film and gas body in slug-annular flow, thus forming the foam-slug-annular flow. With increasing U_{GS} , foam-annular flow is developed. In this flow pattern, foams exist in the gas core but not present in the liquid film. Churn flow is formed in the channel at relatively high U_{GS} and U_{LS} . Unlike other two-phase systems, in which one phase disperses into another phase body because of high inertia, a lot of foam occurs in liquid body and gas core, as well as at gas-liquid interface. At relative high U_{GS} ($U_{LS} > 3\text{m/s}$), the foams hold the entire liquid slug, and much higher pressure drops are measured, three times higher with respect to Nitrogen-water two-phase system under same working conditions.

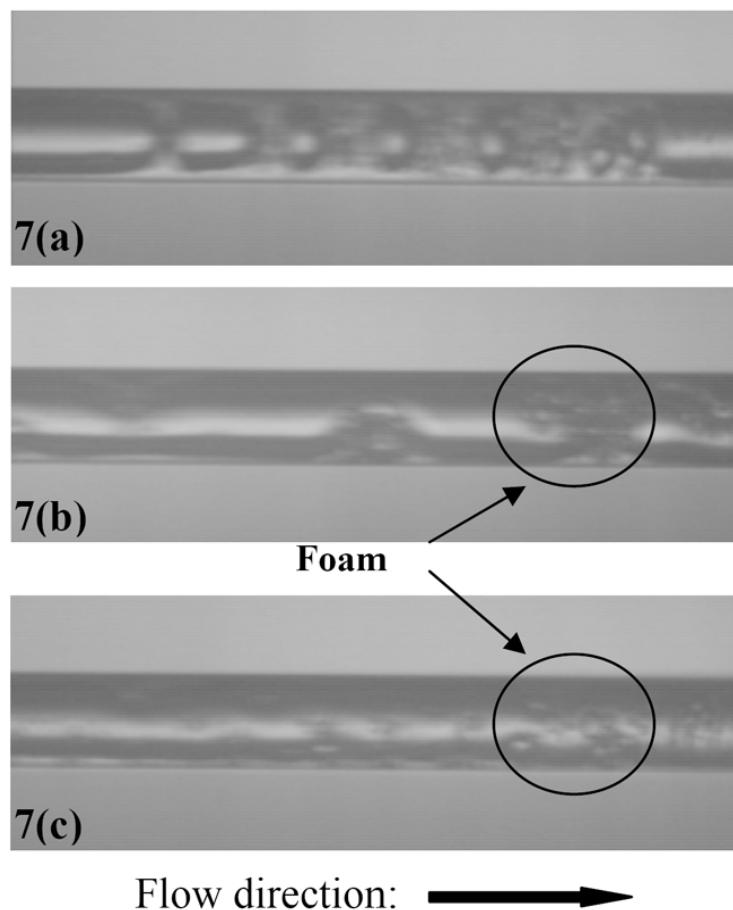


Figure 2-7: Foam flow patterns of Nitrogen-SDS solution (0.2610% SDS) horizontal flow in the circular microchannel ($d_i = 496\mu\text{m}$): (a) foam-slug flow ($U_{LS} = 0.086\text{ m/s}$, $U_{GS} = 3.103\text{ m/s}$); (b) foam-slug-annular flow ($U_{LS} = 0.051\text{ m/s}$, $U_{GS} = 4.228\text{ m/s}$); (c) foam-annular flow ($U_{LS} = 0.034\text{ m/s}$, $U_{GS} = 28.18\text{ m/s}$)

It is known that the surfactant, especially anionic surfactant such as SDS is usually a foaming agent. The SDS molecule, like all the other anionic surfactant molecules, has hydrophilic head and hydrophobic tail, and they will migrate to the liquid surface to minimize the surface potential energy of the system by accumulating at the liquid-gas interface. This effect activates the formation of foams and the force of repulsion between the ionized molecular head and tail can keep the foam stable (Rosen, 2004). For the slug-annular, annular and churn flow, the gas-liquid interface is very large but unstable due to the high gas velocities. Therefore, stable foams are formed in the Nitrogen-SDS solution flow. This phenomenon may be useful for chemical process in which large gas-liquid interface is needed, such as gas absorption or gas-liquid reaction.

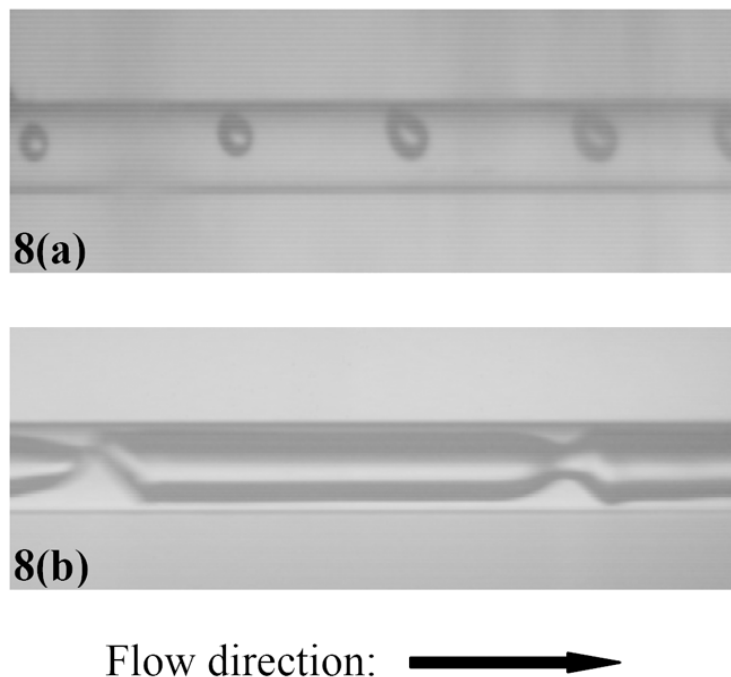


Figure 2-8: Two representative flow patterns of Nitrogen-ethanol horizontal flow with different details compared to Nitrogen-water flow in the circular microchannel ($d_i = 496\mu\text{m}$): (a) bubbly flow ($U_{LS} = 0.866 \text{ m/s}$, $U_{GS} = 0.049 \text{ m/s}$); (b) slug-annular flow ($U_{LS} = 0.069 \text{ m/s}$, $U_{GS} = 2.067 \text{ m/s}$)

Typical flow patterns were also observed in the Nitrogen-ethanol system. However,

detail features of flow patterns may be different from Nitrogen-water system. For example, the gas bubbles deviate from the centre of the microchannel, and closer to the upper side of the channel (Figure 2-8(a)), which may be related to the buoyancy of the gas bubbles and the decrease of the liquid surface tension. More asymmetry was observed in slug-annular flow (Figure 2-8(b)) (Li and Wang, 2003). In addition, slug-bubbly flow and wavy flow were not observed.

Figure 2-9 displays the comparison of two-phase flow regime maps for working fluids having different surface tensions.

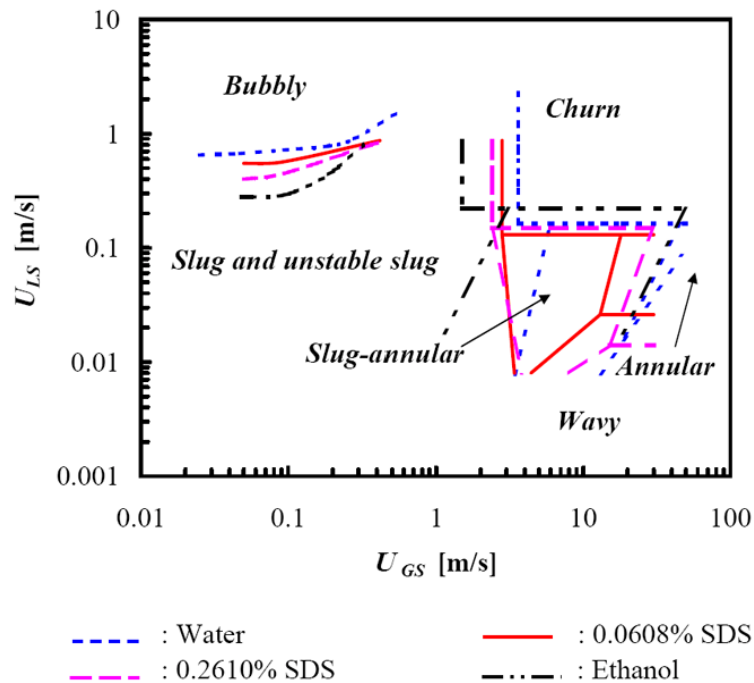


Figure 2-9: Comparison of two-phase horizontal flow regime maps in circular microchannels ($d_i = 496\mu\text{m}$) with different surface tension

In spite of the disturbance caused by the presence of foams, it is obvious that the regions of slug and unstable slug flow reduce with decreasing surface tension. The bubbly flow is easier to form at lower surface tension since the surface energy needed to form and elongate small gas bubbles decreases. The earlier transition from slug to slug-annular flow is mainly because that the liquid phase is easier to break through because of the decreasing surface tension. Earlier transition from slug to churn flow occurs at lower surface tension. However,

for the transitions between slug, slug-annular and churn flow, the influence of surface tension can not be well identified due to the disturbance of foams. Wavy flow region also reduces with decreasing surface tension, even not observed in ethanol case. According to Bretherton (1961), the liquid film thickness increases with decreasing surface tension, therefore wavy flow region is smaller when surface tension is lower. These observations correspond well to the “zone divisions” proposed by Akbar et al. (2003).

2.3 Comparison with existing flow regime maps and available transition criteria

2.3.1 Comparison with existing flow regime maps

The flow pattern maps of the nitrogen-water system are compared with three existing flow regime maps, i.e. that of Triplett et al. (1999), of Yang and Shieh (2001) and of Hassan et al. (2005). These three flow pattern maps are selected because they are all based on the systematic experiments of two-phase horizontal flow in microchannels, which are close to the present work. In experiments of Triplett, air and water were used as working fluids, and the test channel was circular with $d_i = 1.097$ mm. As shown in Figure 2-10(A), the regime map of Triplett agrees well with ours for the regions of bubbly, slug and annular flow, with the exception for the transition from slug-annular and annular to churn flow. This difference may be caused by different experimental conditions, such as temperature, or by the differences in gas liquid inlet conditions, channel diameter and fabrication. Good agreement was also found in comparison with Hassan’s flow map (Figure 2-10(C)). However, it can be noted from Figure 2-10(B) that the Flow regime map of Yang and Shieh (2001) does not correspond well with the present regime maps.

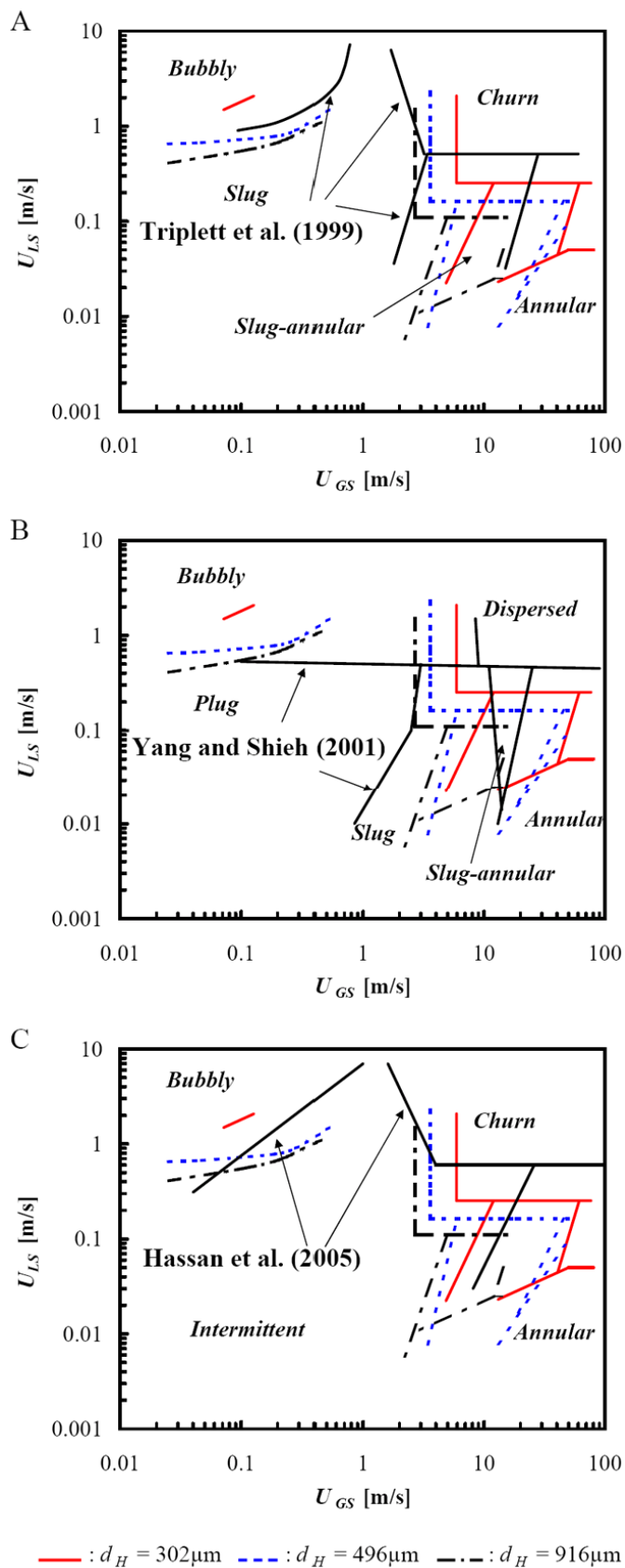


Figure 2-10: Comparison with existing flow regime maps of (A): Triplett et al. (1999); (B): Yang and Shieh (2001); (C) Hassan et al. (2005)

2.3.2 Comparison with available transition criteria

Many transition models have been proposed by researchers to predict the flow pattern transitions in small channels. Here, we choose two transition models, that of Akbar et al.(2003) and that of Waelchli and Rudolf von Rohr (2006), for reason that the channel size and fluid properties considered are close to our work.

a) Comparison with the transition model of Akbar et al. (2003)

Akbar et al. (2003) suggested that the Weber number ($We = U^2 d_H \rho / \sigma$) is more appropriate to be used as coordinate to predict the flow regime transitions:

Surface tension dominated zone:

$$\text{For } We_{LS} < 3.0: \quad We_{GS} < 0.11We_{LS}^{0.315} \quad (2.13)$$

$$\text{For } We_{LS} > 3.0: \quad We_{GS} < 1.0 \quad (2.14)$$

Annular flow zone:

$$We_{GS} > 11.0We_{LS}^{0.14} \quad \text{and} \quad We_{LS} < 3.0 \quad (2.15)$$

Dispersed flow zone:

$$We_{LS} > 3.0 \quad \text{and} \quad We_{GS} > 1.0 \quad (2.16)$$

The comparison between Akbar's model and the present flow regime maps using Weber number as coordinates are displayed in Figures 2-11(A)-(C). It can be noted that the Akbar's model can well predict the annular flow region under all experimental conditions, but it is not the case for other flow patterns. Note that the dispersed flow in Akbar's model, which occurs at higher gas and liquid velocities than churn flow, was not observed in the present work. According to the "zone division" of Akbar et al. (2003), the transition flow zone consists slug-annular flow, a part of unstable slug flow and a part of churn flow. In addition, the surface tension dominated zone includes bubbly flow, slug and plug flow. As a result, the Akbar's transition model seems to be acceptable for predicting the transitions of flow patterns.

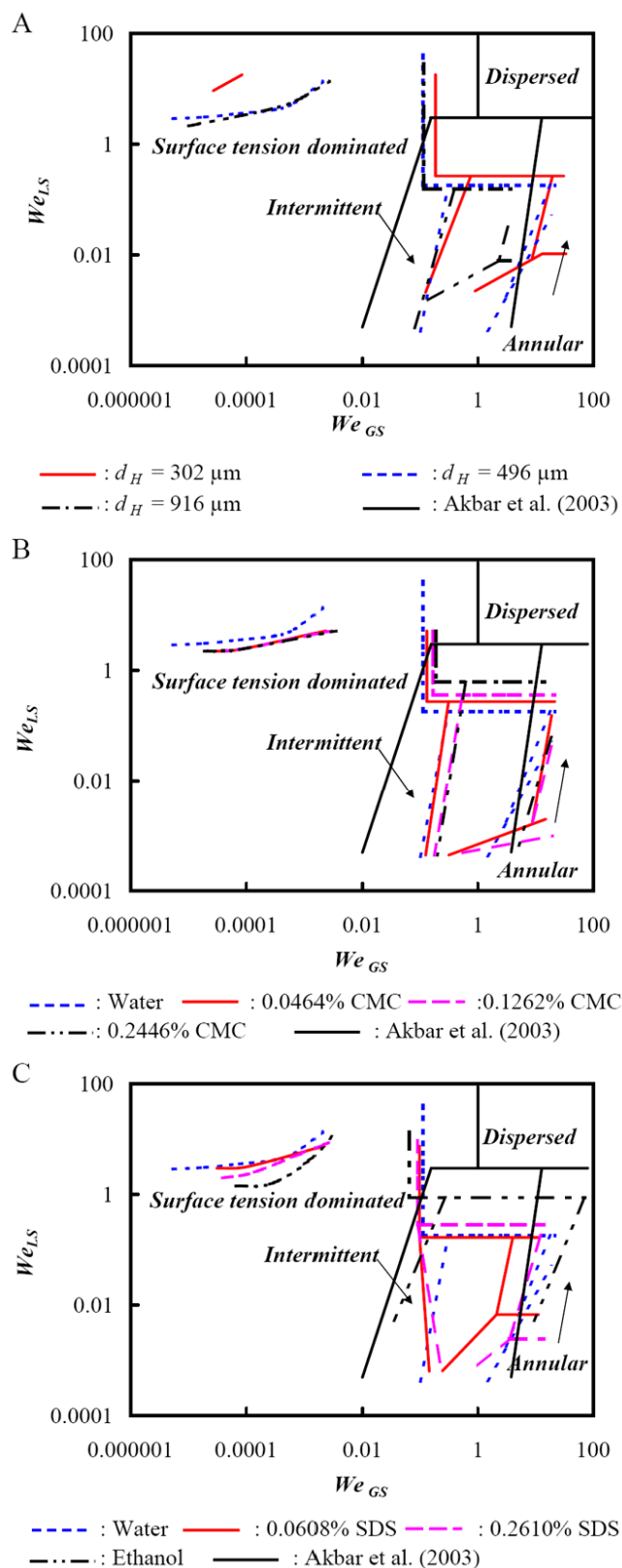


Figure 2-11: Comparison with the flow pattern transition model of Akbar et al. (2003): (A) with various channel diameters; (B) with various liquid viscosities; (C) with various surface tensions

Also note that Weber number is more appropriate to be used as coordinates than superficial velocities, for that the effects of surface tension and channel diameter can be taken into account. But it fails to reveal the effect of liquid viscosity on two phase flow patterns, as shown in Figure 2-11(B).

b). Comparison with the transition model of Waelchli and Rudolf von Rohr (2006)

Waelchli and Rudolf von Rohr (2006) suggested that $Re_{G,L}^{0.2} We_{G,L}^{0.4}$ be used as coordinates, and it showed good agreement with their experimental results. As expressed in Eq. (2.17), $Re_{G,L}^{0.2} We_{G,L}^{0.4}$ can be considered as a transformation of $U_{G,L}$, with additional factors adapted to the variation of fluid physical properties and channel diameters.

$$Re_{G,L}^{0.2} We_{G,L}^{0.4} = U_{G,L} \left(\frac{d_H^3 \cdot \Delta\rho^3}{\mu_{G,L} \cdot \sigma^2} \right)^{0.2} \rightarrow K_{G,L} U_{G,L} \quad (2.17)$$

Figure 2-12 shows a comparison of Waelchli and Rudolf von Rohr's model with our experimental results. Several features may be observed. Firstly, the transition lines of the model are in poor agreement with the present experimental data. Secondly, the effect of channel diameter on two phase flow patterns can be well revealed by using $Re_{G,L}^{0.2} We_{G,L}^{0.4}$ as coordinates, as show in Figure 2-12(A). However, they may not be appropriate to predict the influences of liquid physical properties.

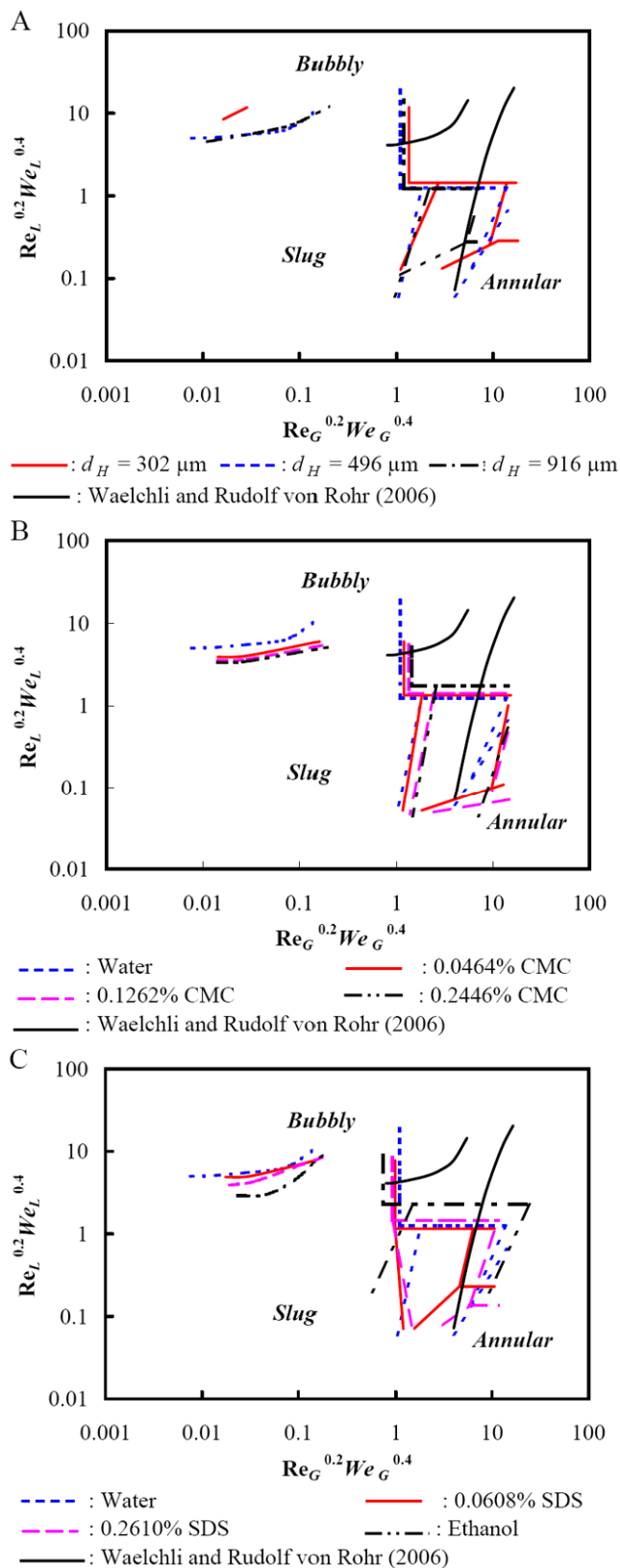


Figure 2-12: Comparison with the flow pattern transition model of Waelchli and Rudolf von Rohr (2006): (A) with various channel diameters; (B) with various liquid viscosities; (C) with various surface tensions

2.4 Transition criteria based on the present experimental data

Based on the above discussion, it can be concluded that the effects of channel size and liquid physical properties on the gas-liquid flow patterns in microchannels are significant. The existing transition models can not properly correlate our experimental data. As a result, we try to propose here a new transition model.

For the two-phase flow patterns transition in the circular horizontal microchannels, it can be known that the influence factors that should be taken into account are fluids viscosities, $\mu_{L,G}$, surface tension, σ , superficial velocities, $U_{LS,GS}$, channel inner diameter, d_i , channel surface roughness, k_s (in the present study, the microchannels were fabricated through precise hot-stretching and very clean giving: $k_s = 0.001$ mm), and fluids densities, $\rho_{L,G}$. The influence of temperature is not considered for that all the experiments are conducted under 25 °C. Using π -theorem (the detail can be found in Waelchli and Rudolf von Rohr, 2006; Zlokarnik, 1983), six dimensionless groups can be obtained as follows:

$$\text{Re}_L = \frac{\rho_L U_{LS} d_i}{\mu_L}$$

$$\text{Re}_G = \frac{\rho_G U_{GS} d_i}{\mu_G}$$

$$\text{Ca}_L = \frac{\mu_L U_{LS}}{\sigma}$$

$$\text{Ca}_G = \frac{\mu_G U_{GS}}{\sigma}$$

$$\delta = \frac{k_s}{d_i}$$

$$\mu_{ra} = \frac{\mu_L}{\mu_G}$$

A function f can be expressed based on the dimension analysis for the flow patterns transition boundaries as:

$$f(\text{Re}_L, \text{Re}_G, \text{Ca}_L, \text{Ca}_G, \delta, \mu_{ra}) = 0 \quad (2.18)$$

Usually, f is an exponential function which can only be extracted from experimental results, and we used the form for the present study as:

$$c_0 \text{Re}_L^{c_1} \text{Ca}_L^{c_2} \delta^{c_3} \mu_{ra}^{c_4} = \text{Re}_G^{c_5} \text{Ca}_G^{c_6} \delta^{c_7} \mu_{ra}^{c_8} \quad (2.19)$$

According to Eq. (2.19), when the transition lines of all the gas-liquid systems are plotted in the figures, $\text{Re}_G^{c_5} \text{Ca}_G^{c_6} \delta^{c_7} \mu_{ra}^{c_8}$ can be used as x-axis and $\text{Re}_L^{c_1} \text{Ca}_L^{c_2} \delta^{c_3} \mu_{ra}^{c_4}$ as y-axis, as shown in Figure 2-13. According to the experimental data, a parameter-variation yields the exponents as follows.

For transition from bubbly to slug flow:

$$\text{x-axis: } \text{Re}_G^{0.3} \text{Ca}_G^{0.7} \delta^{-0.4} \quad (\text{the value in the present work: from 0.0026 to 5.085})$$

$$\text{y-axis: } \text{Re}_L^{0.3} \text{Ca}_L^{0.7} \delta^{-0.4} \mu_{ra}^{-0.4} \quad (\text{from 0.0054 to 2.30})$$

For transitions from slug flow to churn and slug-annular flow:

$$\text{x-axis: } \text{Re}_G^{0.3} \text{Ca}_G^{0.7} \delta^{-0.4} \mu_{ra}^{-0.2} \quad (\text{from 0.0015 to 2.80})$$

$$\text{y-axis: } \text{Re}_L^{0.3} \text{Ca}_L^{0.7} \delta^{-0.4} \mu_{ra}^{-0.6} \quad (\text{from 0.0025 to 0.95})$$

For transitions from churn to slug-annular and annular flow:

$$\text{x-axis: } \text{Re}_G^{0.9} \text{Ca}_G^{0.1} \delta^{0.2} \quad (\text{from 0.077 to 174.7})$$

$$\text{y-axis: } \text{Re}_L^{0.9} \text{Ca}_L^{0.1} \delta^{0.2} \mu_{ra}^{0.5} \quad (\text{from 2.06 to 1058})$$

Because of different flow mechanism, three transitions are discussed separately. It can be noted that in the transitions from churn to slug-annular and annular flow, the exponent of Ca is 0.1, smaller than other two transitions. It indicates that the influence of surface tension is less important under higher gas velocities. It also can be noted that all the axis are proportional to U_{GS} and U_{LS} , e.g., Eq. (2.20) and Eq. (2.21). It can be considered as additional factors which relate the channel size and liquid physical properties are used to correct U_{GS} and U_{LS} .

$$\text{Re}_G^{0.3} \text{Ca}_G^{0.7} \delta^{-0.4} = d_i^{0.7} \mu_G^{0.4} \rho_G^{0.3} \sigma^{-0.7} U_{GS} \quad (2.20)$$

$$\text{Re}_L^{0.3} \text{Ca}_L^{0.7} \delta^{-0.4} \mu_{ra}^{-0.4} = d_i^{0.7} \mu_G^{0.4} \rho_L^{0.3} \sigma^{-0.7} U_{LS} \quad (2.21)$$

All the transitions are plotted in Figure 2-13(A)-(C) and good agreement is observed. Note that for the transitions from slug to slug-annular flow and from churn to slug-annular flow, Nitrogen-SDS solutions have not been considered, due to the disturbance of foams.

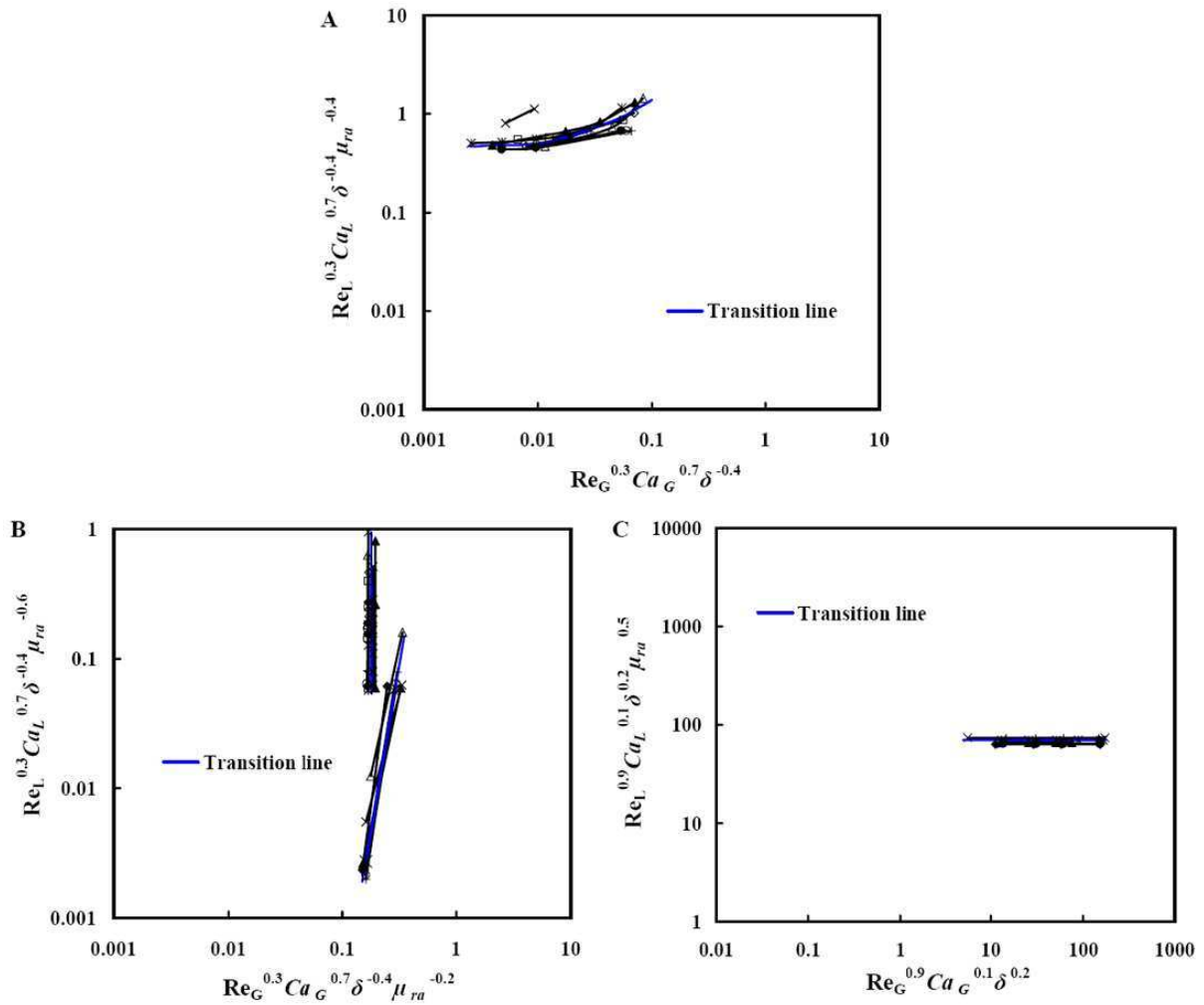


Figure 2-13: The flow pattern transitions with based on the experimental data: (A) the transition from bubbly to slug flow; (B) the transitions from slug to churn and to slug-annular flow; (C) the transitions from churn to slug-annular and to annular flow

We admit that the transition criteria presented here are based only on the experimental data obtained in the current work, without the effective comparison with others, thus may lack

of universality at this stage. However, the aim of this effort is not to claim that our model is better than the previous ones, because the available experiments data in literature on the effects of liquid physical properties are still rare. And the present model is far from complete, i.e. other influencing factors such as temperature, channel section, orientation, channel surface characteristics and inlet structure are not considered, which is also the subject of our ongoing work, as well as further refinement of the model by comparison with others.

2.5 Conclusions

Gas-liquid flow in horizontal circular microchannels with diameter of 302 μm , 496 μm , and 916 μm was experimentally investigated. Special emphasis has been put on the influences of channel size and liquid physical properties on gas-liquid flow patterns. Flow pattern maps were constructed and compared with existing models in literature in order to discuss the transition trends from one flow pattern to another. A new model was proposed which takes the effects of channel size and liquid physical properties into account. Based on the analysis and discussions above, we list the main observations as follows:

(1). Typical flow patterns, i.e. bubbly, slug, slug-annular, annular and churn flow were observed during all the tests. In addition, transitional flow patterns, such as bubbly-slug and unstable-slug flow as well as wavy flow also appeared. Dispersed bubbly flow and dispersed flow were not observed.

(2). Channel size influences the two-phase flow patterns remarkably. With decreasing channel diameter, the transitions from slug to bubbly flow, to churn and to annular flow occur at higher U_{GS} and U_{LS} . In other words, the surface tension dominated region as defined by Akbar et al. (2003) widened.

(3). Liquid physical properties (viscosity and surface tension) have obvious effects on two-phase flow patterns. On one hand, when liquid viscosity increases, the transitions from slug to churn and to slug-annular flow happen at higher U_{GS} and U_{LS} , while the transition to bubbly flow remains almost unvaried. On the other hand, the smaller the surface tension is, the earlier the transitions from slug to bubbly flow, to churn flow and to slug-annular flow, which can be considered as shrinkage of surface tension dominated region.

(4). The flow pattern maps presented by Triplett et al. (1999) and by Hassan et al. (2005) correspond well to our experimental results. However, the maps of Yang and Shieh (2001) are in poor agreement with the present results.

(5). The Akbar's transition model can only predict the transition from slug-annular to annular flow under our tested conditions. The transition model proposed by Waelchli and Rudolf von Rohr (2006) can not well predict the present flow regime maps either.

(6). A new model which considers the effects of channel size and liquid physical properties is proposed. Three empirical correlations are proposed for predicting the transitions from slug to bubbly flow, from slug to churn and slug-annular flow, and from churn to slug-annular and annular flow, respectively.

Gas-liquid two phase pressure drop characteristics will be presented in the next chapters, in which the main trend of pressure drop with the U_{GS} and U_{LS} and the dependent of pressure drop on the two-phase flow patterns will be presented. The pressure drop characteristics of pressure drop in the inertia-dominated region and that in surface tension-dominated region will be deeply discussed, respectively.

References

- Akbar, M.K., Plummer, D.A., Ghiaasiaan, S.M., 2003. On gas-liquid two-phase flow regimes in microchannels. *International Journal of Multiphase Flow* 29, 855-865.
- Barajas, A.M., Panton, R.L., 1993. The effects of contact-angle on 2-phase flow in capillary tubes. *International Journal of Multiphase Flow* 19, 337-346.
- Barnes, H.A., 2000. *Handbook of elementary rheology* University of Wales, Institute of Non-Newtonian Fluid Mechanics, Wales.
- Bretherton, F.P., 1961. The motion of long bubbles in tubes. *Journal of Fluid Mechanics* 10, 166-188.
- Chen, W.L., Twu, M.C., Pan, C., 2002. Gas-liquid two-phase flow in micro-channels. *International Journal of Multiphase Flow* 28, 1235-1247.
- Coleman, J.W., Garimella, S., 1999. Characterization of two-phase flow patterns in small diameter round and rectangular tubes. *International Journal of Heat and Mass Transfer* 42, 2869-2881.
- Hassan, I., Vaillancourt, M., Pehlivan, K., 2005. Two-phase flow regime transitions in microchannels: A comparative experimental study. *Microscale Thermophysical Engineering* 9, 165-182.
- Li, J.-M., Wang, B.-X., 2003. Size effect on two-phase regime for condensation in micro/mini tubes. *Heat Transfer—Asian Research* 32, 65-71.
- Rebrov, E.V., 2010. Two-phase flow regimes in microchannels. *Theoretical Foundations of Chemical Engineering* 44, 355-367.
- Rosen, M.J., 2004. *Surfactants and Interfacial Phenomena* 3rd ed. Honoken, New Jersey: John Wiley & Sons.
- Shao, N., Gavriilidis, A., Angeli, P., 2009. Flow regimes for adiabatic gas-liquid flow in microchannels. *Chemical Engineering Science* 64, 2749-2761.
- Spisak, W., 1986. *Two-phase flow of gas-highly viscous liquid*. Wroclaw Technical University, Wroclaw, Poland.
- Triplett, K.A., Ghiaasiaan, S.M., Abdel-Khalik, S.I., Sadowski, D.L., 1999. Gas-liquid two-phase flow in microchannels - Part I: two-phase flow patterns. *International Journal of Multiphase Flow* 25, 377-394.
- Waelchli, S., Rudolf von Rohr, P., 2006. Two-phase flow characteristics in gas-liquid microreactors. *International Journal of Multiphase Flow* 32, 791-806.
- Wahlin, B., Wahl, T., Gonzalez-Castro, J.A., Fulford, J., Robeson, M., 2005. Task committee on experimental uncertainty and measurement errors in hydraulic engineering: an update, in: Raymond, W. (Ed.). ASCE, p.

447.

- Yang, C.-Y., Shieh, C.-C., 2001. Flow pattern of air-water and two-phase R-134a in small circular tubes. *International Journal of Multiphase Flow* 27, 1163-1177.
- Yang, Z.C., Bi, Q.C., Liu, B., Huang, K.X., 2010. Nitrogen/non-Newtonian fluid two-phase upward flow in non-circular microchannels. *International Journal of Multiphase Flow* 36, 60-70.
- Yue, J., Luo, L., Gonthier, Y., Chen, G., Yuan, Q., 2008. An experimental investigation of gas-liquid two-phase flow in single microchannel contactors. *Chemical Engineering Science* 63, 4189-4202.
- Yue, J., Luo, L., Gonthier, Y., Chen, G., Yuan, Q., 2009. An experimental study of air-water Taylor flow and mass transfer inside square microchannels. *Chemical Engineering Science* 64, 3697-3708.
- Zhao, T.S., Bi, Q.C., 2001. Co-current air-water two-phase flow patterns in vertical triangular microchannels. *International Journal of Multiphase Flow* 27, 765-782.
- Zlokarnik, M., 1983. Model scale-up in chemical-engineering. *Chemie Ingenieur Technik*. 55, 363-372.

CHAPTER 3: TWO-PHASE PRESSURE DROP MODEL FOR INERTIA-DOMINATED REGION

As an extension of the study presented in the last chapter on gas-liquid flow patterns in horizontal circular microchannel, this chapter mainly concentrates on the characteristics of two-phase pressure drop, and of course its dependency on two-phase flow patterns.

The experimental results show that the two-phase pressure drop in microchannels is highly flow pattern dependent, and the main trend can be divided into three regions: bubbly and slug flow region (surface tension-dominated), unstable flow region (transitional region) and slug-annular, annular and churn flow region (inertia-dominated region), and will be exhibited in this chapter. The two-phase pressure drop data in *inertia-dominated region* will be compared with many existing homogeneous-flow models and Lockhart-Martinelli models using various Chisholm parameter (C) correlations. And an effort will be made for proposing a modified Lockhart-Martinelli model in which the effects of channel diameter and liquid properties on the C -value will be taken into account.

3.1 Introduction

Pressure drop, one of the most important hydrodynamic aspects of gas-liquid flow, is an essential element for the design of two-phase processes in the chemical industry and others gas-liquid systems, i.e. boiling and condensation in pipes. Two methods are generally used to predict the pressure drop of gas-liquid flow, i.e. homogeneous mixture model and separated-flow model (Collier and Thome, 1994).

Homogeneous mixture model, also named homogeneous-flow model, is a simple model which assumes that gas and liquid flow have identical velocity, thus can be considered as a single phase flow with two-phase mixture density and viscosity (Holland and Bragg, 1995; Lee et al., 2010). Generally, in homogeneous-flow model, the two-phase frictional pressure drop is calculated from:

$$\left(\frac{dP_{fri}}{dZ} \right)_{hom} = f_{tp} \frac{G^2}{2d_H \rho_{tp}} \quad (3.1)$$

In which, ρ_{tp} is two-phase mixture density defined as:

$$\rho_{tp} = \left(\frac{x_e}{\rho_G} + \frac{1-x_e}{\rho_L} \right)^{-1} \quad (3.2)$$

The two-phase Darcy friction factor f_{tp} is a function of two-phase mixture Reynolds number (McAdams et al., 1942), which defined as:

$$\text{Re}_{tp} = \frac{Gd_H}{\mu_{tp}} \quad (3.3)$$

For laminar two-phase flow ($\text{Re}_{tp} \leq 2100$) in pipes (Saisorn and Wongwises, 2008):

$$f_{tp} = \frac{64}{\text{Re}_{tp}} \quad (3.4)$$

And for turbulent flow ($\text{Re}_{tp} > 2100$)

$$f_{tp} = \frac{0.3164}{\text{Re}_{tp}^{0.25}} \quad (3.5)$$

in which μ_{tp} is two-phase mixture viscosity, which is the key parameter for homogeneous-flow model. Different expressions for μ_{tp} have been proposed, as tabulated in Table 3-1. For two-phase flow in mini- or microchannel, several authors found that the homogeneous-flow model could well predict the pressure drop based on their experimental results ((Agostini et al., 2008; Choi et al., 2008; Liu and Wang, 2008; Saisorn and Wongwises, 2008; Triplett et al., 1999; Ungar and Cornwell, 1992) while others also found that the predicted results deviated obviously from their experimental data (Niu et al., 2009; Su et al., 2010).

Table 3-1: Different expressions of the two-phase mixture viscosity for homogeneous-flow model

Authors	Correlation
McAdams et al. (1942)	$\mu_{tp} = \left(\frac{x_e}{\mu_G} + \frac{1-x_e}{\mu_L} \right)^{-1}$
Cicchitti et al. (1960)	$\mu_{tp} = x_e \mu_G + (1-x_e) \mu_L$
Owens (1961)	$\mu_{tp} = \mu_L$
Dukler et al. (1964)	$\mu_{tp} = \beta \mu_G + (1-\beta) \mu_L$
Beattie and Whalley (1982)	$\mu_{tp} = \mu_L (1-\beta)(1+2.5\beta) + \beta \mu_G, \quad \beta = \rho_L x_e / [\rho_L x_e + \rho_G (1-x_e)]$
Lin et al. (1991)	$\mu_{tp} = \mu_L \mu_G / \left[\mu_G + x_e^n (\mu_L - \mu_G) \right], \quad n = 1.4 \text{ when } 0 < x_e < 0.25$
Awad and Muzychka (2008)	$\mu_{tp} = \frac{1}{2} \left[\mu_L \frac{2\mu_L + \mu_G - 2(\mu_L - \mu_G)x_e}{2\mu_L + \mu_G + (\mu_L - \mu_G)x_e} + \mu_G \frac{2\mu_G + \mu_L - 2(\mu_G - \mu_L)(1-x_e)}{2\mu_G + \mu_L + (\mu_G - \mu_L)(1-x_e)} \right]$

On the other hand, many researchers preferred using separated-flow model to predict the two-phase pressure drop in mini or microchannels, since the interaction between two phases was considered, which would be significant when the channel size is in the mini or micro scale (Choi et al., 2011; English and Kandlikar, 2006). The most widely used separated-flow

model was proposed by Lockhart and Martinelli (1949). They used two-phase friction multiplier to relate the two-phase frictional pressure drop to the single-phase frictional pressure drop, expressed as:

$$\left(\frac{dP_{fri}}{dZ}\right)_{sep} = \left(\frac{dP_{fri}}{dZ}\right)_L \phi_L^2 = \left(\frac{dP_{fri}}{dZ}\right)_G \phi_G^2 \quad (3.6)$$

And the Lockhart-Martinelli parameter is given by:

$$X^2 = \left(\frac{dP_{fri}}{dZ}\right)_L / \left(\frac{dP_{fri}}{dZ}\right)_G \quad (3.7)$$

The most widely used correlation to calculate the two-phase frictional multiplier was proposed by Chisholm and Laird (1958), expressed as:

$$\phi_L^2 = 1 + \frac{C}{X} + \frac{1}{X^2} \quad (3.8)$$

In which, C is the Chisholm parameter. Combining Eqs.3.6-3.8 yields:

$$\left(\frac{dP_{fri}}{dZ}\right)_{sep} = \left(\frac{dP_{fri}}{dZ}\right)_L + C \sqrt{\left(\frac{dP_{fri}}{dZ}\right)_L \left(\frac{dP_{fri}}{dZ}\right)_G} + \left(\frac{dP_{fri}}{dZ}\right)_G \quad (3.9)$$

From Eq. (3.9), it can be known that the two-phase frictional pressure drop based on Lockhart-Martinelli model is composed of three parts: the liquid phase pressure drop, the gas phase pressure drop and the pressure drop caused by the interaction between liquid and gas phase. Thus, the C parameter can be considered as a parameter dealing with two-phase interaction. Chisholm and Laird (1958) first gave out four C -values depending on the gas and liquid flow conditions (whether the flows are turbulent or laminar) for two-phase flow in common size tubes. Later, Mishima and Hibiki (1996) found that the value of Chisholm's parameter would decrease with decreasing tube diameter when they investigated the two-phase flow in the circular small tubes, and they proposed a C -value correlation related to tube diameter. After that, extensive investigations were carried out to study two-phase flow pressure drop characteristics in mini or microchannels, and many modified C correlations were proposed, as listed in Table 3-2. Most of the C correlations were related to channel diameter and dimensionless numbers, i.e. Reynolds number, Weber number or confinement number. Recently, more and more researchers considered that the C -value depended dramatically on the fluid physical properties and channel diameter (English and Kandlikar,

2006; Kawahara et al., 2009; Ma et al., 2010). Meanwhile, we have discussed in detail in the last chapter the significant influences of liquid physical properties and channel diameter on the two phase flow pattern. Consequently, the two-phase pressure drop in microchannels is highly related to the gas-liquid flow patterns, as also reported by other authors (Cheng et al., 2008; Choi et al., 2010, 2011; Moreno Quibén and Thome, 2007a, b; Rebrov, 2010). Nevertheless, this relationship has not been considered in most of two-phase pressure drop models.

Based on the experimental results obtained in the last chapter, a typical trend of two-phase pressure drop highly related to the two-phase flow patterns in the microchannel will be depicted in this chapter. Three flow regions will be defined according to flow patterns, i.e., surface-tension dominated region, transitional region and inertia-dominated region. Then the experimental pressure drop results in the “*inertia-dominated region*” will be compared to various existing predictive methods, and the influences of channel size and liquid physical properties on the C -value will be deeply discussed and exhibited. Finally, a modified correlation will be proposed for a better prediction for this region.

Table 3-2: Chisholm parameter C and various expressions of C correlation for two-phase flow in mini or microchannel

Authors	Gas-liquid	Channel geometry	Correlation							Observations
Chisholm and Laird (1958)	-	-	Both liquid and gas flow turbulent: $C = 20$; liquid flow laminar and gas flow turbulent: $C = 12$; liquid flow turbulent and gas flow laminar: $C = 10$; both liquid and gas flow laminar: $C = 5$.							Modify the Lockhart-Martinelli model with Chisholm number: C .
Mishima and Hibiki (1996)	Air/water	Circular small tubes and rectangular ducts; hydraulic diameters: 1 mm – 4 mm.	$C = 21(1 - e^{-0.319 \times 10^3 d_H})$ for rectangular ducts; $C = 21(1 - e^{-0.333 \times 10^3 d_i})$ for circular small tubes. $C = c_0 \lambda^{c_1} \psi^{c_2} \text{Re}_L^{c_3}$							The effect of channel size on C considered.
Lee and Lee (2001)	Air/water	Rectangular channels with small height: (0.4, 1, 2, 4 mm) × 20 mm;	Liquid	Gas	c_0	c_1	c_2	c_3	The C correlation defined using three dimensionless parameters in which liquid properties, flow rates and channel size considered.	
			Laminar	Laminar	6.833×10^{-8}	-1.317	0.719	0.557		
			Laminar	Turbulent	6.185×10^{-2}	0	0	0.726		
			Turbulent	Laminar	3.627	0	0	0.174		
Turbulent	Turbulent	0.408	0	0	0.451					
Qu and Mudawar (2003)	Vapor/water	Parallel rectangular microchannel: 0.231 mm × 0.713 mm.	$C = 21(1 - e^{-0.319 \times 10^3 d_H})(0.00418G + 0.0613)$							The C correlation incorporates the effects of channel size and mass velocity.
Yue et al. (2004)	Nitrogen/water	Rectangular microchannel ($d_H = 0.528$ and 0.333 mm).	$C = 0.411822X^{-0.0305} \text{Re}_L^{0.600428}$							The single phase pressure drop ratio X considered as a significant factor in the C correlation.
Lee and Mudawar (2005)	Vapor/R134a	Rectangular micro-channel: 0.231 mm × 0.713 mm.	$C = c_0 \text{Re}_L^{c_1} \text{We}_L^{c_2}$,							Liquid phase Re and We number used to modify the C value.
			laminar-laminar: $C = 2.16 \text{Re}_L^{0.047} \text{We}_L^{0.60}$; laminar liquid-turbulent vapor: $C = 1.45 \text{Re}_L^{0.25} \text{We}_L^{0.23}$.							

Table 3-2 (Continued)

Authors	Gas-liquid	Channel geometry	Correlation	Observations
English and Kandlikar (2006)	Air/water	Rectangular minichannel: 1.124 mm × 0.93 mm	$C^* = C(1 - e^{-319D_h})$; $C = 5$ for laminar-laminar flow.	Modified model of Mishima and Hibiki (1996).
Hwang and Kim (2006)	Vapor/R134a	Circular steel microtubes with diameters: 0.244, 0.430, 0.792 mm.	$C = 0.227 \text{Re}_L^{0.452} X^{-0.320} N_{conf}^{-0.820}$. $N_{conf} = \sqrt{\frac{\sigma}{g(\rho_L - \rho_G)}} / d_i$	Confinement number considered in the C correlation.
Chen et al. (2007)	Air/water	Three rectangular channels with width of 3.0 mm and depth of 3.0, 6.0, 9.0 mm.	$C = aX^b$; $a = 5.55 - 0.7555 \times A^{-0.805} + 0.00439 \times \text{Re}_T$ and $b = 0.1001 + 0.0005 \times A^{0.895}$.	Channel aspect ratio, liquid phase Re and single phase pressure drop ratio X were considered in the C correlation.
Choi et al. (2008)	Vapor/R410A	Circular smooth minichannels with diameters: 1.5 mm and 3.0 mm.	$C = 5.5564 \text{Re}_{tp}^{0.2837} \text{We}_{tp}^{-0.288}$	C considered as a correlation of total two-phase flow Reynolds number and Weber number
Lee and Lee (2008)	Air/water	Circular mini-tubes with diameters: 1.62 and 2.16 mm.	$C = c_0 \lambda^{c_1} \psi^{c_2} \text{Re}_L^{c_3}$; for their data: $C = 2.161 \times 10^{-21} \lambda^{-3.703} \psi^{-0.995} \text{Re}_L^{0.486}$	-
Kawahara et al. (2009)	Nitrogen/water, ethanol and ethanol aqueous	Circular tube with diameter: 0.25 mm.	$C = bBo^{0.04} \text{Re}_L^{0.25} \text{We}_G^{-0.12}$, $b = 1.38$ for the flow without contraction, and $b = 0.55$ for the flow with contraction.	Bond number and inlet contraction were considered in the correlation.
Niu et al. (2009)	Mixture of CO ₂ and Nitrogen/ polyethylene glycol dimethyl ether	Circular channels with inner diameter: 1 mm.	$C = 0.0049 \text{Re}_L^{0.98} \text{Re}_G^{1.08} \text{We}_{tp}^{-0.86}$	Re_L , Re_G and We_{tp} considered as the dramatic influence factor on C .
Lee et al. (2010)	-	Collected experimental data in channels ($d_H = 0.207$ mm ~ 14 mm)	$C = 121.6(1 - e^{-22.7Bo})x_e^{1.85}$	Bond number and gas mass fraction employed to calculate the C in their work.

Table 3-2 (Continued)

Authors	Gas-liquid	Channel geometry	Correlation	Observations
Li and Wu (2010)	-	Collected experimental data in mini-channel ($d_H = 0.148 \text{ mm} \sim 3.0 \text{ mm}$).	$Bo \leq 1.5$, $C = 11.9Bo^{0.45}$; and $1.5 < Bo \leq 11$, $C = 109.4(Bo \text{Re}_L^{0.5})^{-0.56}$; $Bo \geq 11$, Beattie and Whalley's homogeneous-flow model predict well the data	Three Bo regions considered respectively, and Bond number considered as a significant factor.
Ma et al. (2010)	Air/water, ethanol and n -propanol	Four rectangular microchannels: depth $100 \mu\text{m} \times$ width (200, 400, 800, 2000 μm).	$C = aCa^b$; $Ca = \mu_L U_{LS} / \sigma$, $a = 7.59 - 0.4237A^{-0.9485} + 0.0023 \text{Re}_L$, $b = 0.223 + 0.2A^{0.9778}$; A is the aspect ratio of rectangular microchannels.	Effects of surface tension and channel aspect ratio were investigated and taken into account in the C correlation.
Saisorn and Wongwises (2010)	Nitrogen and air/water	Circular micro-channels with diameter: 0.15, 0.22, 0.53 mm.	$C = 7.599 \times 10^{-3} \lambda^{-0.631} \psi^{0.005} \text{Re}_L^{-0.008}$	-
Su et al. (2010)	Nitrogen/40% methyldiethanolamine aqueous solution	Circular channels with diameters: 0.56 mm, 1.00 mm, 1.80 mm.	$C = c_0 \text{Re}_L^{c_1} X^{c_2} We_G^{c_3}$; for both laminar gas and liquid flow: the values of c_0 , c_1 , c_2 , c_3 respectively are 0.0704, 1.7720, -2.7901, -0.6384; for turbulent gas flow and laminar liquid flow: 0.5426, 0.3882, -0.2211, 0.3064.	Re_L , X and We_G considered as influencing factor and two flow regime considered.
Zhang et al. (2010)	-	Collected experimental data in mini-channel ($d_H = 0.014 \text{ mm} \sim 6.25 \text{ mm}$).	Liquid-gas: $C = 21(1 - e^{-0.674/Lo^*})$; Liquid-vapor: $C = 21(1 - e^{-0.142/Lo^*})$.	Dimensionless Laplace constant considered in the C correlation to replace the channel diameter.

3.2 Experimental condition and data reduction

The experimental setup, the geometry of the test section and the experimental procedures has been described in detail in the last chapter. The method for uncertainties analysis was also presented in the last chapter, and in this work the estimated maximum uncertainty was 1% for pressure drop measurements, 1.7% for flow velocity, 1.9% for Reynolds number and 3.2% for the Weber number. The uncertainties made by instruments and error in measured channel dimensions were also taken into account.

In the present work, the experiments were implemented in the test section shown in the Figure 2-2 of the last chapter. Two-phase flow in three circular microchannels made in quartz glass with diameters of 302, 496 and 916 μm and identical length of 10 cm, was investigated in this study. Generally, the total two-phase pressure drop consists of three parts: the gravitational pressure drop (static pressure drop), the acceleration pressure drop (momentum pressure drop) and the frictional pressure drop:

$$\Delta P_{TP} = \Delta P_{fri} + \Delta P_{acc} + \Delta P_{gra} \quad (3.10)$$

Since the experiments were conducted in the horizontal microchannel, thus:

$$\Delta P_{gra} = 0 \quad (3.11)$$

and

$$\Delta P_{fri} = \Delta P_{TP} - \Delta P_{acc} \quad (3.12)$$

And the two-phase acceleration pressure drop is given by (Yan, 2007):

$$\Delta P_{acc} = G^2 \left[\left(\frac{x_e}{\rho_G \varepsilon_G} + \frac{(1-x_e)^2}{\rho_L (1-\varepsilon_G)} \right)_{out} - \left(\frac{x_e}{\rho_G \varepsilon_G} + \frac{(1-x_e)^2}{\rho_L (1-\varepsilon_G)} \right)_{in} \right] \quad (3.13)$$

In which, G is total two-phase mass flux defined as:

$$G = U_{LS} \rho_L + U_{GS} \rho_G \quad (3.14)$$

And ε_G is the void fraction. In literature, many correlations were proposed to estimate the void fraction of two-phase flow in horizontal pipes. Among them, two typical correlations

were widely used:

Armand's correlation (Armand, 1946):

$$\varepsilon_G = 0.833\beta \quad (3.15)$$

In which β is the gas volumetric fraction defined as:

$$\beta = \frac{U_{GS}}{U_{GS} + U_{LS}} \quad (3.16)$$

And Kawahara's non-linear correlation (Kawahara et al., 2002):

$$\varepsilon_G = \frac{0.03\beta^{0.5}}{1 - 0.97\beta^{0.5}} \quad (3.17)$$

Many researchers found that the Armand's correlation can well predict the gas void fraction in microchannels under a wide range of experimental conditions, especially under slug flow (Taylor flow) (Choi et al., 2011; Kawahara et al., 2009; Serizawa et al., 2002; Warnier et al., 2008; Yue et al., 2008; Zhao and Bi, 2001). Some researchers also reported that when the channel diameters are smaller than 150 μm , the Kawahara's correlation shows better agreement with the experimental results (Chung and Kawaji, 2004; Kawahara et al., 2002; Saisorn and Wongwises, 2010). In this work, actually, no matter which correlation is used to estimate the void fraction for the data reduction of two-phase pressure drop only very small error would remain because ΔP_{acc} is very small compared to ΔP_{TP} (less than 1.9% under all experimental conditions). Since the diameters of three microchannels employed in present work are 302, 496 and 916 μm , Armand's correlation is more suitable and adopted in the data processing of the present work.

3.3 Dependence of pressure drop on the flow regimes

It is reported that the gas-liquid two-phase pressure drop in a mini or microchannel depends on the flow regimes (Cheng et al., 2008; Choi et al., 2011; Jassim and Newell, 2006; Moreno Quibén and Thome, 2007a, b; Nino et al., 2002; Nino et al., 2006; Rebrov, 2010). Nino et al. (2002) conducted experiments of the two-phase pressure drop using a variety of fluids in two multi-port microchannels with hydraulic diameters of 1.54 mm and 1.02 mm.

They found that two-phase pressure drop was highly flow-regime dependent and proposed models for intermittent flow (bubbly flow and slug flow) regime and annular flow regime, respectively, to predict the pressure drop in multi-port microchannels. However, the inevitable problem of gas and liquid flow maldistribution between multi-channels may make their model unsuitable for single mini or microchannel. Based on experiments using nitrogen-water as two-phase system in rectangular microchannels with hydraulic diameters of, 143, 322 and 490 μm , Choi et al. (2011) found that the typical trend of two-phase pressure drop could be divided into three regions: (a) the bubbly, slug and elongated bubble flow regimes; (b) the multiple flow regimes (transitional regime); (c) the liquid ring flow regime. In the first and third regions, the pressure drop increased with the increasing gas superficial velocity (U_{GS}), whereas a reverse tendency was observed in transitional regime, which could be caused by the collapse of the elongated bubbles. Unfortunately, they did not propose a reasonable two-phase pressure drop model taking this typical trend into account.

In the present study, a typical trend of pressure drop similar to that of Choi et al. (2011) was also experimentally observed, as shown in Figure 3-1. For all working liquids used in the present experiments and liquid superficial velocity (U_{LS}), the results show the same trend which can also be divided into three regions according to flow patterns:

Region I: The bubbly and slug flow (the slug flow in the present paper includes slug and elongated bubble flow in Choi's paper) region. In this region, the U_{GS} was relatively low, and the two-phase pressure drop increased with increasing U_{GS} .

Region II: The unstable slug flow region or transitional region. The unstable slug flow, which was similar to the multiple flow in Choi's paper, is a transitional flow pattern between slug flow and slug-annular or churn flow. The two-phase pressure drop does not increase obviously with U_{GS} , but shows some instability in this region.

Region III: The slug-annular, annular (liquid ring flow in Choi's paper) and churn flow region. The U_{GS} is relatively high, and two-phase pressure drop increases monotonously with the U_{GS} , but with a higher increasing rate with respect to region I.

Inspired by the region division theory of Akbar et al. (2003) for two-phase flow regime

map in microchannel, in which flow map was divided into four regions: the surface tension-dominated region (including bubbly and slug flow), inertia-dominated zone 1 (including annular and slug-annular or so-called wavy-annular slow), inertia-dominated zone 2 (dispersed flow) and transition zone, the three pressure drop regions in the present work can be rewritten according to the flow mechanisms as:

Region I: The surface tension-dominated region.

Region II: The transitional region.

Region III: The inertia-dominated region.

Since each region has its dominating driven-force and proper flow mechanism, the two-phase pressure drop in each region will be treated separately. In this chapter, only that in *inertia-dominated (region III)* will be discussed, by comparing our experimental data with the predicted two-phase pressure drops using various homogeneous-flow models and Lockhart-Martinelli models. The study of pressure drop in the surface tension-dominated region (region I) will be presented in the following chapter.

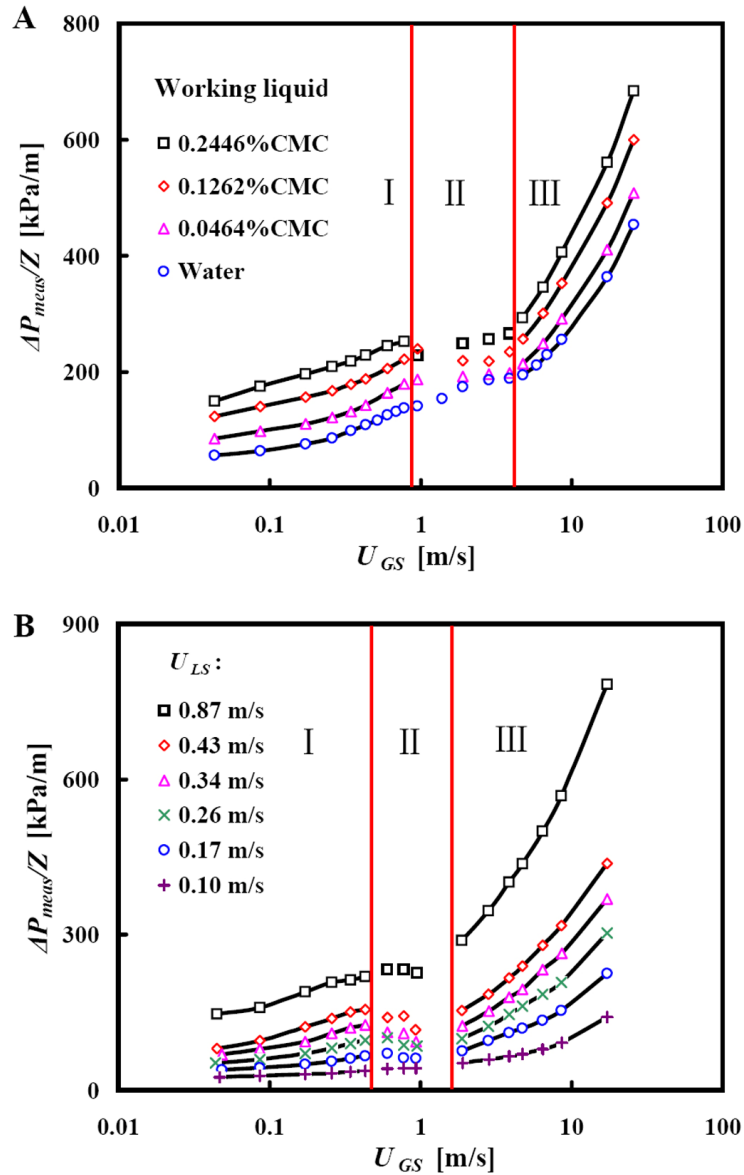


Figure 3-1: The dependence of two-phase pressure drop on the flow patterns in circular horizontal microchannel ($d_i = 496 \mu\text{m}$): (A) Gas: nitrogen, $U_{LS} = 0.34 \text{ m/s}$; (B) nitrogen-ethanol two-phase flow. (I) The surface tension-dominated region (bubbly and slug flow regimes); (II) The transitional flow region (unstable slug flow regime); (III) The inertia-dominated region (slug-annular, annular and churn flow regimes)

3.4 Two-phase pressure drop in circular horizontal microchannel in inertia-dominated region (slug-annular, annular and churn flow regimes)

For convenience to analysis the departure of the predicted values from the experimental results, mean relative deviation and the percentage of points falling within the relative deviation of 30% are used, defined as:

$$E_m = \frac{1}{N} \sum_{i=1}^N \left| \frac{\Delta p_{exp,i} - \Delta p_{pre,i}}{\Delta p_{exp,i}} \right| \times 100\% \quad (3.18)$$

And

$$P_{30\%} = \frac{n_{\text{points falling within 30\%}}}{N_{\text{total points}}} \times 100\% \quad (3.19)$$

3.4.1 The comparison of experimental results with existing homogeneous-flow model correlations

The measured two-phase pressure drop of three two-phase flow systems (nitrogen-ethanol, nitrogen-0.2446%CMC solution and nitrogen-water) in circular microchannel with diameter of 496 μm were compared with various homogeneous-flow models, as shown in Figure 3-2. The mean relative deviation between experimental data and predicted results, and the percentage of points falling within the relative deviation of 30% are tabulated in Table 3-3. It can be observed that the predictions of McAdams et al. (1942) and Beattie and Whalley (1982) are the best among homogeneous-flow models, and the others absolutely fail in prediction for two-phase flow in microchannels, as also reported by other researchers (Choi et al., 2008; Niu et al., 2009; Pamitran et al., 2010; Saisorn and Wongwises, 2008; Su et al., 2010; Triplett et al., 1999). However, it can be observed from Table 3-3 that even for the predictions of the McAdams' or Beattie and Whalley's model, the mean relative deviations from measured results are rather high and no more than 56.25% points fall within the relative deviation of 30%. Therefore, the homogeneous-flow model may not be the proper method to predict the two-phase pressure drop in the inertia-dominated region, for it postulates that the gas phase has the same velocity as liquid and the interaction between two

phases is ignored.

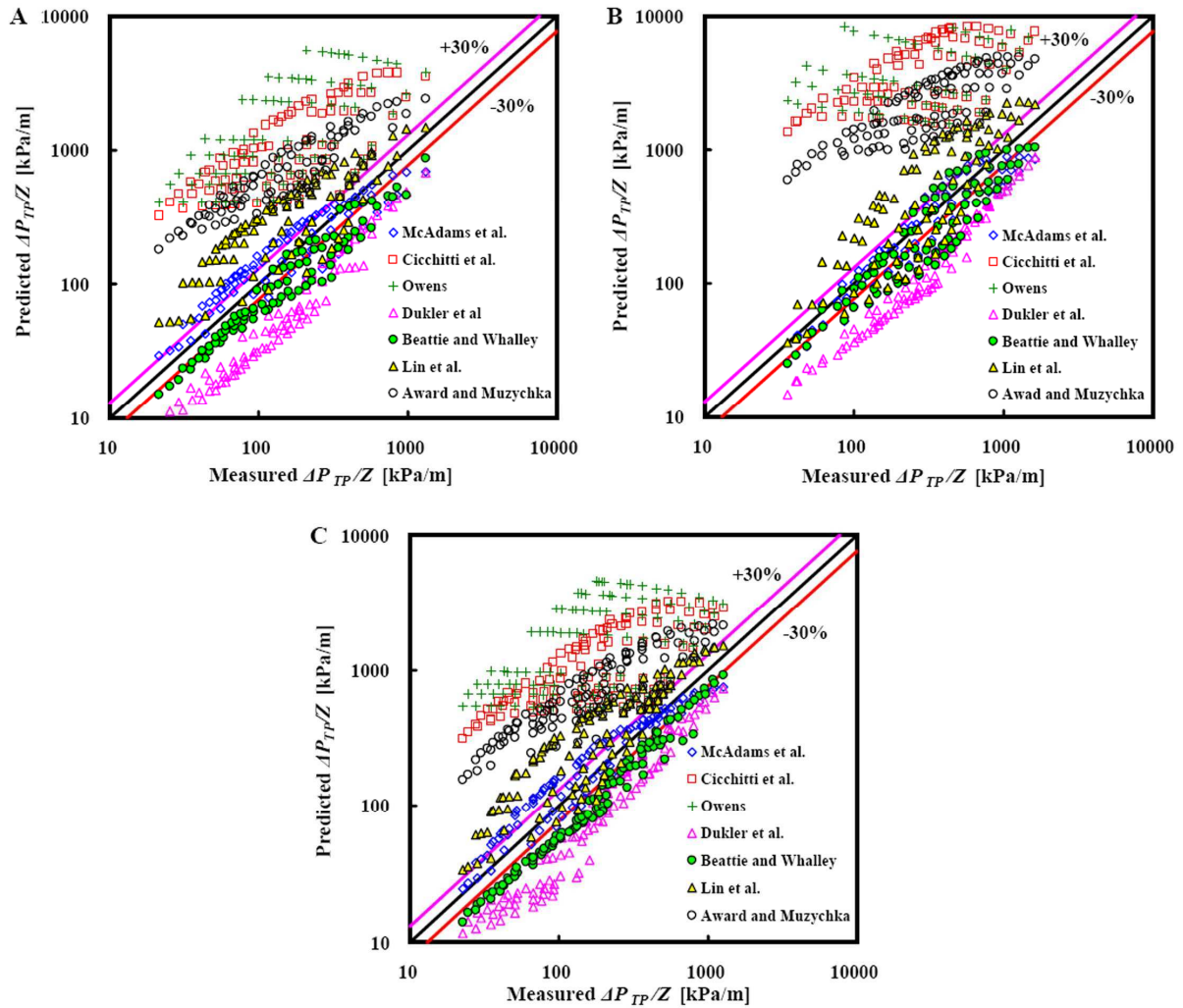


Figure 3-2: The comparison of measured two-phase pressure drop (in the inertia-dominated region) in circular horizontal microchannel ($d_i = 496 \mu\text{m}$) with predictions of homogeneous-flow models. (A): The nitrogen-ethanol two-phase flow; (B): The nitrogen and 0.2446% CMC aqueous solution two-phase flow; (C): The nitrogen-water two-phase flow

Table 3-3: Mean relative deviation between predicted results of various homogeneous-flow models and the measured two-phase pressure drop (in the inertia-dominated region) in circular horizontal microchannel ($d_i = 496 \mu\text{m}$), and the percentage of points falling within the relative deviation of 30%

Homogeneous-flow correlations	Two-phase systems					
	Nitrogen-ethanol		Nitrogen-0.2446% CMC solution		Nitrogen-water	
	E_m (%)	$P_{30\%}$ (%)	E_m (%)	$P_{30\%}$ (%)	E_m (%)	$P_{30\%}$ (%)
McAdams et al. (1942)	35.16	37.50	30.51	52.75	31.09	56.25
Cicchitti et al. (1960)	693.6	0	1546	0	653.6	0
Owens (1961)	997.2	0	2079	0	1093	0
Dukler et al. (1964)	60.64	0	59.15	0	50.73	4.46
Beattie and Whalley (1982)	31.96	48.86	30.52	50.55	37.52	22.32
Lin et al. (1991)	120.0	15.90	89.89	27.47	96.96	21.43
Awad and Muzychka (2010)	374.4	1.14	706.5	0	341.5	1.79

3.4.2 The comparison of experimental results with existing Lockhart-Martinelli model correlations

The mean relative deviation between experimental two-phase pressure drop data in the inertia-dominated region and predicted results of the Lockhart-Martinelli models using various C correlations, and the percentage of points falling within the relative deviation of 30% are tabulated in Table 3-4. It can be noted that Lockhart-Martinelli models using C correlations of Chisholm (1958), Yue et al. (2004), Kawahara et al. (2009) and Lee et al. (2010) have better agreement than others for relative lower E_m (%) and higher $P_{30\%}$ (%). The comparison of the measured two-phase pressure drop data with the predicted results of these four models is also depicted in Figure 3-3. Although remarkable departure is found between the predicted results and the present experimental data, and a lot of points do not fall within the relative deviation of 30%, the Lockhart-Martinelli model seems to have more potential with respect to the homogeneous-flow model. Thus, a modified Lockhart-Martinelli model with a new C correlation will be proposed based on the experimental data of the present work.

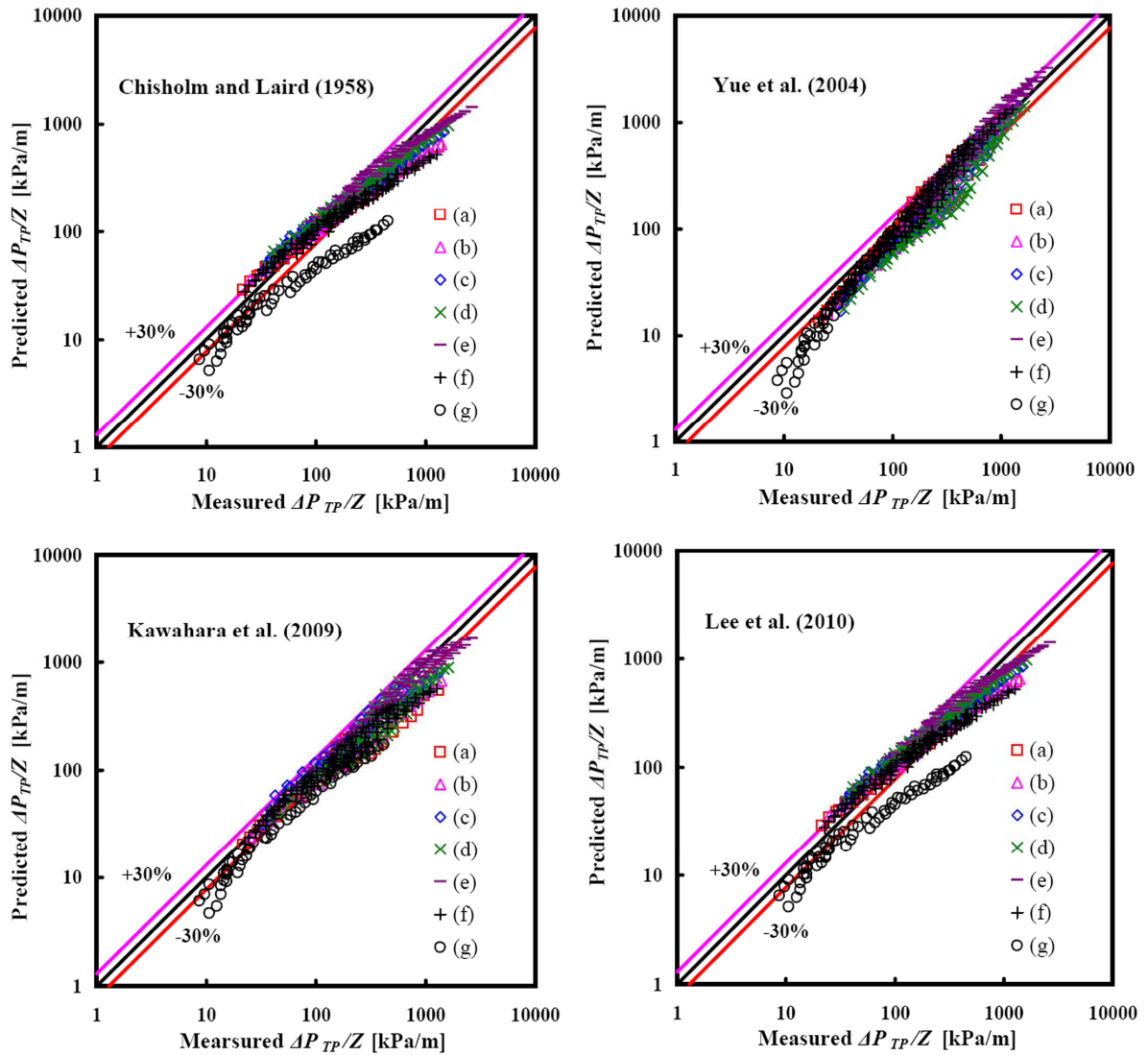


Figure 3-3: The comparison of measured two-phase pressure drop (in the inertia-dominated region) in circular horizontal microchannels with predictions of Lockhart-Martinelli models using various C correlations. In this figure, the different symbols represent: (a) the nitrogen-ethanol two-phase flow in microchannel with $d_i = 496 \mu\text{m}$; (b), (c) and (d) the nitrogen and 0.0464% CMC, 0.1262% CMC and 0.2446% CMC aqueous solution two-phase flow in microchannel with $d_i = 496 \mu\text{m}$, respectively; (e), (f) and (g) the nitrogen-water two-phase flow in microchannels with $d_i = 302 \mu\text{m}$, $d_i = 496 \mu\text{m}$ and $d_i = 916 \mu\text{m}$, respectively

Table 3-4: Mean relative deviation between predicted results of Lockhart-Martinelli model using various *C* correlations and the measured two-phase pressure drop (in the inertia-dominated region) in circular horizontal microchannels, and the percentage of points falling within the relative deviation of 30%

Authors	Two-phase system													
	Nitrogen-ethanol		Nitrogen-0.0464% CMC solution		Nitrogen-0.1262% CMC solution		Nitrogen-0.2446% CMC solution		Nitrogen-water					
	$D_i = 496 \mu\text{m}$				$D_i = 496 \mu\text{m}$				$D_i = 302 \mu\text{m}$		$D_i = 496 \mu\text{m}$		$D_i = 916 \mu\text{m}$	
	E_m (%)	$P_{30\%}$ (%)	E_m (%)	$P_{30\%}$ (%)	E_m (%)	$P_{30\%}$ (%)	E_m (%)	$P_{30\%}$ (%)	E_m (%)	$P_{30\%}$ (%)	E_m (%)	$P_{30\%}$ (%)	E_m (%)	$P_{30\%}$ (%)
Chisholm and Laird (1958)	20.40	77.27	21.27	71.43	19.51	79.12	18.00	82.42	21.10	81.32	23.33	68.75	45.43	30.30
Mishima and Hibiki (1996)	29.00	52.27	32.46	27.47	28.72	51.65	27.47	56.04	43.54	21.98	33.62	46.43	43.20	30.30
Lee et Lee (2001)	68.14	0	68.72	0	67.04	0	66.32	0	67.42	0	65.37	0	79.54	0
Qu and Mudawar (2003)	43.20	18.18	38.92	27.47	38.36	28.57	38.89	30.77	32.80	38.46	40.92	19.64	48.28	27.27
Yue et al. (2004)	19.61	90.91	22.43	67.03	28.71	46.15	32.77	39.56	21.45	76.92	18.80	96.43	27.62	54.55
Lee and Mudawar (2005)	45.25	20.45	53.24	6.59	50.59	14.29	50.19	12.09	43.01	20.88	53.73	2.68	64.67	0
English and Kandlikar (2006)	58.84	0	60.06	0	57.68	0	56.86	0	61.88	0	59.48	0	71.24	0
Hwang and kim (2006)	62.24	0	64.99	0	64.25	0	64.04	0	64.37	0	62.63	0	74.64	0
Choi et al. (2008)	134.4	13.64	177.0	7.69	176.5	4.40	167.7	4.40	188.9	1.10	186.6	10.71	110.8	19.70
Lee et Lee (2008)	68.17	0	68.54	0	67.06	0	66.33	0	64.82	2.20	45.12	31.25	250.5	10.61

Table 3-4 (continued)

Authors	Two-phase system													
	Nitrogen-ethanol		Nitrogen-0.0464% CMC solution		Nitrogen-0.1262% CMC solution		Nitrogen-0.2446% CMC solution		Nitrogen-water					
	$D_i = 496 \mu\text{m}$				$D_i = 496 \mu\text{m}$				$D_i = 302 \mu\text{m}$		$D_i = 496 \mu\text{m}$		$D_i = 916 \mu\text{m}$	
	E_m (%)	$P_{30\%}$ (%)	E_m (%)	$P_{30\%}$ (%)	E_m (%)	$P_{30\%}$ (%)	E_m (%)	$P_{30\%}$ (%)	E_m (%)	$P_{30\%}$ (%)	E_m (%)	$P_{30\%}$ (%)	E_m (%)	$P_{30\%}$ (%)
Kawahara et al. (2009)	21.74	70.45	23.42	64.84	24.70	59.34	26.62	57.14	12.18	93.41	20.72	72.32	45.63	3.03
Niu et al. (2009)	21.29	73.86	131.6	7.69	73.05	15.38	47.95	27.47	178.9	0	207.3	4.46	209.3	9.09
Lee et al. (2010)	20.40	77.27	21.27	71.43	19.51	78.02	18.00	82.42	21.10	79.12	23.33	67.86	45.43	27.27
Li and Wu (2010)	21.50	71.59	38.01	31.87	34.06	37.36	33.03	43.96	47.04	15.38	39.01	35.71	49.05	16.67
Ma et al. (2010)	36.63	30.68	45.03	9.89	39.02	20.88	36.40	30.77	41.31	14.29	48.08	4.46	67.65	0
Saisorn and Wongwises (2010)	43.98	15.91	29.99	51.65	44.10	12.09	49.86	0	21.58	74.73	24.26	63.39	27.04	62.12
Su et al. (2010)	1935	13.64	2506	6.59	273.3	19.78	79.46	17.58	8635	6.59	36085	0	22564	4.55
Zhang et al. (2010)	22.47	68.18	39.73	26.37	35.87	30.77	34.84	39.56	48.68	14.29	40.61	33.93	50.46	15.15
New correlation	7.41	97.73	8.55	98.90	9.39	96.70	11.98	94.51	13.11	100	7.97	99.11	17.89	80.52

3.5 New correlation for modified Lockhart-Martinelli model

In this section, the effects of channel diameter, liquid viscosity and surface tension on the two-phase pressure drop in circular horizontal microchannel were systematically and experimentally investigated, which will be discussed and a modified C correlation will be proposed to modify the Lockhart-Martinelli model.

3.5.1 The influence of channel diameter

Figure 3-4 shows the influence of channel diameter on the C -value under the same liquid velocity and liquid properties conditions. The C -value is obtained from the measured two-phase pressure drop, calculated by the following equation derived from Eq. (3.9):

$$C = \left[\left(\frac{dP_{fri}}{dZ} \right)_{meas} - \left(\frac{dP_{fri}}{dZ} \right)_L - \left(\frac{dP_{fri}}{dZ} \right)_G \right] / \sqrt{\left(\frac{dP_{fri}}{dZ} \right)_L \left(\frac{dP_{fri}}{dZ} \right)_G} \quad (3.20)$$

From Figure 3-4, it can be noted that the C -value increases with the channel diameter. This trend was also reported by many other researchers (Lee and Lee, 2001; Mishima and Hibiki, 1996). Actually, such trend is agreed by most of the researchers, which just can be derived from their C correlations. For example, the C correlation of Lee and Mudawar (2005) is expressed by:

$$\text{Laminar liquid-laminar vapor: } C = 2.16 \text{Re}_L^{0.047} \text{We}_L^{0.60} \quad (3.21)$$

$$\text{Laminar liquid-turbulent vapor: } C = 1.45 \text{Re}_L^{0.25} \text{We}_L^{0.23} \quad (3.22)$$

The Eq. (3.21) and Eq. (3.22) can be rewritten in the form:

$$C = 2.16 \left(\frac{U_{LS} \rho_L d_H}{\mu_L} \right)^{0.047} \left(\frac{U_{LS}^2 \rho_L d_H}{\sigma} \right)^{0.60} = 2.16 \frac{U_{LS}^{1.25} \rho_L^{0.65} d_H^{0.65}}{\mu_L^{0.047} \sigma^{0.60}} \quad (3.23)$$

$$C = 1.45 \left(\frac{U_{LS} \rho_L d_H}{\mu_L} \right)^{0.25} \left(\frac{U_{LS}^2 \rho_L d_H}{\sigma} \right)^{0.23} = 1.45 \frac{U_{LS}^{0.71} \rho_L^{0.48} d_H^{0.48}}{\mu_L^{0.25} \sigma^{0.23}} \quad (3.24)$$

From Eq. (3.23) and Eq. (3.24), it also can be known that the C -value would increase with the channel diameter when other influence factors keep constant.

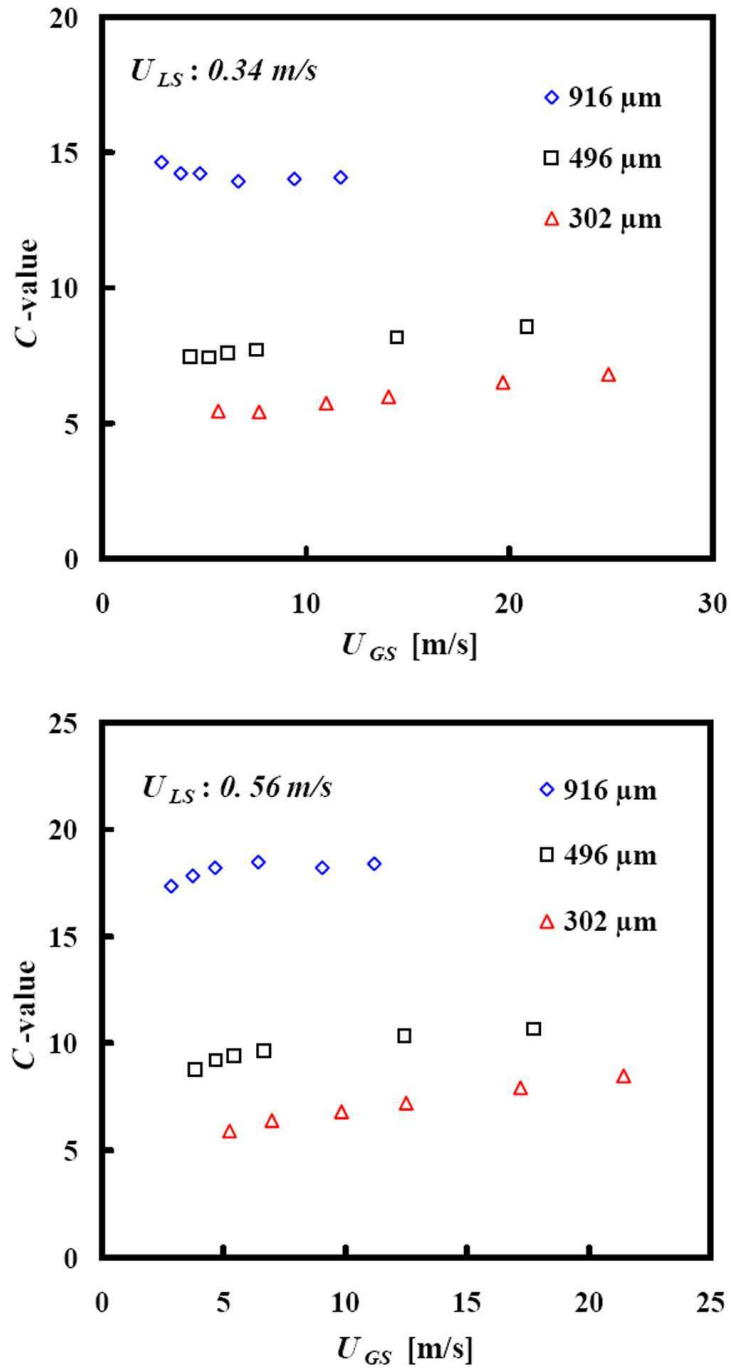


Figure 3-4: The Chisholm parameter C -value as a function of gas superficial velocity in circular horizontal microchannels with different diameters in the inertia-dominated region

3.5.2 The influence of liquid viscosity and surface tension

The influences of liquid viscosity and surface tension on C -value in the inertia-dominated region are depicted in Figures 3-5 and 3-6. Note that in the last chapter, we

have shown that the dynamic viscosity of CMC aqueous solution increases with increasing CMC concentration. And at very low concentration, the other physical properties of these three CMC aqueous solutions such as surface tension and density are almost constant. Therefore, in Figure 3-5, the decreasing C -value with the decreasing CMC concentration indicates that the increasing liquid viscosity has a negative effect on C -value.

Figure 3-6 shows the comparison between the C -value of nitrogen-water and that of nitrogen-ethanol two-phase flow in microchannel ($d_i = 496 \mu\text{m}$) at the same U_{LS} . These two systems have close values of viscosity and density, but a large difference in surface tension: the surface tension of nitrogen-water system is more than three times higher than that of nitrogen-ethanol system. From Figure 3-6, it can be noted that the C -values of the two systems are almost identical, implying the insignificant influence of surface tension on the C -value. This phenomenon is just in correspondence with the two-phase flow mechanism of the inertia-dominated region, in which the inertia is significantly larger than the surface tension force. Consequently, it can be considered that the influence of surface tension on two-phase pressure drop (thus the C -value) would be very small with respect to that of inertia, even negligible.

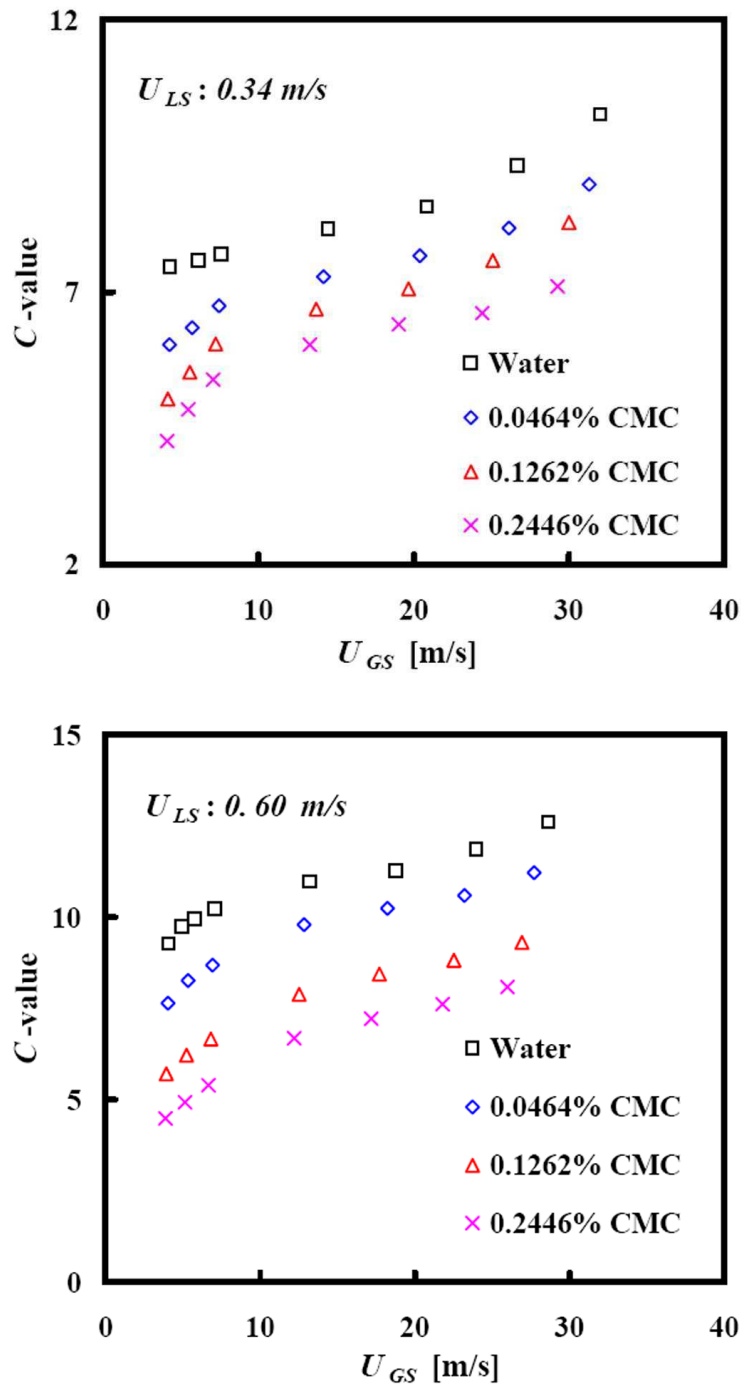


Figure 3-5: The Chisholm parameter C -value against gas superficial velocity in circular horizontal microchannel with inner diameter of $496 \mu\text{m}$ under different liquid viscosity in the inertia-dominated region at 25°C . Liquid viscosities at 25°C : 0.2446% CMC solution ($U_{LS} = 0.34 \text{ m/s}$: $\mu_{eff} = 3.5 \text{ mPa}\cdot\text{s}$; $U_{LS} = 0.60 \text{ m/s}$: $\mu_{eff} = 3.3 \text{ mPa}\cdot\text{s}$) > 0.1262% CMC solution ($U_{LS} = 0.34 \text{ m/s}$: $\mu_{eff} = 2.6 \text{ mPa}\cdot\text{s}$; $U_{LS} = 0.60 \text{ m/s}$: $\mu_{eff} = 2.5 \text{ mPa}\cdot\text{s}$) > 0.0464% CMC solution ($U_{LS} = 0.34 \text{ m/s}$: $\mu_{eff} = 1.6 \text{ mPa}\cdot\text{s}$; $U_{LS} = 0.60 \text{ m/s}$: $\mu_{eff} = 1.6 \text{ mPa}\cdot\text{s}$) > water ($0.89 \text{ mPa}\cdot\text{s}$)

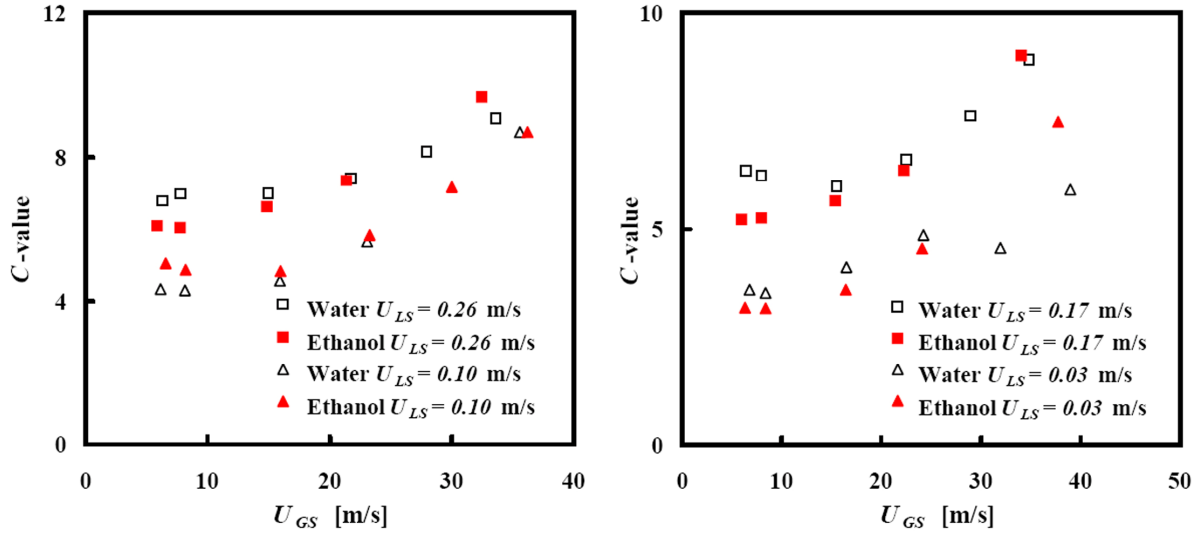


Figure 3-6: The Chisholm parameter C-value of nitrogen-water (surface tension: 72.0 mN/m at 25°C) and nitrogen-ethanol (surface tension: 21.5 mN/m at 25°C) two-phase system as a function of gas velocity in circular horizontal microchannel with diameter of 496 μm in the inertia-dominated region

3.5.3 The proposal of new C correlation

As discussed above, the Chisholm parameter C can be considered as a parameter which represents the interaction between the two phases. Therefore, the variables which have to be taken into account in the C correlation should be the superficial velocities (U_{LS} and U_{GS}), acceleration of gravity (g), the densities (ρ_L and ρ_G), their surface tension (σ), the viscosities (μ_L and μ_G), the channel angle of inclination with respect to the gravity force (θ) and the channel diameter (d_i). Neglecting the effect of surface tension and gravity on C -value, and θ equal to zero for horizontal flow, the effective variables are U_{LS} , U_{GS} , ρ_L , ρ_G , μ_L , μ_G and d_i . By using π -theorem, two dimensionless parameters can be proposed:

$$\text{Re}_L = \frac{U_{LS} \rho_L d_i}{\mu_L} \quad (3.25)$$

$$\text{Re}_G = \frac{U_{GS} \rho_G d_i}{\mu_G} \quad (3.26)$$

The C correlation for the two-phase flow in circular horizontal microchannel in the inertia-dominated region can be expressed as:

$$C = f(\text{Re}_L, \text{Re}_G) \quad (3.27)$$

by using a least square regression of all the experimental data of the present work, the Eq. (3.27) can be determined and rewritten as:

$$C = (1.17 + 0.53 \text{Re}_G^{0.39}) \text{Re}_L^{0.31} \quad (3.28)$$

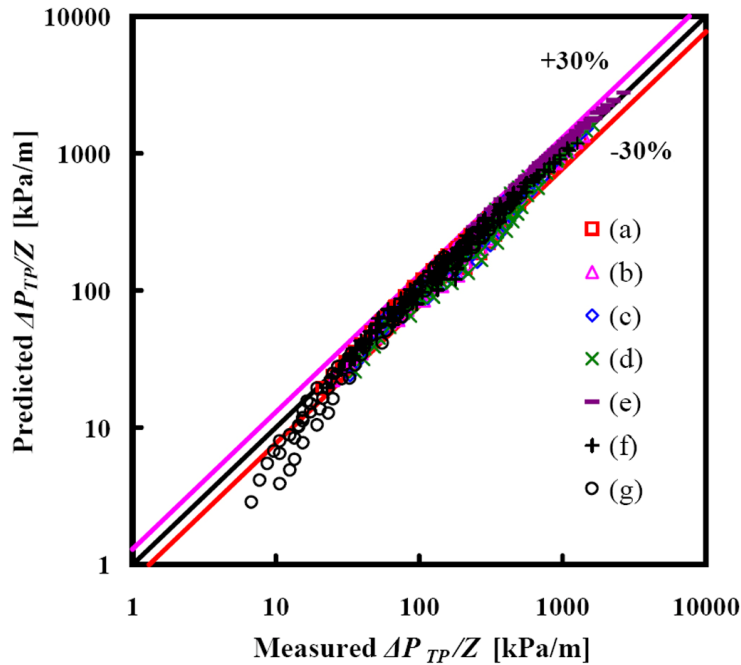


Figure 3-7: The comparison of measured two-phase pressure drop (in the inertia-dominated region) in horizontal circular microchannels with predictions of the new model. In this figure, the various symbols represent (a) the nitrogen-ethanol two-phase flow in microchannel with $d_i = 496 \mu\text{m}$; (b), (c) and (d) the nitrogen and 0.0464% CMC, 0.1262% CMC and 0.2446% CMC aqueous solution two-phase flow in microchannel with $d_i = 496 \mu\text{m}$, respectively; (e), (f) and (g) the nitrogen-water two-phase flow in microchannels with $d_i = 302 \mu\text{m}$, $d_i = 496 \mu\text{m}$ and $d_i = 916 \mu\text{m}$, respectively

The comparison of measured two-phase pressure drop (in the inertia-dominated region) with predictions based on the modified Lockhart-Martinelli model using present proposed C correlation is shown in the Figures (3-7)-(3-9). The mean relative deviation of predicted results from the measured two-phase pressure drop in present work and the percentage of points falling within the relative deviation of 30% for the new correlation are presented in the last row of Table 3-4. It can be noted that the predictions of the new correlation show a very good agreement with the experimental data, for rather low E_m , e.g. 7.41% for nitrogen-ethanol, 7.97% for nitrogen-water, less than 12% for nitrogen-CMC solutions, and rather high $P_{30\%}$, e.g. 97.73% for nitrogen-ethanol, 99.11% for nitrogen-water, more than 94% for nitrogen-CMC solutions, and even 100% for nitrogen-water two-phase flow in the channel with diameter of 302 μm .

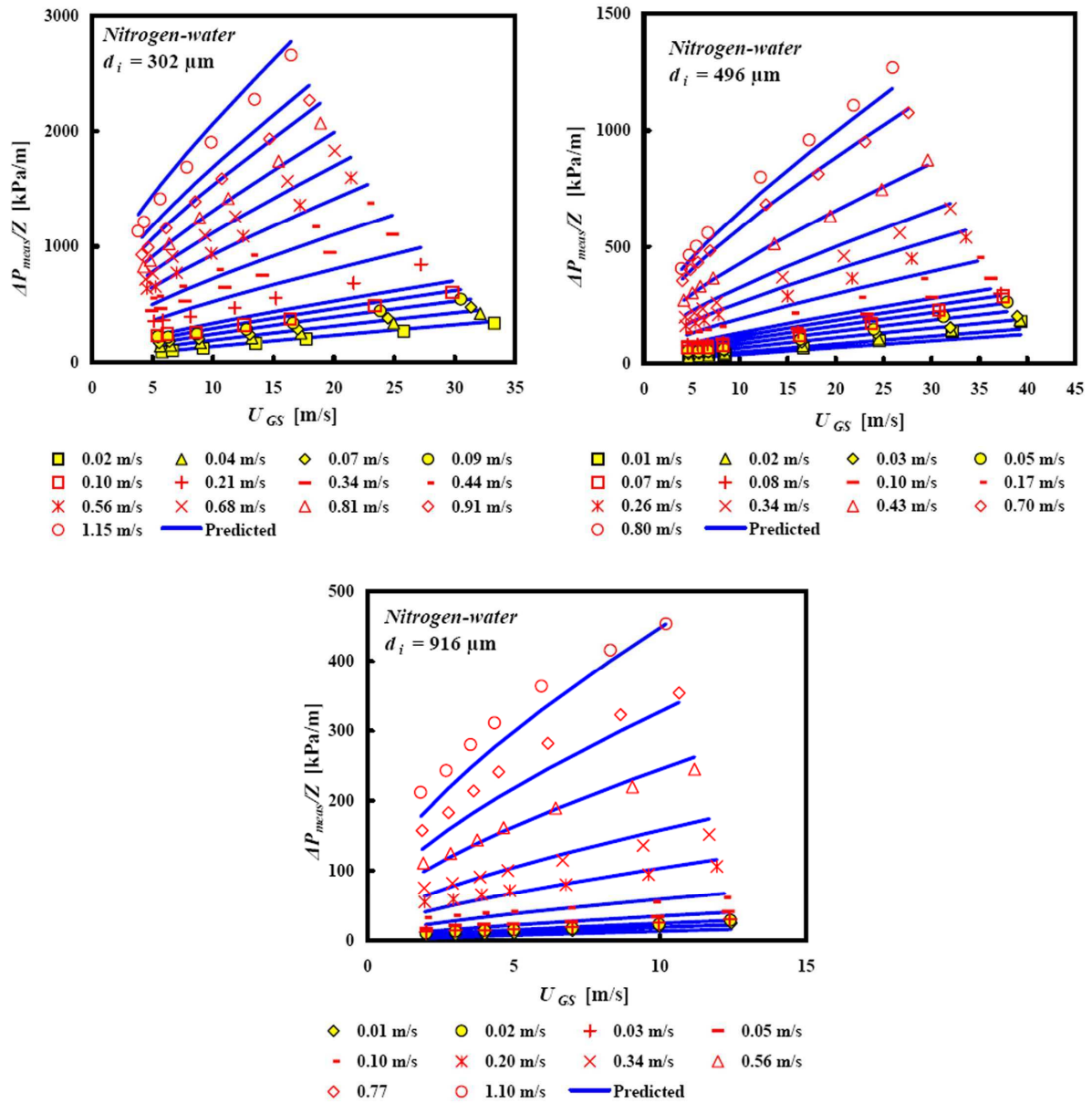


Figure 3-8: The comparison between the measured two-phase pressure drop in circular horizontal microchannels in the inertia-dominated region and the predicted results of the new model: nitrogen-water two-phase system in microchannels with inner diameter of 302, 496 and 916 μm

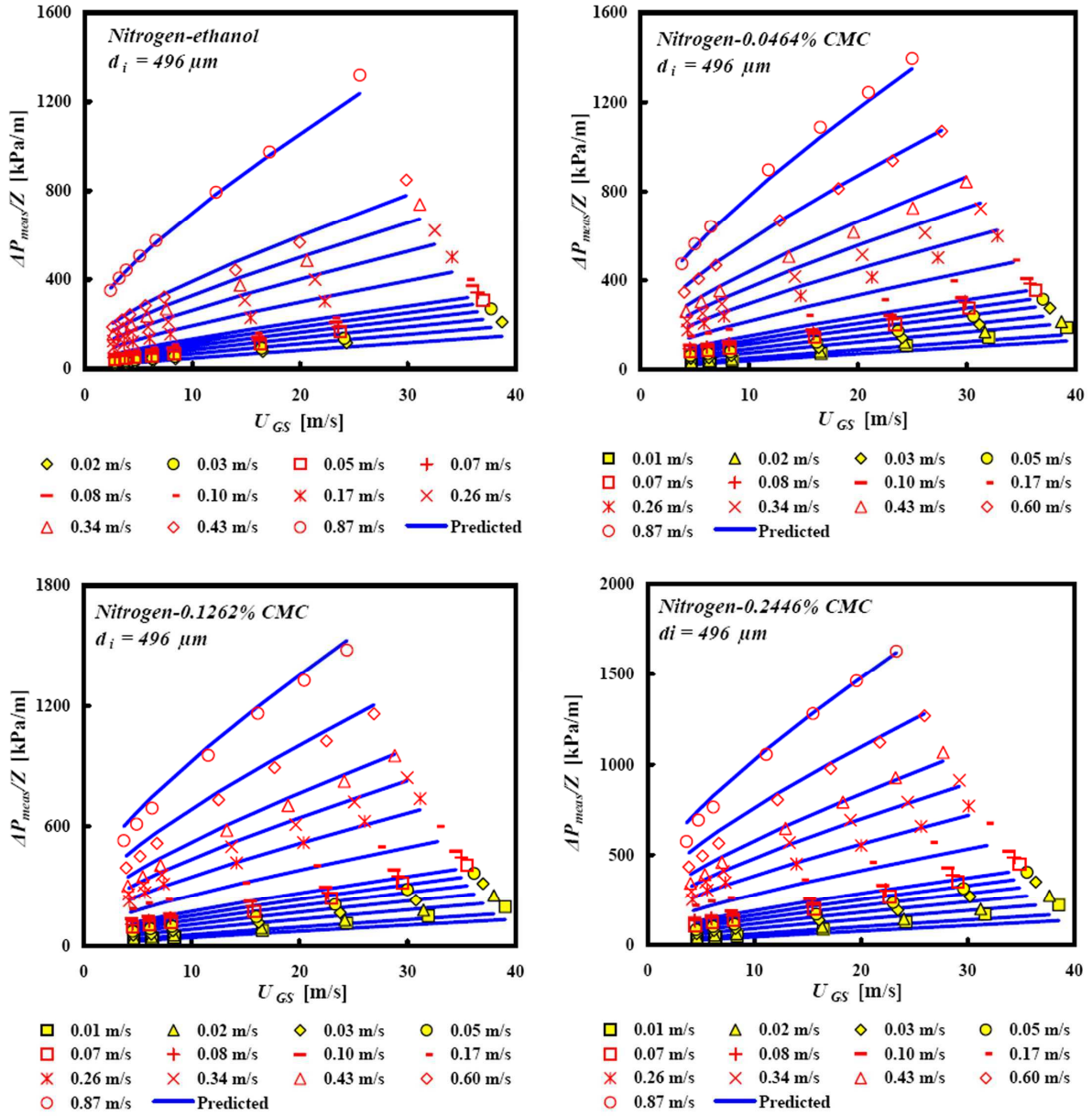


Figure 3-9: The comparison between the measured two-phase pressure drop in the circular horizontal microchannel in the inertia-dominated region and the predicted results of the new model: nitrogen-ethanol two-phase flow and three nitrogen-CMC aqueous solutions two-phase flow system with different concentration: 0.0464%, 0.1262% and 0.2446% in the microchannel with inner diameter of $496 \mu\text{m}$

3.5.4 Verification of the modified Lockhart-Martinelli model using presently proposed C correlation

The modified model proposed in the present work is verified with several groups of experimental pressure drop data in mini or microchannels reported in literature (Kawahara et al., 2002; Niu et al., 2009; Triplett et al., 1999; Yue et al., 2004), as shown in Figure 3-10. Although a lot of researches have been reported, the original data of two-phase pressure drop in mini or microchannel are difficult to obtain, and four groups of data are collected for verification. The minimum gas velocities of these data ($U_{GS} = 1.10$ m/s for Triplett's data; $U_{GS} = 8$ m/s for Kawahara's data; $U_{GS} = 2.85$ m/s for Yue's data; $U_{GS} = 1.75$ m/s for Niu's data) are determined according to the transition criteria proposed in the part I of this paper to ensure that the experimental results employed for verification fall within the inertia-dominated region. It is shown in Figure 3-10 that the present model can well predict the experimental data employed here, not only for circular microchannel, but also for rectangular microchannel ($E_m = 11.40\%$ and $P_{30\%} = 99.13\%$ for Yue's data). Good agreement between the predictions and these data also indicates that the present proposed model can well predict the effects of channel size (from $100\ \mu\text{m}$ to $1.1\ \text{mm}$) and the liquid properties ($E_m = 15.44\%$ and $P_{30\%} = 100\%$ for Niu's data; and liquid physical properties of polyethylene glycol dimethyl ether at 20°C : $\rho_L = 1.027\ \text{kg/m}^3$, $\mu_L = 4.3\ \text{mPa}\cdot\text{s}$, $\sigma = 34\ \text{mN/m}$) on the two-phase pressure drop in the inertia-dominated region.

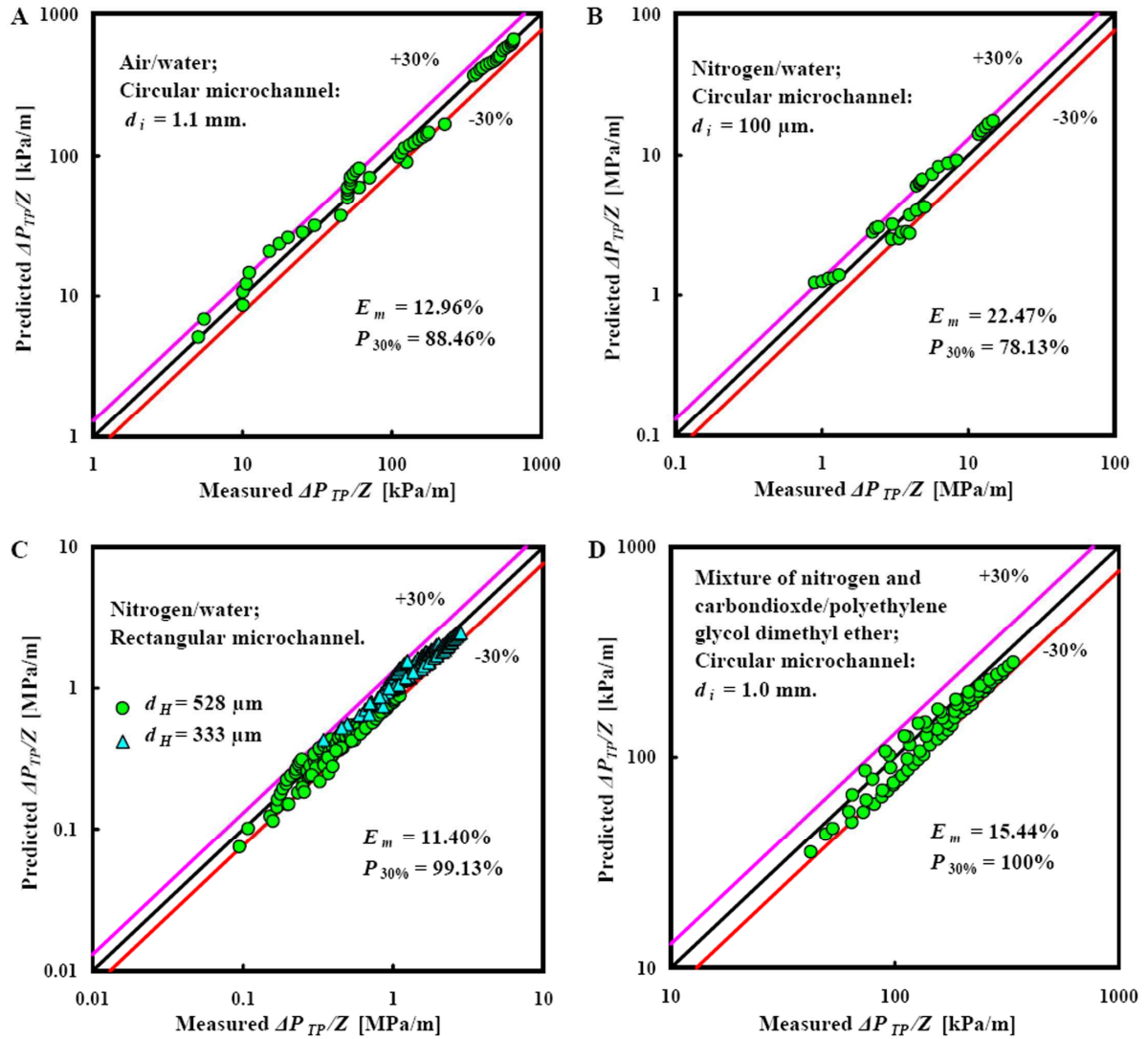


Figure 3-10: Verification of the modified Lockhart-Martinelli model using presently proposed C correlation with experimental data in literature. (A) data in Fig.3 (a) of Triplett et al., 1999; (B) data in Fig.12 of Kawahara et al., 2002; (C) Yue et al., 2004; (D) Niu et al., 2009

3.6 Conclusions

Based on the analysis and discussions of the experimental data presented above, we list the major findings as follows:

(1) The two-phase pressure drop was found highly dependent on the flow patterns, and the typical trend could be divided into three regions: (I) bubbly and slug flow regimes (the surface tension-dominated region); (II) unstable slug flow regime (the transition region); (III)

slug-annular, annular and churn flow regimes (the inertia-dominated region). It matches the Akbar's division of entire gas-liquid two-phase flow pattern map in microchannels according to the two-phase flow mechanism.

(2) Homogeneous-flow model cannot well predict the two-phase pressure drop in microchannels for that the interaction between two phases is not considered. Lockhart-Martinelli models using Chisholm parameter (C) correlations proposed by Chisholm (1958), Yue et al. (2004), Kawahara et al. (2009) and Lee et al. (2010) could provide better (but unsatisfied) predictions with respect to our experimental data.

(3) The C -value increases with channel diameter and decreases with liquid viscosity. The influence of surface tension on C -value is inconspicuous in the inertia-dominated region.

(4) A new and simple C correlation based on Reynolds numbers of gas and liquid was developed to modify the Lockhart-Martinelli model for prediction of the two-phase pressure drop in the inertia-dominated region. The predictions show very good agreement with our experimental data and others' reported in literature.

The study of pressure drop characteristics of gas-liquid flow in circular horizontal microchannels in the surface tension-dominated region will be presented in the next chapter, since the two-phase flow mechanisms in that region is rather different from that in the inertia-dominated region. New methods that differ from the current Lockhart-Martinelli model may be indispensable for better prediction of the two-phase pressure drop.

References

- Agostini, B., Revellin, R., Thome, J.R., Fabbri, M., Michel, B., Calmi, D., Kloter, U., 2008. High heat flux flow boiling in silicon multi-microchannels - Part III: Saturated critical heat flux of R236fa and two-phase pressure drops. *International Journal of Heat and Mass Transfer* 51, 5426-5442.
- Akbar, M.K., Plummer, D.A., Ghiaasiaan, S.M., 2003. On gas-liquid two-phase flow regimes in microchannels. *International Journal of Multiphase Flow* 29, 855-865.
- Armand, A.A., 1946. The resistance during the movement of a two-phase system in horizontal pipes *Izvestiya Vses. Teplotekh. Inst.* 1, 16-23.
- Awad, M.M., Muzychka, Y.S., 2008. Effective property models for homogeneous two-phase flows. *Experimental Thermal and Fluid Science* 33, 106-113.
- Beattie, D.R.H., Whalley, P.B., 1982. A simple two-phase frictional pressure drop calculation method. *International Journal of Multiphase Flow* 8, 83-87.
- Chen, I.Y., Chen, Y.-M., Liaw, J.-S., Wang, C.-C., 2007. Two-phase frictional pressure drop in small rectangular channels. *Experimental Thermal and Fluid Science* 32, 60-66.
- Cheng, L., Ribatski, G., Moreno Quibén, J., Thome, J.R., 2008. New prediction methods for CO₂ evaporation inside tubes: Part I - A two-phase flow pattern map and a flow pattern based phenomenological model for two-phase flow frictional pressure drops. *International Journal of Heat and Mass Transfer* 51, 111-124.
- Chisholm, D., Laird, A.D.K., 1958. Two-phase flow in rough tubes. *Trans. ASME* 80, 276-286.
- Choi, C.W., Yu, D.I., Kim, M.H., 2010. Adiabatic two-phase flow in rectangular microchannels with different aspect ratios: Part II - bubble behaviors and pressure drop in single bubble. *International Journal of Heat and Mass Transfer* 53, 5242-5249.
- Choi, C.W., Yu, D.I., Kim, M.H., 2011. Adiabatic two-phase flow in rectangular microchannels with different aspect ratios: Part I - Flow pattern, pressure drop and void fraction. *International Journal of Heat and Mass Transfer* 54, 616-624.
- Choi, K.-I., Pamitran, A.S., Oh, C.-Y., Oh, J.-T., 2008. Two-phase pressure drop of R-410A in horizontal smooth minichannels. *International Journal of Refrigeration* 31, 119-129.
- Chung, P.M.Y., Kawaji, M., 2004. The effect of channel diameter on adiabatic two-phase flow characteristics in microchannels. *International Journal of Multiphase Flow* 30, 735-761.

- Cicchitti, A., Lombardi, C., Silvestri, M., Soldaini, G., Zavattarelli, R., 1960. Two-phase cooling experiments: pressure drop, heat transfer and burnout measurements. *Energia nuclear*, Milano 7, 407-425.
- Collier, J.G., Thome, J.R., 1994. *Convective boiling and condensation*. Oxford University Press, New York, USA
- Dukler, A.E., Wicks, M., Cleveland, R.G., 1964. Frictional pressure drop in two-phase flow: A. A comparison of existing correlations for pressure loss and holdup. *AIChE Journal* 10, 38-43.
- English, N.J., Kandlikar, S.G., 2006. An experimental investigation into the effect of surfactants on air-water two-phase flow in minichannels. *Heat Transfer Engineering* 27, 99-109.
- Holland, F.A., Bragg, R., 1995. *Flow of incompressible Newtonian fluids in pipes and channels*, Fluid Flow for Chemical Engineers (Second Edition). Butterworth-Heinemann, Oxford, pp. 70-95.
- Hwang, Y.W., Kim, M.S., 2006. The pressure drop in microtubes and the correlation development. *International Journal of Heat and Mass Transfer* 49, 1804-1812.
- Jassim, E.W., Newell, T.A., 2006. Prediction of two-phase pressure drop and void fraction in microchannels using probabilistic flow regime mapping. *International Journal of Heat and Mass Transfer* 49, 2446-2457.
- Kawahara, A., Chung, P.M.Y., Kawaji, M., 2002. Investigation of two-phase flow pattern, void fraction and pressure drop in a microchannel. *International Journal of Multiphase Flow* 28, 1411-1435.
- Kawahara, A., Sadatomi, M., Nei, K., Matsuo, H., 2009. Experimental study on bubble velocity, void fraction and pressure drop for gas-liquid two-phase flow in a circular microchannel. *International Journal of Heat and Fluid Flow* 30, 831-841.
- Lee, C.Y., Lee, S.Y., 2008. Pressure drop of two-phase plug flow in round mini-channels: Influence of surface wettability. *Experimental Thermal and Fluid Science* 32, 1716-1722.
- Lee, H.J., Lee, S.Y., 2001. Pressure drop correlations for two-phase flow within horizontal rectangular channels with small heights. *International Journal of Multiphase Flow* 27, 783-796.
- Lee, H.J., Liu, D.Y., Alyousef, Y., Yao, S.C., 2010. Generalized two-phase pressure drop and heat transfer correlations in evaporative micro/minichannels. *Journal of Heat Transfer-Transactions of the ASME* 132.
- Lee, J., Mudawar, I., 2005. Two-phase flow in high-heat-flux micro-channel heat sink for refrigeration cooling applications: Part I--pressure drop characteristics. *International Journal of Heat and Mass Transfer* 48, 928-940.
- Li, W., Wu, Z., 2010. A general correlation for adiabatic two-phase pressure drop in micro/mini-channels. *International Journal of Heat and Mass Transfer* 53, 2732-2739.
- Lin, S., Kwok, C.C.K., Li, R.Y., Chen, Z.H., Chen, Z.Y., 1991. Local frictional pressure drop during vaporization

- of R-12 through capillary tubes. *International Journal of Multiphase Flow* 17, 95-102.
- Liu, D.S., Wang, S.D., 2008. Flow pattern and pressure drop of upward two-phase flow in vertical capillaries. *Industrial & Engineering Chemistry Research* 47, 243-255.
- Lockhart, R.W., Martinelli, R.C., 1949. Proposed correlation of data for isothermal 2-phase, 2-component flow in pipes *Chemical Engineering Progress* 45, 39-48.
- Ma, Y., Ji, X., Wang, D., Fu, T., Zhu, C., 2010. Measurement and correlation of pressure drop for gas-liquid two-phase flow in rectangular microchannels. *Chinese Journal of Chemical Engineering* 18, 940-947.
- McAdams, W.H., Woods, W.K., Heroman, L.C., 1942. Vaporization inside horizontal tubes-II. Benzene-oil mixture. *Trans. ASME* 64, 193.
- Mishima, K., Hibiki, T., 1996. Some characteristics of air-water two-phase flow in small diameter vertical tubes. *International Journal of Multiphase Flow* 22, 703-712.
- Moreno Quibén, J., Thome, J.R., 2007a. Flow pattern based two-phase frictional pressure drop model for horizontal tubes, Part II: New phenomenological model. *International Journal of Heat and Fluid Flow* 28, 1060-1072.
- Moreno Quibén, J., Thome, J.R., 2007b. Flow pattern based two-phase frictional pressure drop model for horizontal tubes. Part I: Diabatic and adiabatic experimental study. *International Journal of Heat and Fluid Flow* 28, 1049-1059.
- Nino, V.G., Hrnjak, P.S., Newell, T.A., 2002. Characterization of two-phase flow in microchannels, Air Conditioning and Refrigeration Center, College of Engineering. University of Illinois at Urbana-Champaign.
- Nino, V.G., Jassim, E.W., Hrnjak, P.S., Newell, T.A., 2006. Flow-regime-based model for pressure drop predictions in microchannels. *Hvac&R Research* 12, 17-34.
- Niu, H.N., Pan, L.W., Su, H.J., Wang, S.D., 2009. Flow pattern, pressure drop, and mass transfer in a gas-liquid concurrent two-phase flow microchannel reactor. *Industrial & Engineering Chemistry Research* 48, 1621-1628.
- Owens, W.L., 1961. Two-phase pressure gradient. *International Development in Heat Transfer, Part II*, ASME, New York.
- Pamitran, A.S., Choi, K.I., Oh, J.T., Hrnjak, P., 2010. Characteristics of two-phase flow pattern transitions and pressure drop of five refrigerants in horizontal circular small tubes. *International Journal of Refrigeration-Revue Internationale Du Froid* 33, 578-588.

- Qu, W., Mudawar, I., 2003. Measurement and prediction of pressure drop in two-phase micro-channel heat sinks. *International Journal of Heat and Mass Transfer* 46, 2737-2753.
- Rebrov, E.V., 2010. Two-phase flow regimes in microchannels. *Theoretical Foundations of Chemical Engineering* 44, 355-367.
- Saisorn, S., Wongwises, S., 2008. An inspection of viscosity model for homogeneous two-phase flow pressure drop prediction in a horizontal circular micro-channel. *International Communications in Heat and Mass Transfer* 35, 833-838.
- Saisorn, S., Wongwises, S., 2010. The effects of channel diameter on flow pattern, void fraction and pressure drop of two-phase air-water flow in circular micro-channels. *Experimental Thermal and Fluid Science* 34, 454-462.
- Serizawa, A., Feng, Z., Kawara, Z., 2002. Two-phase flow in microchannels. *Experimental Thermal and Fluid Science* 26, 703-714.
- Su, H.J., Niu, H.N., Pan, L.W., Wang, S.D., Wang, A.J., Hu, Y.K., 2010. The characteristics of pressure drop in microchannels. *Industrial & Engineering Chemistry Research* 49, 3830-3839.
- Triplett, K.A., Ghiaasiaan, S.M., Abdel-Khalik, S.I., LeMouel, A., McCord, B.N., 1999. Gas-liquid two-phase flow in microchannels: Part II: void fraction and pressure drop. *International Journal of Multiphase Flow* 25, 395-410.
- Ungar, E.K., Cornwell, J.D., 1992. Two-phase pressure drop of ammonia in small diameter horizontal tubes, *AIAA, Aerospace Ground Testing Conference*, 17th, Nashville, TN, p. 12.
- Warnier, M.J.F., Rebrov, E.V., de Croon, M.H.J.M., Hessel, V., Schouten, J.C., 2008. Gas hold-up and liquid film thickness in Taylor flow in rectangular microchannels. *Chemical Engineering Journal* 135, S153-S158.
- Yan, C., 2007. *Gas-liquid two-phase flow*. Harbin: Harbin Engineering University Press.
- Yue, J., Chen, G.W., Yuan, Q., 2004. Pressure drops of single and two-phase flows through T-type microchannel mixers. *Chemical Engineering Journal* 102, 11-24.
- Yue, J., Luo, L.G., Gonthier, Y., Chen, G.W., Yuan, Q., 2008. An experimental investigation of gas-liquid two-phase flow in single microchannel contactors. *Chemical Engineering Science* 63, 4189-4202.
- Zhang, W., Hibiki, T., Mishima, K., 2010. Correlations of two-phase frictional pressure drop and void fraction in mini-channel. *International Journal of Heat and Mass Transfer* 53, 453-465.
- Zhao, T.S., Bi, Q.C., 2001. Pressure drop characteristics of gas-liquid two-phase flow in vertical miniature triangular channels. *International Journal of Heat and Mass Transfer* 44, 2523-2534.

CHAPTER 4: HYDRODYNAMIC CHARACTERISTICS OF TAYLOR FLOW IN CIRCULAR MICROCHANNELS

As a continuation of the study on the two-phase pressure drop in the inertia-dominated region in the last chapter, this chapter mainly deals with hydrodynamic characteristics of Taylor flow in circular microchannels, which is the major two-phase flow pattern in the surface tension-dominated region. In this chapter, the fundamental hydrodynamic characteristics of Taylor flow, such as Taylor bubble velocity, void fraction will be investigated, as well as the formation mechanism of the Taylor flow in the circular microchannels, especially, on which the effects of channel diameter and liquid properties will be presented. Furthermore, the two-phase pressure drop characteristics of Taylor flow will also be studied.

4.1 Introduction

In the last chapter, the two-phase pressure drop in the inertia-dominated region was systematically studied. As an extension, the hydrodynamic characteristics of surface tension-dominated region will be discussed in this chapter. As shown in the two-phase flow pattern maps, the two-phase flow patterns in the surface tension-dominated region, i.e. bubbly flow, slug flow or Taylor flow, take an important part, which is the most familiar two-phase flow pattern of all in the microchannels. In the present study, the bubbly flow is very similar to the Taylor flow in shape and in formation mechanism, except that the lengths of gas bubbles are shorter than that of Taylor flow. Therefore, this chapter mainly concerns the hydrodynamic characteristics of Taylor flow in circular microchannels.

Many researchers (Günther et al., 2004; Thulasidas et al., 1997; Trachsel et al., 2005) found that the liquid phase axial back mixing would decrease significantly because of the gas bubbles in the Taylor flow, besides, the liquid phase radial mixing could be enhanced by the internal circulation in the liquid slug. In addition, gas-liquid reactions or gas-liquid-solid reactions would be improved due to the liquid film between the gas bubbles and the channel wall (Kreutzer et al., 2001; liu et al., 2009; Vandu et al., 2005). Consequently, it is generally agreed that Taylor flow have excellent performances in mass transfer and chemical reactions. Thus, the hydrodynamic characteristics of the Taylor flow, which is the fundamental knowledge to research the gas-liquid or gas-liquid-solid reaction performance in the microchannels, are worthy to deeply study.

During the experiments described in the Chapter 2, besides investigating the effects of channel diameter and liquid physical properties on the two-phase flow pattern and pressure drop characteristics, the two-phase pressure drop in the Taylor flow region was also measured in three circular microchannels ($d_i = 302, 496, 916 \mu\text{m}$). In the meanwhile, the video of Taylor flow was also recorded by a high speed camera, based on which, important parameters of Taylor flow were measured, i.e. bubble velocities, the length of gas bubbles and liquid slugs. In this chapter, hydrodynamic characteristics of Taylor flow, such as Taylor bubble velocity, void fraction and two-phase pressure drop will be discussed, especially the effects of channel

diameter and liquid physical properties. The results will also be compared with the available prediction models, and the reasons responsible for the observed deviation will be analyzed.

4.2 Results and discussion

4.2.1 Taylor bubble velocity and void fraction

Taylor bubble velocity is one of the most important parameters in the Taylor flow. Due to the liquid film between the gas bubbles and channel wall, Taylor bubble velocity is different from velocity of liquid slug. And many researchers considered that Taylor bubble velocity was related to the liquid slug velocity and Ca number in the microchannels. Based on the theoretical analysis of gas bubble's motion in the small tube, Bretherton (1961) proposed the correlation as follow:

$$U_B = \frac{U_{Liquid}}{1-1.29(3Ca)^{2/3}} = \frac{U_{Liquid}}{1-2.68Ca^{2/3}} \quad (4.1)$$

Where $Ca < 0.003$. Liquid slug velocity U_{Liquid} can be deduced from the volume continuity equation and equal to the sum of gas superficial velocity and liquid superficial velocity, described as:

$$U_{Liquid} = U_{GS} + U_{LS} = U_{TP} \quad (4.2)$$

But Liu et al. (2005) found that the predictions of following correlation corresponded well with their experimental results, which expressed as:

$$U_B = \frac{U_{TP}}{1-0.61Ca^{1/3}} \quad (4.3)$$

Where $0.0002 < Ca < 0.003$. However, according to the experimental investigation of air-water two-phase flow in the capillary with inner diameter from 1 to 4 mm, Mishima and Hibiki (1996) suggested that a simple linear correlation could predict well the experimental data, which expressed as:

$$U_B = 1.1U_{TP} \quad (4.4)$$

In the present work, Taylor bubble velocities had linear relationship with the liquid slug velocities, which is very similar to Mishima's correlation, as shown in the Figure 4-1.

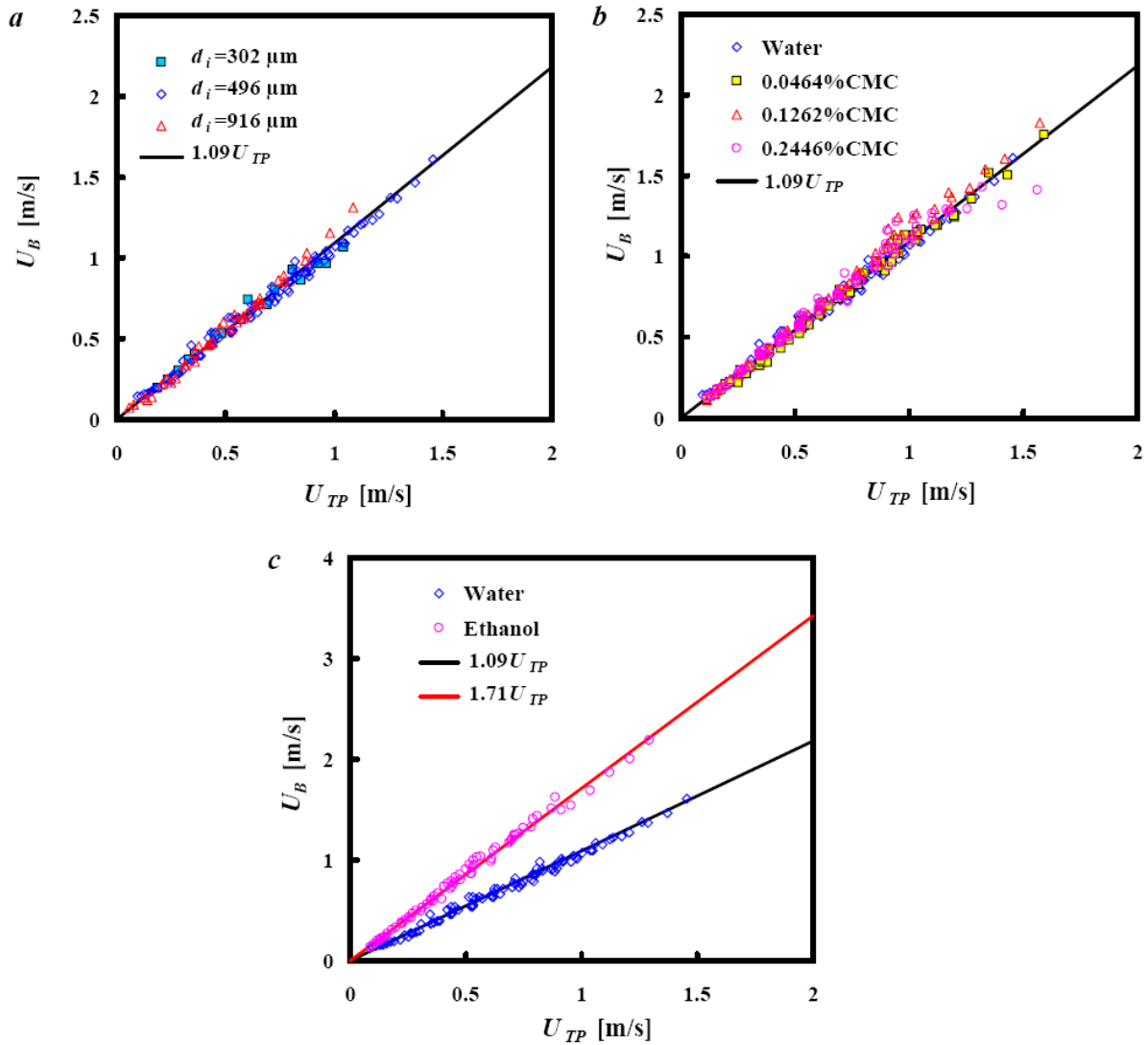


Figure 4-1: Taylor bubble velocities versus the mean velocities in liquid slug in circular microchannels: (a) with different channel diameter; (b), (c) with different liquid physical properties in microchannel with diameter of $496 \mu\text{m}$

From the Figure 4-1(a), it can be noted that the effects of channel diameter on the relationship between Taylor bubble velocities and liquid slug velocities are not obvious. As the discussion in the Chapter 2, it was known that the efficient viscosity of CMC solution would increase with the CMC concentration. Therefore, we can obtain that the effects of liquid viscosity are also so slight, even can be neglected, as shown in the Figure 4-1(b). However, there is significant observed deviation between such linear relationship of nitrogen-water and that of

nitrogen-ethanol two-phase flow system, which can be caused by the variation in the surface tension, two-phase interfacial properties and molecular polarity. But all the linear relationship can be expressed as:

$$U_B = C_0 U_{TP} \quad (4.5)$$

And for nitrogen-water, nitrogen-CMC solution two-phase flow system, $C_0 = 1.09$; for nitrogen-ethanol two-phase flow system, $C_0 = 1.71$. The Eq. 4.5 can be more convenient for application for its simple form, but it still need more experimental verification, which will be our ongoing work in the future.

Void fraction is another important parameter of two-phase flow. Caused by the difference between U_B and U_{TP} , the void fraction ε_G is different from superficial void fraction β , and their relationship depicted in the Figure 4-2. Void fraction is defined as:

$$\varepsilon_G = \frac{U_{GS}}{U_B} \quad (4.6)$$

Generally, there are two type correlations to relate the ε_G to β , one is proposed by Armand (1946), given by:

$$\varepsilon_G = \frac{1}{C_A} \beta, \quad C_A = 1.2 \quad (4.7)$$

Further rewritten as:

$$\varepsilon_G = 0.833\beta \quad (4.8)$$

The other is given by Kawahara et al., (2002), expressed as:

$$\varepsilon_G = \frac{0.03\beta^{0.5}}{1-0.97\beta^{0.5}} \quad (4.9)$$

The comparisons between experimental data and the prediction of the Armand's and Kawahara's correlation are shown in the Figure 4-2, from which it can be noted that Kawahara's correlation absolutely fails in predicting the present experimental results, and obvious deviation is observed when Armand's correlation employed, although similar linear relationships are found. From Figure 4-2(a) and (b), it also can be obtained that channel size

and liquid viscosities hardly affects void fraction in Taylor flow. For nitrogen-water and nitrogen-CMC solutions two-phase flow systems, ε_G almost equals to 0.917β . However, the void fraction of nitrogen-water is obviously different from that of nitrogen-ethanol two-phase flow system, as shown in the Figure 4-2(c), which corresponds to the reason causing the difference of Taylor bubble velocity between the two two-phase flow systems.

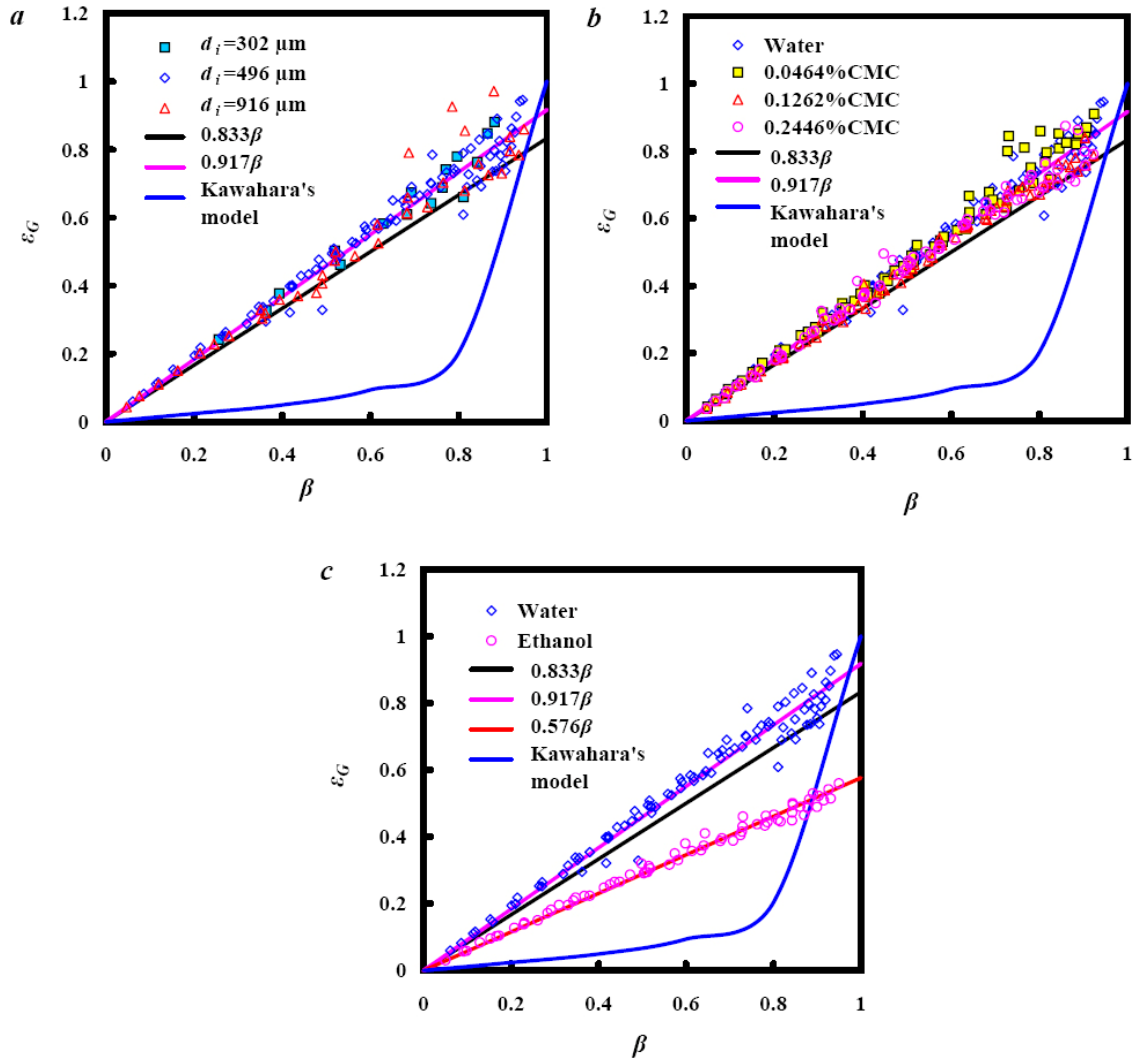


Figure 4-2: void fraction ε_G of Taylor flow in circular microchannels versus homogeneous void fraction β . (a) with different channel diameter; (b), (c) with different liquid physical properties in microchannel with diameter of $496 \mu\text{m}$

4.2.2 Formation mechanism of Taylor bubbles

The formation of Taylor bubbles have been confirmed to be highly dependent on two phase inlet conditions (Garstecki et al., 2005; Garstecki et al., 2006; Salman et al., 2006), which affected significantly on the Taylor bubble length at the entrance of microchannels. Garstecki et al. (2006) have studied the formation mechanism of Taylor bubbles at the T-junction inlet of microchannels, and considered that the break-up mechanism of the gas phase in the in the continuous liquid phase was mainly dependent upon the relative magnitude of forces involved in the Taylor bubbles formation process, i.e. surface tension, shear stress, pressure on the gas phase caused by the continuous fluid, resistance of Taylor bubbles to the continuous fluid. Based on the relative magnitude of forces, formation mechanism of Taylor bubbles was divided into three regions: squeezing regime, dripping regime and jetting regime. When the dominated force in the break-up mechanism was arising from the pressure drop across the emerging bubbles, the Taylor bubble formation process was squeezing dominated, and in the squeezing regime the Ca was considered to be less than 0.02 for their experiments. Then, a simple correlation was proposed to predict the Taylor bubble length in the squeezing regime:

$$L_B / d_i = 1 + \alpha \frac{U_{GS}}{U_{LS}} \quad (4.10)$$

In which α was a fitting parameter, and its value depended upon the structure of the T-junction. Based on the experimental results of gas-liquid flow in the rectangular microchannels with hydraulic diameter of 200, 400 and 667 μm , Yue et al. (2008) found that Eq. (4.10) could predict well the bubble length in the squeezing regime.

In the present study, the values of Ca were less than 0.02 at most operating conditions; therefore the bubble formation process should be dominated by squeezing regime. To examine applicability of Eq. (4.10) for the prediction of Taylor bubble length and to verify the assumption that squeezing regime dominated Taylor bubble formation, the current experimental data were compared with the prediction of Eq. (4.10), as depicted in the Figure 4-3, in which, values of α determined by linear least square regression of experimental data. Approximately, Taylor bubble length could be well represented by the Eq. (4.10) with constant α value. It can be note that the value of α vary with liquid viscosities and surface

tension, but not channel diameter. The reasons can be explored are that the variation of liquid properties can affect the forces involved in the Taylor bubble formation process, such as variation of surface tension, variation of shear stress caused by the change of liquid viscosity, etc.

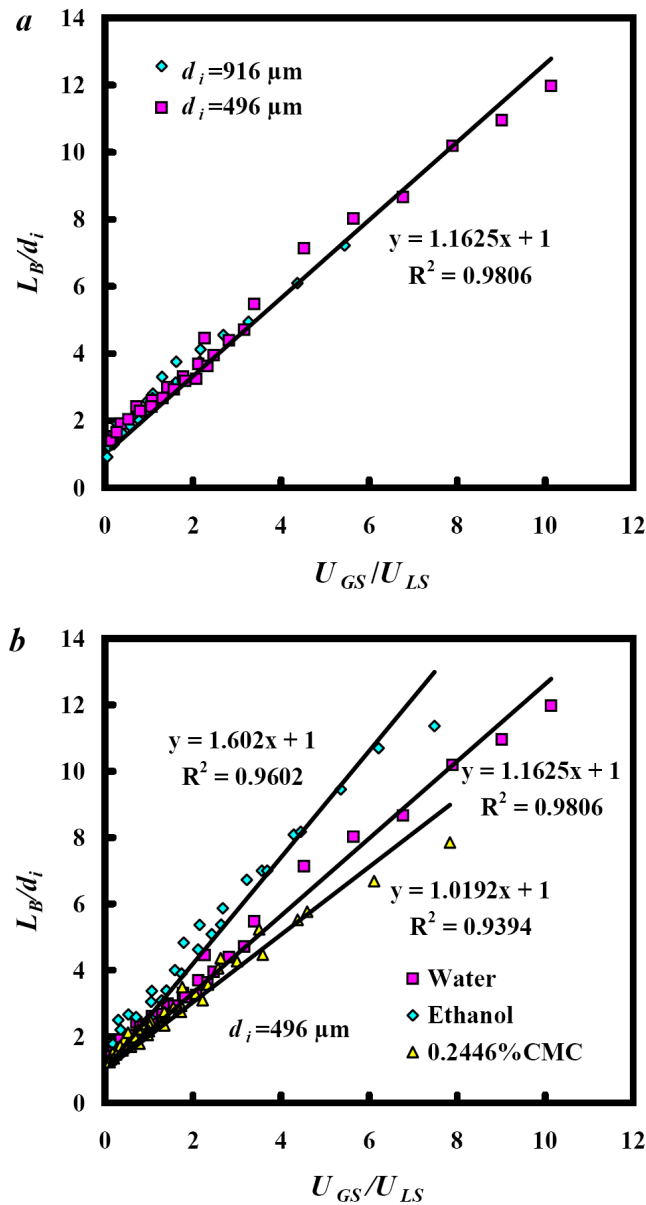


Figure 4-3: L_B / d_i versus U_{GS} / U_{LS} of Taylor flow in squeezing regime in circular microchannels. (a) with different channel diameters: nitrogen-water two-phase flow; (b) with different liquid physical properties in microchannel with diameter of $496 \mu\text{m}$: nitrogen-water, ethanol, 0.2446% CMC two-phase flow, respectively

According to the discussion above, it can be concluded that the Taylor bubble formation mechanism in the present study is dominated by squeezing regime and the Taylor bubble length can be well predicted with the Eq. (4.10), and in which the value of α is highly dependent upon the liquid viscosity and surface tension. The effects of inlet structure, operating orientation and channel section on the Taylor bubble formation, still need experimental and simulation study, necessarily.

4.2.3 Pressure drop characteristics

In the Chapter 3, the two-phase pressure drop in the microchannels was found highly dependent upon the two-phase flow patterns, and the main trend could be divided into three regions: surface tension-dominated region, transition region and inertia-dominated region. The pressure drop in inertia-dominated region was systematically studied and the applicability of homogeneous flow models and separated flow models were examined. It was found that the modified separated flow model could predict the two-phase pressure drop well in the microchannels. However, to predict the pressure drop of Taylor flow, which is the major two-phase flow pattern in the surface tension-dominated region, homogeneous flow model and separated flow model may be not the proper method. To begin with, in the homogeneous flow model, gas and liquid phases are assume to be with equal actual velocities and thoroughly mixed, thus, the two-phase flow can be treated as a single phase flow with average properties of two-phase mixture. As mentioned above, in the Taylor flow, gas bubble velocity is significantly higher than that of liquid phase due to the liquid film between Taylor bubbles and channel wall. Moreover, it is assumed that gas and liquid flow separately in the tube with each phase flowing continuous and occupying a sector of the pipe cross section in the separated flow model. But in the Taylor flow, obviously, the gas phase is discontinuous and the motion of liquid film is very different from that of liquid slug. Finally, Taylor flow can be considered as a transient intermittent flow due to the discontinuous motion of gas bubbles and the alternative exposure of channel wall to the liquid film and liquid slug. Accordingly, Taylor flow can not be regarded as a homogeneous flow or a separated flow, and distinct method will be indispensable for the prediction of two-phase pressure drop in the Taylor flow.

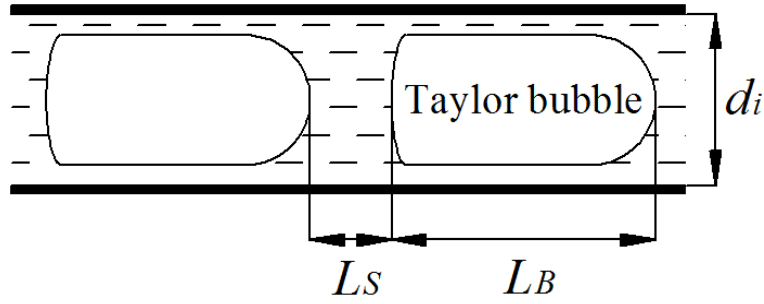


Figure 4-4: Unit cell of Taylor flow

Actually, Taylor flow can be treated as a steady process due to it consists of several or a lot of unit cells (one bubble, the liquid film surrounding the bubble and one slug) which are almost identical, as depicted in the Figure 4-4. Consequently, the pressure drop of Taylor flow can be considered as the sum of the pressure drop of all the unit cells. The frictional pressure drop of one Taylor unit cell consists of three parts: frictional loss in the liquid slug, $\Delta P_{liquid,TUC}$; frictional loss in the liquid film, $\Delta P_{film,TUC}$; the pressure drop over the front and the rear caps, $\Delta P_{cap,TUC}$.

$$\Delta P_{fri,TUC} = \Delta P_{liquid,TUC} + \Delta P_{film,TUC} + \Delta P_{cap,TUC} \quad (4.11)$$

Then the total frictional pressure drop of Taylor flow can be deduced as:

$$\frac{\Delta P_{F,Taylor}}{Z} = \frac{1}{L_B + L_S} (\Delta P_{liquid,TUC} + \Delta P_{film,TUC} + \Delta P_{cap,TUC}) \quad (4.12)$$

in which Z is the length of the microchannel. Generally, for the Taylor flow, both gas flow and liquid flow are in laminar regime (Thulasidas et al., 1997). Therefore, $\Delta P_{liquid,TUC}$ can be regarded as a sum of the additional pressure drop caused by the inner recirculation $\Delta P_{circu,TS}$ and the fully development laminar flow pressure drop in the liquid slug, which is:

$$\Delta P_{liquid,TUC} = \Delta P_{circu,TS} + \frac{64}{\text{Re}_{liquid,TUC}} \frac{L_S \rho_L U_{liquid}^2}{2d_i} \quad (4.13)$$

For the horizontal Taylor flow in the microchannel, liquid film is usually assumed to be nearly at rest (Kreutzer et al., 2005). Thus $\Delta P_{film,TUC}$ is negligible compared to the $\Delta P_{liquid,TUC}$.

The pressure drop over the bubble caps in the circular capillaries can be expressed by the following correlation, which proposed by Bretherton (1961) according to the theoretical study on the motion of bubble in tubes:

$$\Delta P_{cap,TUC} = 7.16(3Ca)^{2/3} \frac{\sigma}{d_i} \quad (4.14)$$

Then the Eq. (4.12) can be further rewritten as:

$$\frac{\Delta P_{F,Taylor}}{Z} = \frac{1}{L_B + L_S} (\Delta P_{circu,TS} + \frac{64}{\text{Re}_{liquid,TUC}} \frac{L_S \rho_L U_{liquid}^2}{2d_i} + \Delta P_{cap,TUC}) \quad (4.15)$$

Kreutzer et al., (2005) implemented experiments to investigate the pressure drop characteristics of Taylor flow in the circular capillary with diameter of 2.3 mm, and verified their experimental findings with CFD simulation. They found that the contribution of $\Delta P_{cap,TUC}$ and $\Delta P_{circu,TS}$ to the frictional loss could be described as an additional function ξ to the friction factor f . ξ was defined as:

$$\xi = a \left(\frac{d_i}{L_S} \left(\frac{\text{Re}_{liquid}}{Ca} \right)^b \right) \quad (4.16)$$

And f could be calculated by:

$$f = \frac{64}{\text{Re}_{liquid}} (1 + \xi) \quad (4.17)$$

Based on the experimental results and numerical findings, it was determined that b in the Eq. (4.16) equaled to 1/3, and $a = 0.07$ for $\text{Re}_{liquid} > 50$, $a = 0.17$ for $\text{Re}_{liquid} \leq 50$.

The total pressure drop of Taylor flow ΔP_{Taylor} in the present work can be expressed as:

$$\Delta P_{Taylor} = \Delta P_{F,Taylor} + \Delta P_{acc} \quad (4.18)$$

In which the ΔP_{acc} calculated by:

$$\Delta P_{acc} = G^2 \left[\left(\frac{x_e}{\rho_G \varepsilon_G} + \frac{(1-x_e)^2}{\rho_L (1-\varepsilon_G)} \right)_{out} - \left(\frac{x_e}{\rho_G \varepsilon_G} + \frac{(1-x_e)^2}{\rho_L (1-\varepsilon_G)} \right)_{in} \right] \quad (4.19)$$

and

$$G = U_{LS}\rho_L + U_{GS}\rho_G \quad (4.20)$$

Thus

$$\Delta P_{F,Taylor} = \Delta P_{Taylor} - \Delta P_{acc} \quad (4.21)$$

In the last section of this chapter, it was obtained that:

$$\varepsilon_G = 0.917\beta \quad (4.22)$$

for nitrogen-water and nitrogen-CMC solutions two-phase systems, and

$$\varepsilon_G = 0.576\beta \quad (4.23)$$

for nitrogen-ethanol two-phase systems.

Finally, the $f \text{Re}_{liquid}$ can be measured from the experimental data as:

$$\left(f \text{Re}_{liquid} \right)_{meas} = \frac{2 \frac{\Delta P_{F,Taylor}}{Z} d_i^2}{U_{TP} \mu_L} \frac{L_B + L_S}{L_S} \quad (4.24)$$

The measured $f \text{Re}_{liquid}$ as a function of L_s / d_i is plotted in the Figure 4-5, as well as its comparison with the prediction of Kreutzer's correlation Eq. (4.17). It can be noted from Figure 4-5 (a) (b) (d) (e) (f) that the most of experimental data are higher than predictions of Eq. (4.17) with $a = 0.07$, but lower than that of Eq. (4.17) with $a = 0.17$. However, Eq. (4.17) would over-predict the experimental data of nitrogen-ethanol two-phase system are significantly, no matter which a value employed, as shown in Figure 4-5 (c).

Walsh et al. (2009) experimentally investigated the hydrodynamic characteristics of Taylor flow in capillaries, and five liquids with various liquid properties were employed in their work. Based on the results, they suggested that $a = 1.92/16 = 0.12$ and $b = 1/3 \approx 0.33$ in the Eq. (4.17). As exhibited in the Figure 4-5, it can be known that Walsh's correlation can predict well the experimental data of nitrogen-water and nitrogen-CMC solutions. Figure 4-6 plots the comparison of measured $f \text{Re}_{liquid}$ with predictions of Walsh's correlation, and the deviations between them are lower than 20% for the most of data.

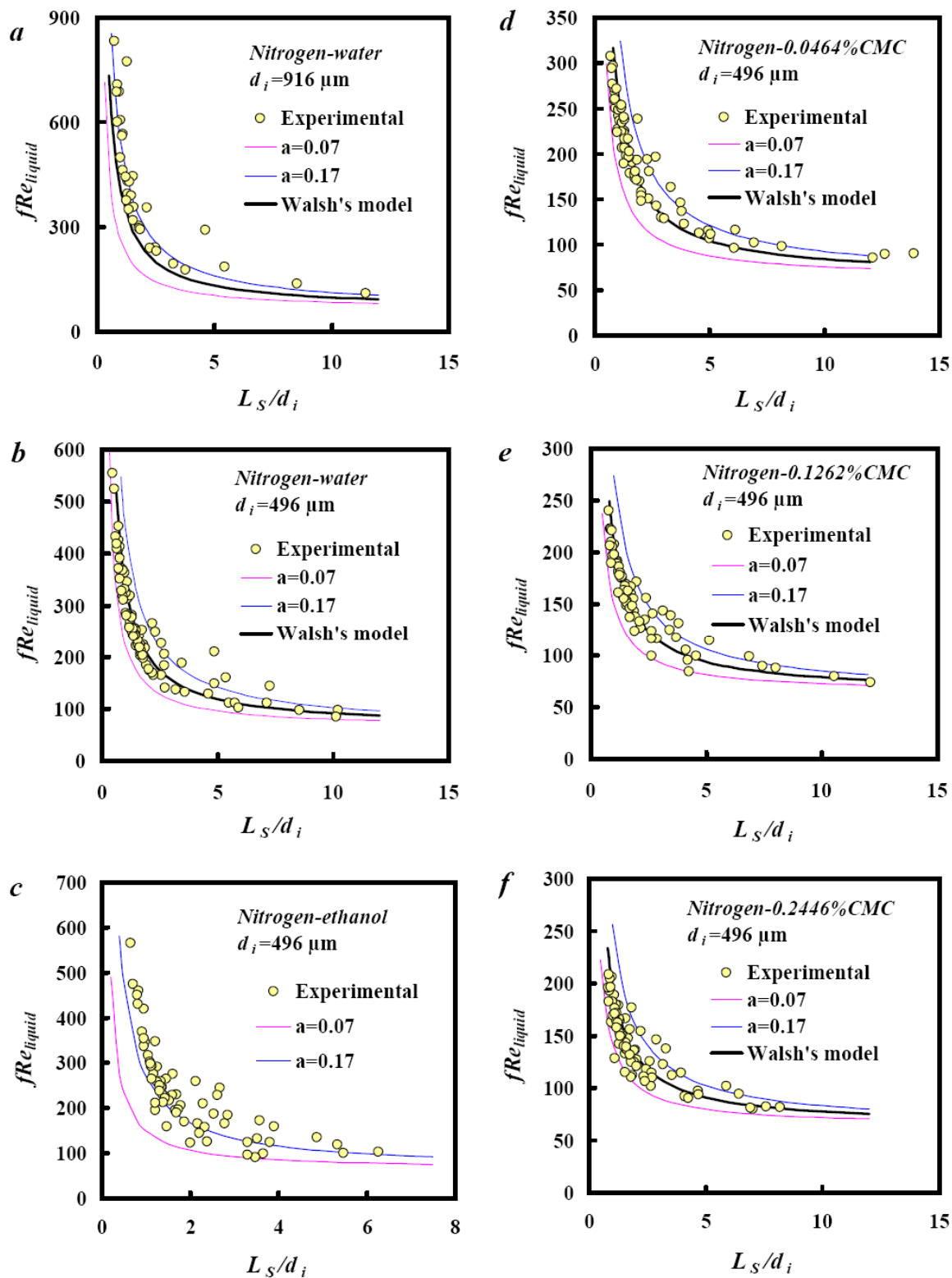


Figure 4-5: fRe_{liquid} versus L_s/d_i of Taylor flow in circular microchannels with different channel diameters and liquid physical properties

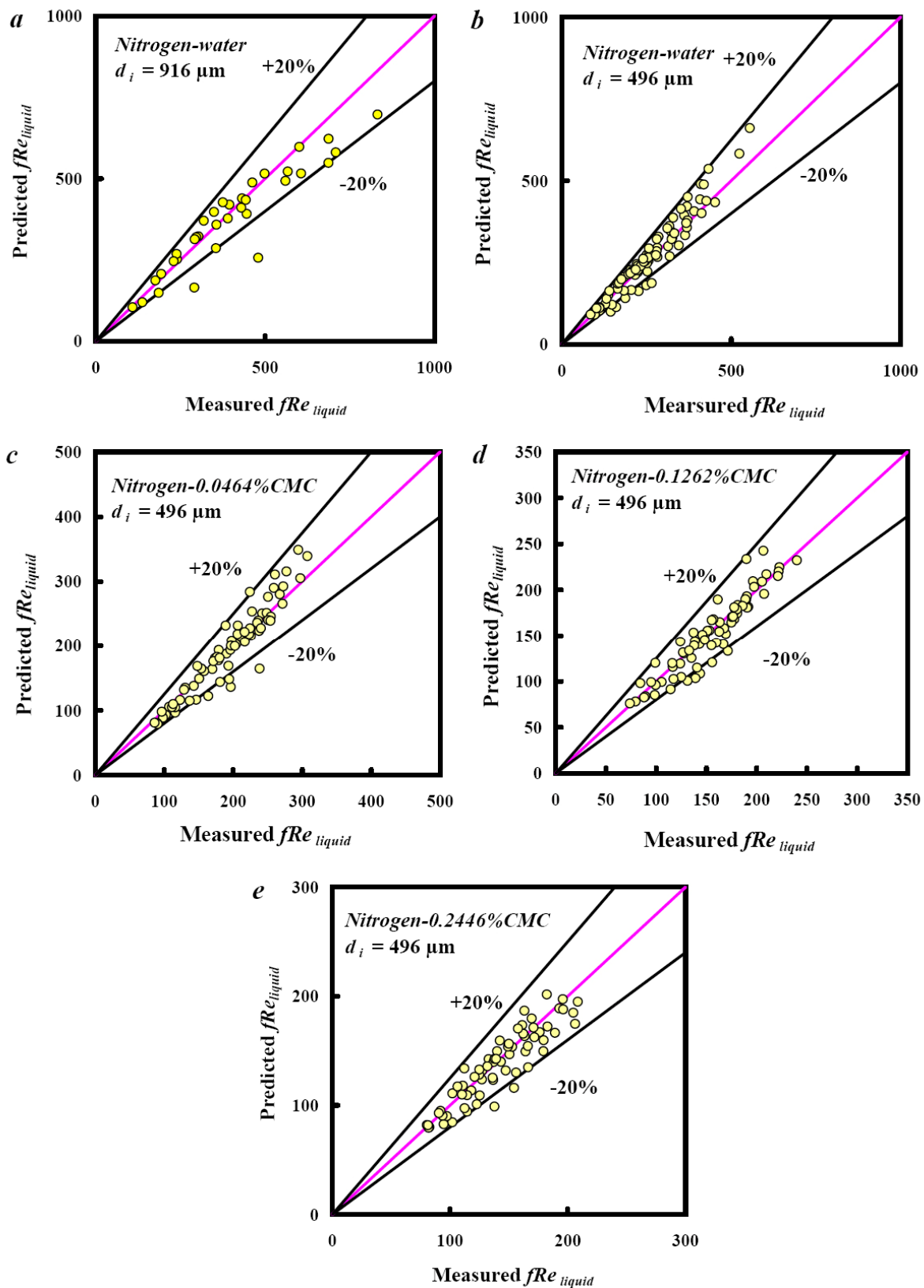


Figure 4-6: The comparison between experimental results of $f Re_{liquid}$ and prediction of Walsh's correlation

However, both Kreutzer's correlation and Walsh's correlation would under-predict the experimental data of nitrogen-ethanol two-phase system, as shown in the Figure 4-7. Kreutzer's correlation is based on the assumption that the Ca should be sufficiently small, less than 0.04. In the present study, for the Taylor flow of nitrogen-water and nitrogen-CMC solutions two-phase flow systems, Ca values are less than 0.05 ($0.0001 < Ca < 0.05$), in accordance with the Kreutzer's assumption, consequently, the experimental data can be predicted well using Kreutzer's model modified by Walsh et al. But for the Taylor flow of nitrogen-ethanol two-phase flow system, Ca ranges from 0.006 to 0.11, in which certain part of experimental data exceed the Kreutzer's assumption. It was found that (Thulasidas et al., 1997), for higher Ca value, the liquid film could not be assumed at rest, and the relative magnitude of inertia force increased causing the aggravation of recirculation in the liquid slug. Therefore, Kreutzer's model will under-predict the frictional loss caused by the motion of liquid film and the recirculation in the liquid slug, and that will lead to the failure to predict the experimental data of nitrogen-ethanol two-phase flow system.

4.3 Conclusions

In this chapter, hydrodynamic characteristics of Taylor flow were discussed. Major conclusions can be drawn as follows:

(1) Taylor bubble velocity showed a good linear relationship with the sum of gas and liquid superficial velocity. Similarly, void fraction could be predicted by a simple linear correlation related to gas phase volumetric fraction. But for the nitrogen-ethanol two phase flow, lopes varied from that of others two-phase flow systems in these two linear relations.

(2) In the present work, the formation mechanism of Taylor bubbles was dominated by squeezing regime, and there was a linear relation between the bubble length to channel diameter ratio and gas to liquid superficial velocity ratio, in which the slope highly depended on the liquid viscosity and surface tension.

(3) Kreutzer's model modified by Walsh et al. could predict well the two-phase pressure drop of Taylor flow in the present experiments at relatively low Ca values.

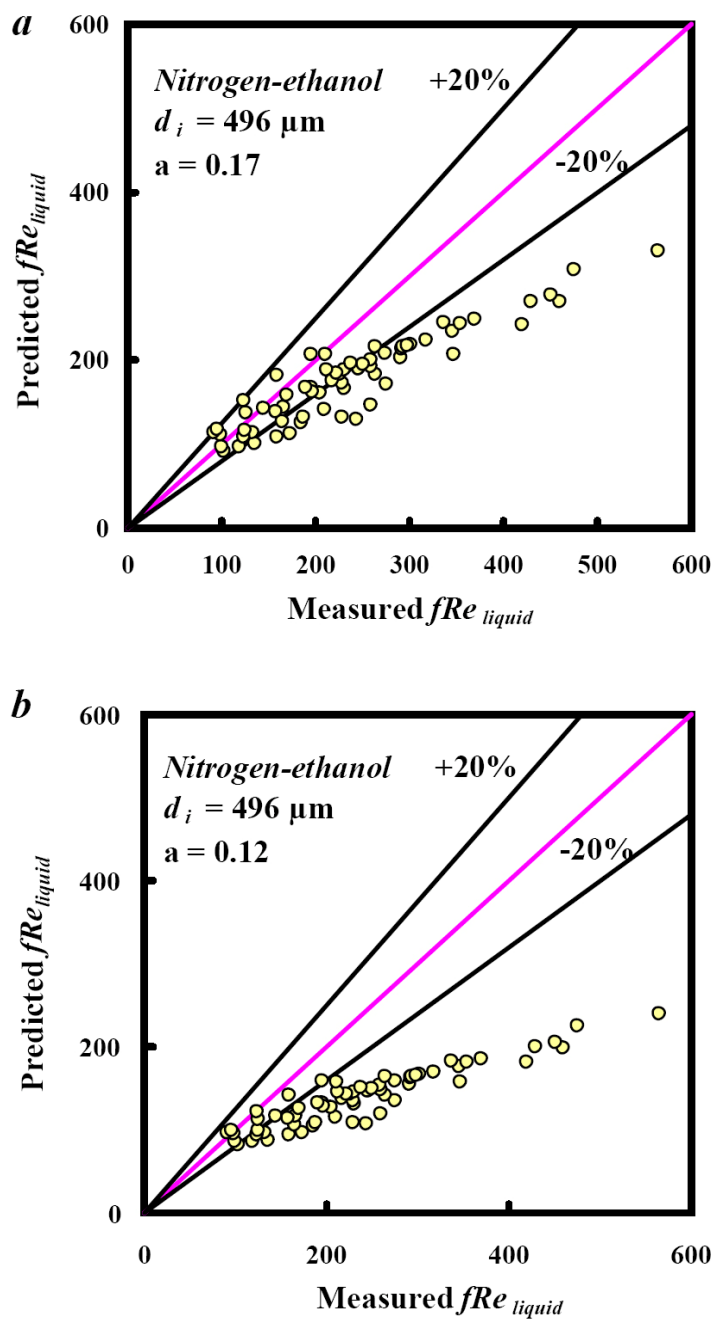


Figure 4-7: The comparison between experimental results of fRe_{liquid} in nitrogen-ethanol two-phase system and prediction of Kreutzer's and Walsh's correlations

References

- Armand, A.A., 1946. The resistance during the movement of a two-phase system in horizontal pipes. *Izvestiya Vses. Teplotekh. Inst.* 1, 16-23.
- Bretherton, F.P., 1961. The motion of long bubbles in tubes. *J. Fluid. Mech.* 10, 166-188.
- Garimella, S., Killion, J.D., Coleman, J.W., 2002. An experimentally validated model for two-phase pressure drop in the intermittent flow regime for circular microchannels. *Journal of Fluids Engineering* 124, 205–214.
- Garstecki, P., Stone, H.A., Whitesides, G.M., 2005. Mechanism for flow-rate controlled breakup in confined geometries: A route to monodisperse emulsions. *Physical Review Letters* 94, 164501.
- Garstecki, P., Fuerstman, M.J., Stone, H.A., Whitesides, G.M., 2006. Formation of droplets and bubbles in a microfluidic T-junction – scaling and mechanism of break-up. *Lab on a Chip* 6, 437-446.
- Günther, A., Khan, S. A., Thalmann, M., Trachsel, F., Jensen, K. F., 2004. Transport and reaction in microscale segmented gas-liquid flow. *Lab on a Chip* 4, 278-286.
- Kawahara, A., Chung, P.M.Y., Kawaji, M., 2002. Investigation of two-phase flow pattern, void fraction and pressure drop in a microchannel. *International Journal of Multiphase Flow* 28, 1411-1435.
- Kreutzer, M.T., Du, D., Heiszwolf, J.J., Kapteijn, F., Moulijn, J.A., 2001. Mass transfer characteristics of three-phase monolith reactors. *Chemical Engineering Science* 56, 6015-6023.
- Kreutzer, M.T., Kapteijn, F., Moulijn, J.A., Kleijn, C.R., Heiszwolf, J., 2005. Inertial and interfacial effects on pressure drop of Taylor flow in capillaries. *AICHE Journal* 51, 2428-2440.
- Liu, D., Zhang, J., Li, D., Kong, Q., Zhang, T., Wang, S., 2009. Hydrogenation of 2-ethylanthraquinone under Taylor flow in single square channel monolith reactor. *AICHE Journal* 55, 726-736.
- Liu, H., Vandu, C. O., Krishna, R., 2005. Hydrodynamics of Taylor flow in vertical capillaries: flow regimes, bubbles rise velocity, liquid slug length, and pressure drop. *Ind. Eng. Chem. Res.* 44, 4884-4897.
- Lockhart, R.W., Martinelli, R.C., 1949. Proposed correlation of data for isothermal two-phase, two-component flow in pipes. *Chemical Engineering Progress* 45, 39-48.
- Mishima, K., Hibiki, T., 1996. Some characteristics of air-water two-phase flow in small diameter vertical tubes. *Int. J. Multiphase Flow* 22, 703-712.
- Salman, W., Gavriilidis, A., Angeli, P., 2006. On the formation of Taylor bubbles in small tubes. *Chemical*

- Engineering Science 61, 6653-6666.
- Thulasidas, T. C., Abraham, M. A., Cerro, R. L., 1997. Flow patterns in liquid slugs during bubble-train flow inside capillaries. *Chemical Engineering Science* 52, 2947-2962.
- Trachsel, F., Gunther, A., Khan, S., Jensen, K. F., 2005. Measurement of residence time distribution in microfluidic systems. *Chemical Engineering Science* 60, 5729-5737.
- Vandu, C. O., Liu, H., Krishna, R., 2005. Mass transfer from Taylor bubbles rising in single capillaries. *Chemical Engineering Science* 60, 6430-6437.
- Walsh, E., Muzychka, Y., Walsh, P., Egan, V., Punch, J., 2009. Pressure drop in two phase slug/bubble flows in mini scale capillaries. *International Journal of Multiphase flow* 25, 879-884.
- Yan, C., 2007. Gas-liquid two-phase flow. Harbin: Harbin Engineering University Press.
- Yue, J., Luo, L., Gonthier, Y., Chen, G., Yuan, Q., 2008. An experimental investigation of gas-liquid two-phase flow in single microchannel contactors. *Chemical Engineering Science* 63, 4189-4202.
- Yue, J., Luo, L., Gonthier, Y., Chen, G., Yuan, Q., 2009. An experimental study of air-water Taylor flow and mass transfer inside square microchannels. *Chemical Engineering Science* 64, 3697-3708.

CHAPTER 5: OXIDATION OF HYDROGENATED 2-ETHYLTETRAHYDROANTHRAQUINONE IN CIRCULAR MICROCHANNEL

This chapter mainly concerns the oxidation of hydrogenated 2-ethyltetrahydroanthraquinone (THEAQH₂) in the circular microchannel, as an attempt on application of microchemical technology in the hydrogen peroxide industrial production process. One aim of this study is to verify the two-phase flow pattern transition model and pressure drop prediction model of inertia-dominated region proposed in the previous chapters. The other aim, also the major one, is to experimentally investigate the oxidation of THEAQH₂ in circular microchannel, especially the characteristics of gas-liquid specific interfacial area and the effects of operating conditions.

5.1 Introduction

Hydrogen peroxide is one of the most important chemical products, which is considered as an ideal, environmental friendly oxidizer, for that the by-products is only water after oxidation. Thus, it is widely used in the municipal wastewater treatment, propellant in aerospace, medical hygiene application, pulp- and paper-bleaching, as well as in others industrial process employed as feed-stock, i.e. electronic material production, pharmaceutical synthesis, organic synthesis, etc. Nowadays, hydrogen peroxide is manufactured almost exclusively by the self-oxidation of 2-alkyl anthrahydroquinone to the corresponding 2-alkyl anthraquinone in the so-called anthraquinone process, which mainly consists of three parts: catalytic hydrogenation, self-oxidation and extraction, generally. In the traditional industrial production process, the self-oxidation step, which is a gas-liquid two-phase reaction process, usually occurs in big tower two-phase reactors with diameter more than 3 m and height more than 20 m, and its limitations are obvious: low efficiency, poor safety, high energy consumption, etc. It is worthy to improve the self-oxidation step to meet the market demands, as well as environmental requirement, and microchemical technology provides a new method for its excellent performance in process intensification.

In this chapter, oxygen-anthraquinone working solution two-phase flow in a circular microchannel and the oxidation of THEAQH₂ in a circular microchannel with diameter of 900 μm and length of 30 cm will be investigated. Specifically, the gas-liquid specific interfacial area will be calculated with the image of flow patterns recorded by a fast camera, and the effects of temperature, operating pressure, and liquid velocity on the oxidation will be discussed.

5.2 Experiments

5.2.1 Set up

The experimental setup constructed for this study is composed of a test section, gas and liquid circuits and the data acquisition system, as depicted in Figure 5-1. A precise pump

(Shimadzu, LC-15C, 0.001-10 mL/min) were used to control the liquid flow in the microchannel. The pulse of the pump was maximally reduced by installation of two buffer tanks, so that constant flow rate and steady flow in the microchannel could be achieved. The temperature of liquid was controlled by using a water bath. Flow rate of gas was controlled and adjusted by mass flow controllers (Seven star: D07-11C, 0-500 mL/min; D07-7A, 0-100 mL/min; D07-7A, 0-30 mL/min; D07-7B, 0-2 L/min). A T type junction connected with the downstream microchannel was prepared for the pre-contact of gas and liquid. To visualize and record the two-phase flow patterns in the microchannels, a fast camera (Canon 5D Mark II, shutter speed: 1/8000 S) was installed at a side of the test channel, with background illumination provided by two homemade LED lamps installed at the opposite side. A pressure difference sensor (Micro, MDM490, 0-70 kPa) was employed to measure the pressure drop of two-phase flow through the microchannel. A back-pressure valve was paired up with a pressure sensor (Micro, MPM489, and 0-1 MPa) to control the operating pressure during experiments.

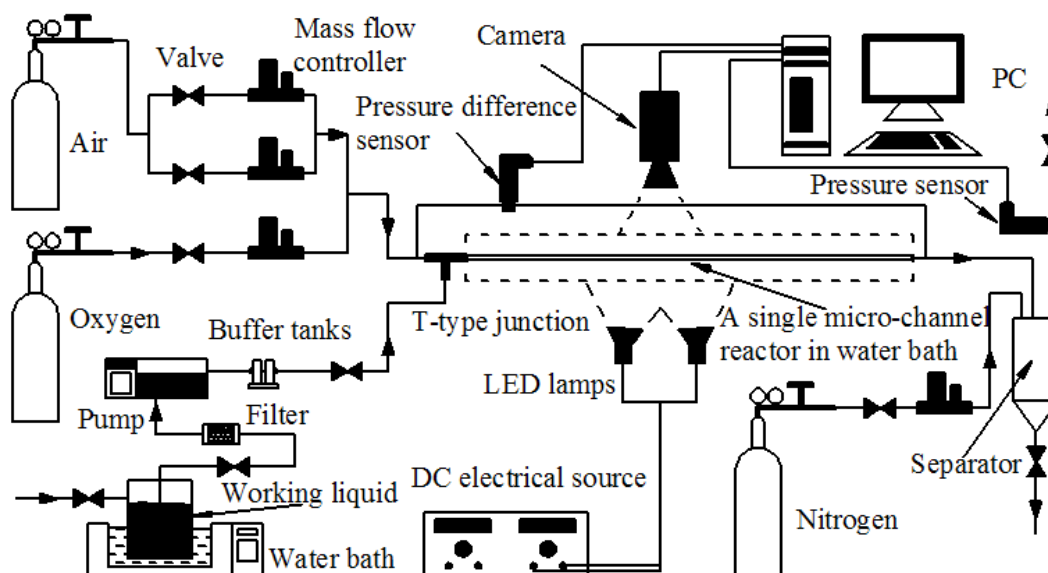


Figure 5-1: Schematic diagram of experimental setup

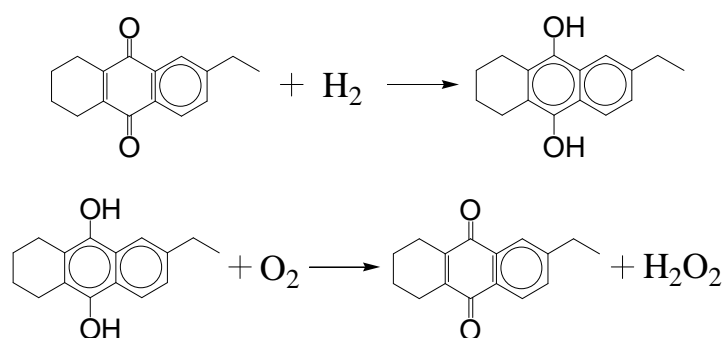
The circular microchannel with diameter of 900 μm and length of 30 cm has been used in the experiments. For convenience of visualization, these microchannels were made of

quartz glass, and fabricated through precise hot-stretching by “Verre et Séparation Technologies S.A.”, Lyon, France. The T junction through which gas and liquid were fed to the main microchannel was made of stainless steel and fabricated by Nanzhong Mould Company.

Before the oxidation in the microchannel and in the separator after the microchannel, the hydrogenated anthraquinone working solution was kept in the atmosphere of nitrogen to prevent it from oxidizing out of the microchannel.

5.2.2 Working solution and analytical method

The anthraquinone working solution was get from a hydrogen peroxide production workshop of SINOPEC CORP, in which there were 33.1 g/L 2-ethylanthraquinone (EAQ) and 91.5 g/L 2-ethyltetrahydroanthraquinone (THEAQ) dissolved in mixture of heavy aromatics and trioctyl phosphate (Zhang, 2008). Table 5-1 tabulated the physical properties of working solution and oxygen. It was confirmed that only THEAQ involved in the hydrogenation, corresponding to THEAQH₂ in oxidation (Berglin and Schoon, 1983; Santacesaria et al., 1987), and the reaction scheme could be expressed as follow:



In the oxidation, the working liquid was catalytic hydrogenated anthraquinone working solution. It would be sampled and completely oxidized with flowing air to obtain hydrogen peroxide as an oxidation product. Hydrogen peroxide in the oxidation mixer was extracted with de-ionized water. In the presence of sulfuric acid, the extraction products were titrated with standard potassium permanganate solution in order to determine the amount of hydrogen peroxide, which corresponding to the amount of THEAQH₂ in the hydrogenated working solution sample, finally, total concentration of THEAQH₂ C_{total} in the hydrogenated anthraquinone working solution could be determined. The amount of hydrogen peroxide

produced in the oxidized working solution could also be determined by titration, and then the amount of THEAQH₂ oxidized in the microchannel would be determined, whose concentration could be expressed as: C_{oxy} . Accordingly, the oxidation conversion could be defined as: $\eta = C_{oxy} / C_{total}$.

Table 5-1: The Physical Properties of Working liquid and oxygen (Poling et al., 2001; Qingdao college of chemical engineering, 2002)

T	Working liquid			Oxygen	
	μ_L	ρ_L	σ	μ_G	ρ_G
°C	mPa·s	kg/m ³	mN/m	mPa·s	kg/m ³ (atmospheric pressure)
20	2.4	892	31.8	2.1	1.33
30	2.1	888	30.7	2.2	1.29
40	1.8	884	29.6	2.2	1.25
50	1.7	880	28.5	2.3	1.21
60	1.5	876	27.4	2.3	1.17
70	1.4	873	26.3	2.4	1.14

5.3 Oxygen-anthraquinone working solution two-phase flow in circular microchannel

5.3.1 Two-phase flow patterns

Oxygen-anthraquinone working solution two-phase flow patterns in circular microchannel with diameter 900 μm were visually investigated, and three typical flow patterns were observed, i.e. slug flow (Taylor flow), slug-annular flow and transitional flow pattern: unstable slug flow. Due to the small flow range of the pump, higher liquid superficial velocities could be achieved, thus, bubbly flow, churn flow did not appear in the present experiments.

In the Chapter 2, a flow pattern transition model was proposed taking effects of channel size, liquid viscosities, and surface tension into account. With the liquid physical properties tabulated in the Table 5-1, the transition line in the proposed model could be derived as lines plotted in the flow pattern regime maps with U_{GS} and U_{LS} as coordinates, which depicted in Figure 5-2. It could be known that the flow pattern transition model predicted well the present experimental data, especially, the transition from unstable slug flow to slug-annular flow. On the other hand, the applicability of transition model for others two-phase flow system in microchannel was verified, for the liquid physical properties of anthraquinone working solution varied from that of liquids employed in the experiments of Chapter 2, base on which the model proposed.

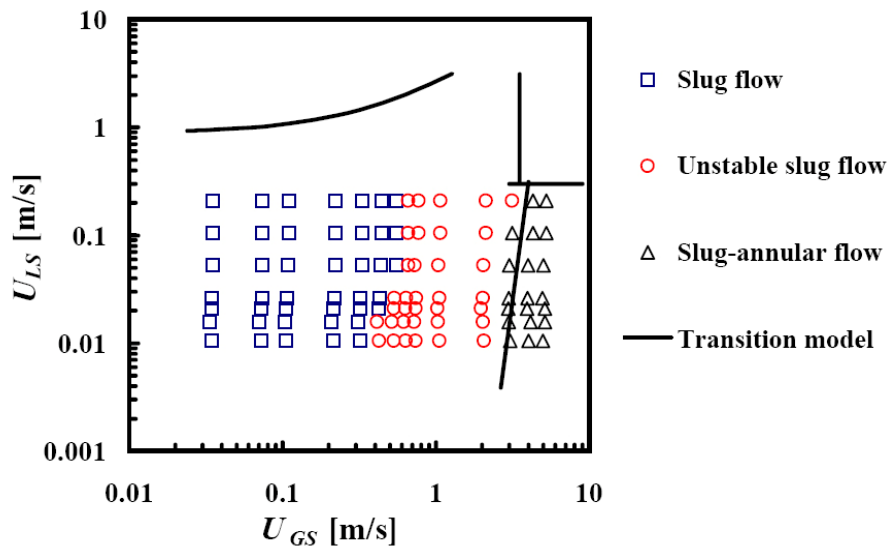


Figure 5-2: The comparison between the flow patterns regime map of the experiments in this chapter and transition model proposed in Chapter 2

5.3.2 Pressure drop

Two-phase pressure drop of oxygen-anthraquinone working solution also was investigated. The typical trend dependent on the flow patterns was also observed as shown in Figure 5-3, whose characteristics have been described in detail. In the present experiments, region I (surface tension-dominated) corresponded to slug flow (Taylor flow), region III

(inertia-dominated) to slug-annular flow.

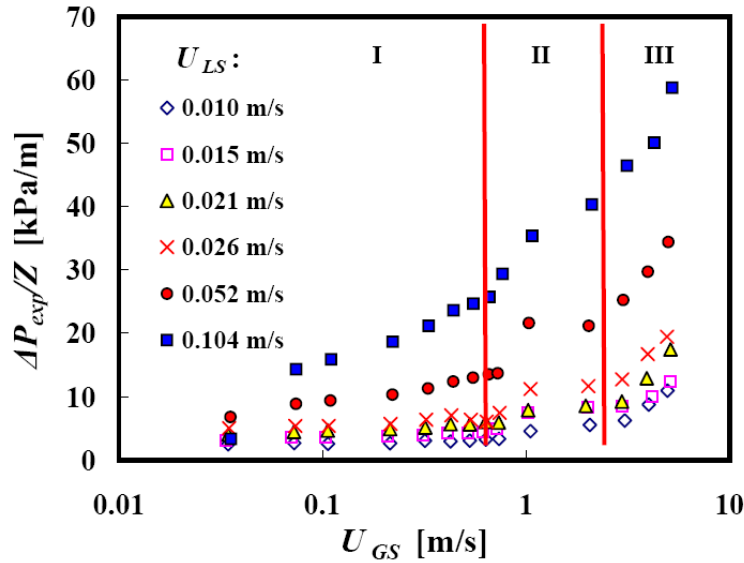


Figure 5-3: The dependence of two-phase pressure drop on the flow patterns in horizontal circular microchannel ($d_i = 900 \mu\text{m}$)

In Chapter 3, the pressure drop in inertia-dominated region was systematically discussed. As a result, a new Chisholm parameter C was proposed to modify the L-M separated flow model for prediction the two-phase pressure drop of inertia-dominated region in microchannel, and good agreement with the data of our previous experiments and that of others was shown. The C correlation can be expressed as:

$$C = (1.17 + 0.53 \text{Re}_G^{0.39}) \text{Re}_L^{0.31} \quad (5.1)$$

The Two-phase pressure drop of oxygen-anthraquinone working solution in inertia-dominated region was compared with the model proposed in Chapter 3, as exhibited in Figure 5-4. It was noted from Figure 5-4, that the prediction corresponded well with the experimental data, and the mean relative deviation of all data was only 14.42%, relative deviation of most data less than 30%. In other words, the model proposed for inertia-dominated region was confirmed again.

However, an important detailed parameter, Taylor bubble velocity, could not be obtained for that the fast camera in the present experiments could only record image, but not the video. Therefore, two-phase pressure drop of Taylor flow have not discussed here.

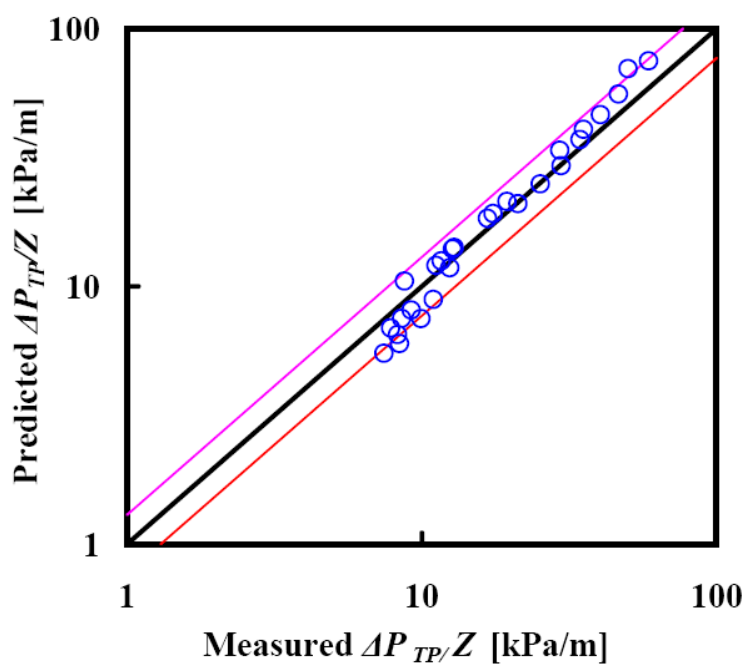


Figure 5-4: The comparison of measured two-phase pressure drop (in the inertia-dominated region) in horizontal circular microchannels with predictions of the new model proposed in Chapter 3

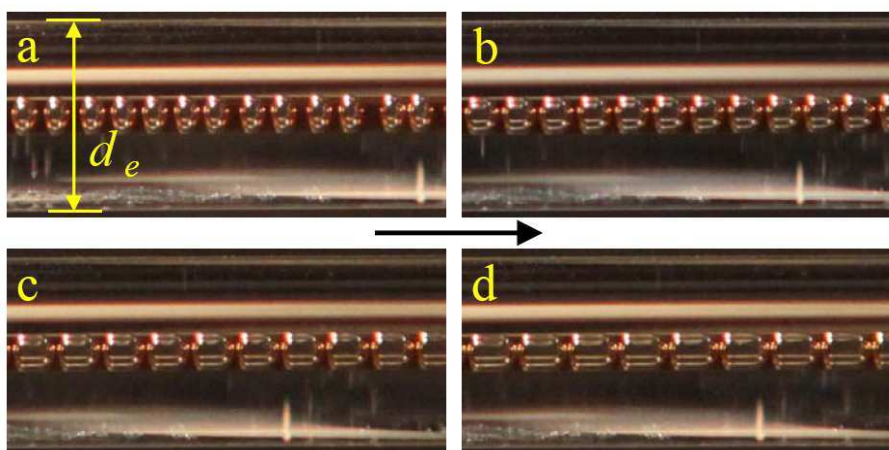


Figure 5-5: Two-phase flow patterns in micro-channel reactor during experiments. Experimental conditions: Temperature 50°C, operating pressure 0.29 MPa, liquid velocity 0.026 m/s. (a): $r_{AS} : 4.4$; (b): $r_{AS} : 8.7$; (c): $r_{AS} : 13.1$; (d): $r_{AS} : 17.5$

5.4 Oxidation of THEAQH₂ in circular microchannel

5.4.1 Gas-liquid specific interfacial area

The two-phase flow pattern during the oxidation in the microchannel was observed to be Taylor flow, and the representative images were exhibited in Figure 5-5, in which the gas-to-liquid ratio r_{As} defined as the ratio of gas superficial velocity under atmospheric pressure to that of liquid phase. Taylor flow could be regarded as a quasi-steady process, with relatively regular Taylor bubbles and liquid slug. So that, it was possible to calculate the gas-liquid specific interfacial area from the two-phase flow images.

As shown in the Figure 5-6, the diameter of Taylor bubble d_b can be calculated by:

$$d_b = d_c - 2T_f \quad (5.2)$$

Where T_f is the thickness of the liquid film, which can be obtained from the correlation proposed by Aussillous and Quere (2000):

$$\frac{T_f}{d_c} = \frac{0.66Ca^{2/3}}{1 + 3.33Ca^{2/3}} \quad (5.3)$$

In which:

$$Ca = \frac{\mu_L U_B}{\sigma} \quad (5.4)$$

Where (Baten et al., 2004):

$$U_B = U_{GS} / \varepsilon_G \quad (5.5)$$

And void fraction ε_G can be calculated by:

$$\varepsilon_G = \frac{V_{Bubble}}{(L_S + L_B)\pi d_c^2 / 4} \quad (5.6)$$

We regard approximately the Taylor bubble as a combination of a cylinder and a hemisphere, for which the interfacial area expressed as:

$$S_B = d_b \pi (L_{cy} + L_{sp1}) + 3\pi d_b^2 / 4 \quad (5.7)$$

Where:

$$L_{cy} + L_{sp1} = L_B - L_{sp2} \approx L_B - d_b / 2 \quad (5.8)$$

Then the gas-liquid specific interfacial area of the microchannel can be obtained from:

$$a_i = \frac{S_B}{(L_S + L_B)\pi d_c^2 / 4} \quad (5.9)$$

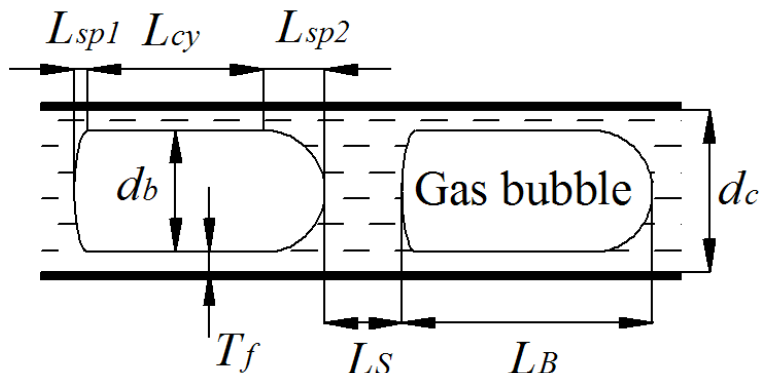


Figure 5-6: The schematic diagram of gas bubbles in Taylor flow

Based on the Eq. (5.9), the specific interfacial area can be calculated for d_c , d_b and L_B are known or obtain from the flow pattern image, as well as U_{GS} calculated from gas flow rate. Four values were determined to be 4560 m^2/m^3 , 4840 m^2/m^3 , 4960 m^2/m^3 and 5040 m^2/m^3 (with the error < 10%), corresponding to the operating conditions in Figure 5-5 (a), (b), (c), (d). Generally, the specific interfacial areas of conventional gas-liquid reactors are less than 200 m^2/m^3 (Ehrfeld et al., 2004). It is dramatically high specific interfacial area that is one of the most important reasons for excellent performance of microchannel reactor in mass transfer processes.

5.4.2 Effects of temperature on oxidation

The effects of temperature on the oxidation were shown in the Figure 5-7, from which it could be noted that C_{oxy} and its corresponding η would increase significantly with temperature. For instance, C_{oxy} was only 0.79 $\text{gH}_2\text{O}_2/\text{L}$, and η only 13.2% with a temperature of 12 °C; but C_{oxy} increased to 4.4 $\text{gH}_2\text{O}_2/\text{L}$, and η to 72.8%, when temperature had reached 70 °C, with others operating condition keeping unchanged.

There were mainly two aspects responsible for this phenomenon. On one hand, the oxidation of was a moderately slow reaction occurring mainly in the bulk liquid, whose rate was affected dramatically by the mass transfer across the gas-liquid interfacial (Santacesaria et al., 1987). Thus, the intrinsic reaction rate would increase with temperature for that it was generally agreed that kinetic constant of the oxidation would rise significantly. On the other hand, mass transfer would be enhanced with the increase of temperature. To start with, gas diffusion in the liquid would accelerate with the increase of temperature; consequently, the mass transfer of oxygen would be enhanced (Lamont and Scott, 1970), which positively related to gas diffusion in the liquid. Moreover, the mass transfer would be intensified by the rise of oxidation kinetic constant. Finally, the solubility of oxygen in the anthraquinone working solution would also be increased with temperature, and that was common phenomenon of oxygen dissolved in a lot of organic solvents (Huang, 2002), such as benzene, toluene, trimethyl benzene, heavy aromatics, etc. Accordingly, the mass transfer driving force would rise, leading to the enhancement of mass transfer. In conclusion, with the increase of temperature, both the intrinsic reaction rate of oxidation and oxygen mass transfer would be intensified, corresponding to the rise of C_{oxy} and η .

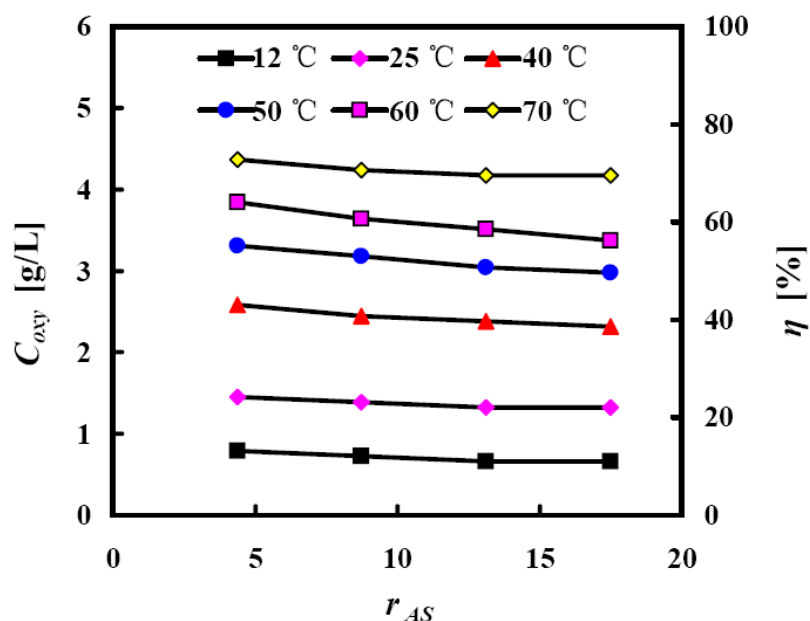


Figure 5-7: The effects of temperature on the oxidation. Experimental condition: Pressure 0.29 MPa, liquid velocity 0.026 m/s

5.4.3 Effects of operating pressure

Generally, operating pressure is another important influencing factor in the gas-liquid reaction process, as well as in the oxidation presented here. As exhibited in Figure 5-8, η under 0.49 MPa was about three times of that under 0.10 MPa with others operating condition unchanged. As mentioned above, the rate of the present oxidation was determined by the intrinsic reaction rate, as well as the mass transfer across the gas-liquid interfacial. On one hand, with the increasing of operating pressure, the mass transfer would be enhanced. On the other hand, the solubility of oxygen in the bulk liquid would increase with higher operating pressure, so that the concentration of oxygen in the liquid phase would become higher. Then, the intrinsic reaction rate would be improved. As a result, the reaction rate of the present oxidation would increase with the operating pressure leading to the rise of C_{oxy} and η as shown in the Figure 5-8.

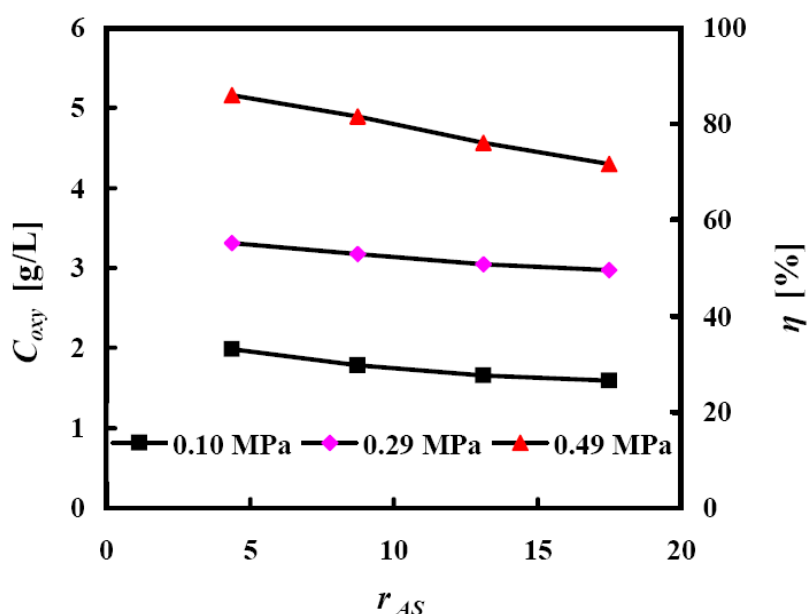


Figure 5-8: The effects of pressure on the oxidation. Experimental conditions: Temperature 50°C, liquid velocity 0.026 m/s

5.4.4 The effects of liquid velocities on the oxidation

In Figure 5-9, it was plotted that the variation of C_{oxy} and η with liquid superficial

velocities of hydrogenated anthraquinone working solution. Obviously, it could be noted that the C_{oxy} and η fallen with the increasing of liquid velocities. The mean residence time of hydrogenated anthraquinone working solution in the microchannel would decrease, when the liquid velocities increased, so that the conversion of the oxidation would be led down inevitably with other operating conditions unchanged. However, with the increasing of the liquid velocities, the amount of hydrogenated anthraquinone working solution through the microchannel per unit of time would increase, and the mass transfer across the gas-liquid interfacial would be enhanced, as well as the intrinsic reaction in the bulk liquid because of the higher mean THEAQH₂ concentration under lower conversion. So that, the hydrogen peroxide space-time yield of the microchannel was improved significantly, as shown in the Figure 5-10.

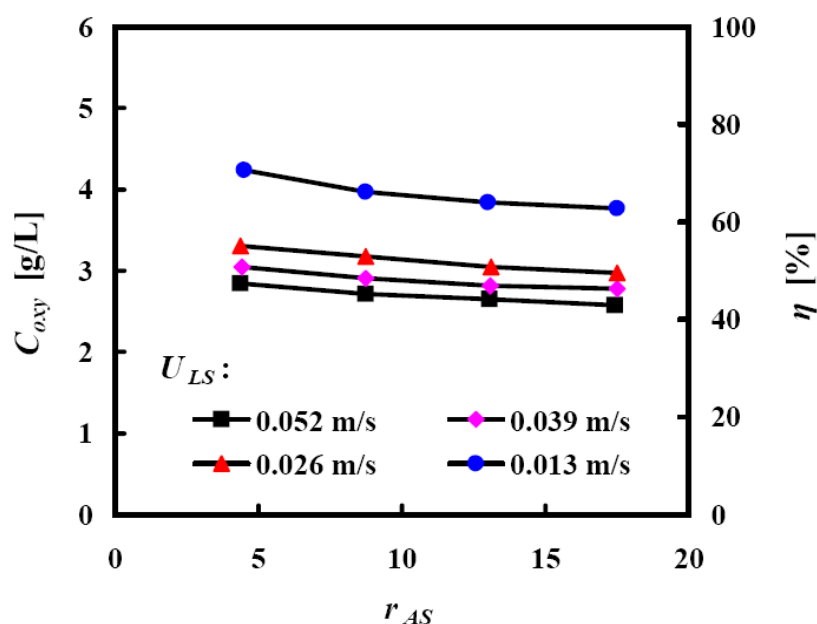


Figure 5-9 The effects of liquid velocity on the oxidation. Experimental conditions: Temperature 50°C, pressure 0.29 MPa

It is a great advantage of microchannel reactor that high hydrogen peroxide space-time yield could be achieved in the THEAQH₂ oxidation process. Actually, the aim to employ microchannel reactor in this oxidation process was to enhance the process to improve the efficiency and to reduce the energy consumption. As a result, the hydrogen peroxide

space-time yield of the microchannel reactor achieved $1790 \text{ kg H}_2\text{O}_2/(\text{m}^3\cdot\text{h})$, when liquid velocity was 0.052 m/s , operating pressure 0.29 MPa and temperature $50 \text{ }^\circ\text{C}$, as shown in Figure 5-10. However, the oxidation process in the hydrogen peroxide production industry is with so low production efficiency, in which, the hydrogen peroxide space-time yield is usually only $15\text{-}36 \text{ kg H}_2\text{O}_2/(\text{m}^3\cdot\text{h})$ (Hu, 2008). Even though the advanced tubular oxidation reactor developed by Kemira company (Hu, 2004), of which the hydrogen peroxide space-time yield is not more than $254 \text{ kg H}_2\text{O}_2/(\text{m}^3\cdot\text{h})$, and the reactor have not been used by many companies yet. Consequently, compared with traditional tower oxidation reactor or advanced tubular reactor, the microchannel reactor has its own potential to improve the oxidation step in the hydrogen peroxide industrial production process.

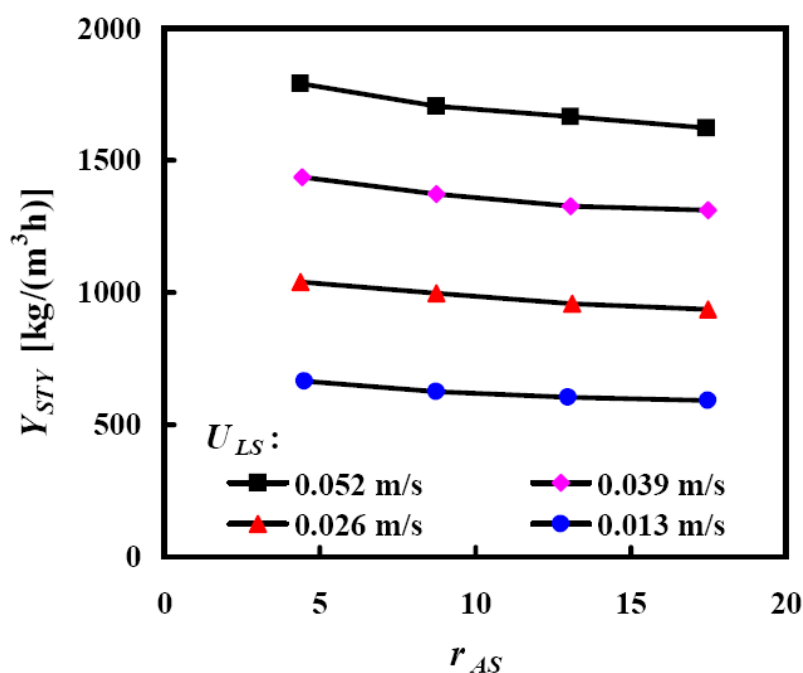


Figure 5-10 The effects of liquid velocity on the space-time yield of hydrogen peroxide.

Experimental conditions: Temperature 50°C , pressure 0.29 MPa .

5.5 Conclusions

The oxygen-anthraquinone working solution two phase flow and the oxidation of THEAQH₂ in the circular microchannel were experimentally investigated in this chapter.

Based on the discussion above, major conclusions could be reached as follow.

(1) Three two-phase flow patterns were observed in the oxygen-anthraquinone working solution two phase flow, i.e. slug flow, unstable slug flow and slug-annular flow. The two-phase flow pattern transition model proposed in the Chapter 2 predicted well the flow patterns in the present experiment. The main trend of two-phase pressure drop also could be divided into three parts, and the pressure drop in the inertia-dominated corresponded well with the prediction of the modified L-M separated-flow model proposed in the Chapter 3.

(2) The gas-liquid two-phase interfacial during the oxidation of THEAQH₂ in the microchannel reactor could achieved more than 5000 m²/m³, which was tens times more than that of traditional reactors.

(3) According to the experiments, it was known that the oxidation rate would increase with the temperature, operating pressure and liquid superficial velocity. And the hydrogen peroxide space-time yield of the microchannel reactor could achieved 1790 kg H₂O₂/(m³·h) in the present experiment, much more than that of others oxidation reactors.

References

- Aussillous, P., Quere, D., 2000. Quick deposition of a fluid on the wall of a tube. *Physics of Fluids* 12, 2367-2371.
- Berglin, T., Schoon, N.H., 1983. Selectivity aspects of the hydrogenation stage of the anthraquinone process for hydrogen-peroxide production. *Industrial & Engineering Chemistry Process Design and Development* 22, 150-153.
- Ehrfeld, W., Hessel, V., Löwe, H., 2004. *Microreactors: new technology for modern chemistry*. Weinheim, Germany: Wiley-VCH.
- Hang, J., 2002. *Handbook of industrial gases*. Beijing, China: Chem. Indus. Press.
- Hu, C., 2004. Current situation of foreign H₂O₂ production plants and production technology. *Chemical Propellants and Polymeric Materials (Chinese)* 2, 1-4.
- Hu, C., 2008. New progress of research and development of anthraquinone process for preparation of hydrogen peroxide and its concentration, purification and stabilization. *Chemical Propellants and Polymeric Materials (Chinese)* 6, 1-9.
- Lamont, J., Scott, D., 1970. An eddy cell model of mass transfer into the surface of a turbulent liquid. *AIChE Journal* 16, 513-519.
- Poling, B.E., Prausnitz, J.M., O'connell, J.P., 2001. *The properties of gases and liquids*. New York: McGraw-Hill, Inc.
- Qingdao college of chemical engineering, 2002. *Graph handbook of chemical properties*. Beijing, China: Chem. Indus. Press.
- Santacesaria, E., Ferro, R., Ricci, S., Carra, S., 1987. Kinetic aspects in the oxidation of hydrogenated 2-ethyltetrahydroanthraquinone. *Industrial & Engineering Chemistry Research* 26, 155-159.
- van Baten, J.M., Krishna, R., 2004. CFD simulations of mass transfer from Taylor bubbles rising in circular capillaries. *Chemical Engineering Science* 59, 2535-2545.
- Zhang, J., 2008. Preparation and studies on catalysts of 2-ethylanthraquinone hydrogenation for H₂O₂ production. PhD. Thesis, Dalian Institute of Chemical Physics, Chinese Academy of Sciences.

CONCLUDING REMARKS

1 Thesis summary

This thesis is mainly concerned with the gas-liquid two-phase flow and reaction characteristics in microchannels. Two-phase flow patterns, the dependence of two-phase pressure drop on the flow patterns, two-phase pressure drop in inertia-dominated region and the hydrodynamic characteristics of Taylor flow have been investigated in circular microchannels, as well as the oxidation of THEAQH₂, which was an important step in the hydrogen peroxide industrial production process. In all the study aspects of this work, special emphasis have been put on the influence of channel size, liquid viscosity and surface tension. In chapters 2~5, the corresponding results, discussions and conclusions have been presented in detail, and the key findings of the present dissertation could be summarized as follows:

(1) In the circular microchannel, there are several typical flow patterns i.e. bubbly flow, slug flow, churn flow, slug-annular flow and annular flow, as well as transitional flow patterns, such as slug-bubbly flow, unstable slug flow and so on. In addition, foam flow patterns will occur when using working liquid containing surfactant.

(2) Channel size, liquid viscosity and surface tension affect two-phase flow patterns in the microchannel dramatically, not only on the detail of the flow patterns, but also on the transition between the flow patterns. The existing flow pattern transition models can not predict well the experimental data, so a new model are proposed taking the effects of channel size, liquid viscosity and surface tension in to account.

(3) The two-phase pressure drop highly depends upon flow patterns, and the corresponding trend can be divided into three parts according to the mechanism, i.e. (I) the surface tension-dominated region (bubbly flow and slug flow), (II) the transitional region (unstable slug flow) and (III) the inertia-dominated region (churn flow, slug-annular flow and annular flow). Homogeneous flow model is not the applicable method to predict two-phase

pressure drop in microchannel. The prediction of modified Lockhart-Martinelli separated flow model corresponds well with the experimental data in the present work and that of other researchers in the inertia-dominated region. The pressure drop of Taylor flow, which is the major flow pattern of surface tension dominated region, can be predicted satisfactorily by Kreutzer's model modified by Walsh et al., when $Ca < 0.05$. But for higher Ca , new model is needed to found.

(4) Taylor bubble velocity and void fraction can be predicted by a simple linear correlation, but for the nitrogen-ethanol two-phase flow, slopes of these correlations vary from that of others two-phase flow systems. In addition, the formation mechanism of Taylor flow can be explained by squeezing regime, and the very important parameter of Taylor flow, gas bubble length, is highly related to the liquid properties.

(5) The experimental results show that the prediction of flow pattern transition model and two-phase pressure drop model proposed in the present work have a good agreement with the data of oxygen-anthraquinone working solution two phase flow in the circular microchannel.

(6) Microchannel reactor has superior reaction performance, when employed in the oxidation of THEAQH₂. During the oxidation, the gas-liquid interfacial can achieve 5000 m²/m³, and the space-time yield of hydrogen peroxide can achieve 1790 kg H₂O₂/(m³·h), tens times more than that of traditional oxidation reactor.

2 Future work perspectives

The present work contributes to the advances in the fundamental knowledge of hydrodynamics and reaction characteristics in gas-liquid microreactors. Although extensive experiments have been performed on the two-phase flow in microchannel, there are still many tasks in this field need to deeply study. Moreover, the present study on the two-phase reaction only represents a first attempt at the application of microreactor in the hydrogen peroxide production industry. There is still much work that can and should be carried out, and in the near future, we recommend as follows:

(1) Foam flow patterns in the microchannel are so special, and rarely reported. On one hand, it has been observed that the pressure drop of the foam flow is several times higher than that of typical flow patterns. On the other hand, the two-phase interfacial area is speculated to be extremely large, which perhaps will be a new method for the enhancement of gas-liquid mass transfer process. Accordingly, extensive experimental work will be implemented to study the hydrodynamics and mass transfer characteristics of foam flow in microchannels.

(2) The flow pattern transition model proposed in the chapter 2 needs plenty of experimental data to verify, and other influencing factors such as temperature, channel section, orientation, channel surface characteristics and inlet structure are not considered. Therefore, it will be the subject of our ongoing work, in which more experiments will be carried out to find a more applicable model.

(3) Computer simulation is great to the study of two-phase flow mechanism in the microchannels, and has been used successfully in this field. For the present work, the formation mechanism of two-phase flow patterns, the mechanism of pressure drop in inertia-dominated and surface tension-dominated region, as well as mass transfer from gas to the liquid, are very different to know clearly only based on the experiments. Therefore, we will use computer software, such as CFD and MATLAB, to numerically study on two-phase flow in microchannels aiming to find a more reasonable prediction model.

(4) The microchannel reactor showed a superior performance in the oxidation step of the hydrogen peroxide production industry. But there are still many problems before using microreactors in the oxidation step, i.e. the effects of channel size, channel section and channel length are not clear, how the two-phase fluid distribute in the multi-microchannels for that the oxidation reactor in the industry must be with multi-channel, etc. We shall conduct more experiments to investigate the influences of operating parameters, channel size, channel section and channel length, etc. on the oxidation. Multi-channel microreactor will be fabricated, for which, fluid distributor will be designed. Oxidation and fluid distribution in the multi-channel reactor will be investigated. Of course, other gas-liquid reaction characteristics in microchannel reactor will also be investigated to find a suitable process to use microreaction technology.

LIST OF FIGURES

<i>Figure 1-1: General classification of two-phase flow patterns in microchannel (Shao et al., 2009)</i>	<i>9</i>
<i>Figure 1-2: Two phase flow pattern in microchannel: (a) bubbly flow; (b) slug or Taylor flow; (c) and (d) churn flow; (e) slug-annular or Taylor-annular flow; (f) annular flow</i>	<i>10</i>
<i>Figure 1-3: Dispersed flow in microchannels</i>	<i>11</i>
<i>Figure 1-4: The images of bubble-train slug flow in microchannels: (a) Two-phase flow in a square microchannel with hydraulic diameter of 0.4 mm of Yue et al. (2008); (b) Two-phase flow in a circular microchannel with diameter of 1 mm of Chen et al. (2002).....</i>	<i>11</i>
<i>Figure 1-5: The two-phase flow pattern regime maps in microchannels: (A) for the experiments of Barajas and Panton (1993); (B) for the experiments of Triplett et al. (1999)</i>	<i>13</i>
<i>Figure 1-6: Universal two-phase flow regime map for horizontal microchannel proposed by Hassan et al. (2005) (JL and JG represent ULS and UGS)</i>	<i>14</i>
<i>Figure 1-7: Two-phase flow regime map with Weber number as coordinates and transition lines proposed by Akbar et al. (2003).....</i>	<i>15</i>
<i>Figure 1-8: Single-reactor chamber of micro packed-bed gas-liquid reactors (Losey et al., 2001).....</i>	<i>24</i>
<i>Figure 1-9: Falling film micro reactor and the principle of contacting liquid and gas reactants</i>	<i>25</i>
<i>Figure 1-10: Micro bubble column reactor and the schematic illustration of contacting liquid and gas reactants</i>	<i>26</i>
<i>Figure 1-11: The comparison of conversion, selectivity, space-time yield of direct fluorination of toluene between in microreactors and in laboratory bubble column (LBC): FFMR, falling film microreactor; MBC, micro bubble column reactor</i>	<i>26</i>
<i>Figure 2-1: Schematic representation of the experimental setup.....</i>	<i>40</i>
<i>Figure 2-2: Detail of the test section. (A) TC I; (B) TC II.....</i>	<i>41</i>
<i>Figure 2-3: Representative flow patterns of Nitrogen-water horizontal flow in the circular microchannels</i>	<i>50</i>
<i>Figure 2-4: Comparison of flow regime maps of Nitrogen-water horizontal flow in circular microchannels with different diameters.....</i>	<i>52</i>
<i>Figure 2-5: The effective viscosity of CMC solution and water as a function of liquid superficial velocity.....</i>	<i>53</i>

<i>Figure 2-6: Comparison of two-phase horizontal flow regime maps in circular microchannels ($d_i = 496 \mu\text{m}$) with different liquid viscosity.....</i>	<i>54</i>
<i>Figure 2-7: Foam flow patterns of Nitrogen-SDS solution (0.2610% SDS) horizontal flow in the circular microchannel ($d_i = 496\mu\text{m}$).....</i>	<i>55</i>
<i>Figure 2-8: Two representative flow patterns of Nitrogen-ethanol horizontal flow with different details compared to Nitrogen-water flow in the circular microchannel ($d_i = 496\mu\text{m}$).....</i>	<i>56</i>
<i>Figure 2-9: Comparison of two-phase horizontal flow regime maps in circular microchannels ($d_i = 496\mu\text{m}$) with different surface tension</i>	<i>57</i>
<i>Figure 2-10: Comparison with existing flow regime maps of (A): Triplett et al. (1999); (B): Yang and Shieh (2001); (C) Hassan et al. (2005).....</i>	<i>59</i>
<i>Figure 2-11: Comparison with the flow pattern transition model of Akbar et al. (2003): (A) with various channel diameters; (B) with various liquid viscosities; (C) with various surface tensions</i>	<i>61</i>
<i>Figure 2-12: Comparison with the flow pattern transition model of Waelchli and Rudolf von Rohr (2006): (A) with various channel diameters; (B) with various liquid viscosities; (C) with various surface tensions.....</i>	<i>63</i>
<i>Figure 2-13: The flow pattern transitions with based on the experimental data: (A) the transition from bubbly to slug flow; (B) the transitions from slug to churn and to slug-annular flow; (C) the transitions from churn to slug-annular and to annular flow.....</i>	<i>66</i>
<i>Figure 3-1: The dependence of two-phase pressure drop on the flow patterns in circular horizontal microchannel ($d_i = 496 \mu\text{m}$).....</i>	<i>83</i>
<i>Figure 3-2: The comparison of measured two-phase pressure drop (in the inertia-dominated region) in circular horizontal microchannel ($d_i = 496 \mu\text{m}$) with predictions of homogeneous-flow models</i>	<i>85</i>
<i>Figure 3-3: The comparison of measured two-phase pressure drop (in the inertia-dominated region) in circular horizontal microchannels with predictions of Lockhart-Martinelli models using various C correlations</i>	<i>88</i>
<i>Figure 3-4: The Chisholm parameter C-value as a function of gas superficial velocity in circular horizontal microchannels with different diameters in the inertia-dominated region.....</i>	<i>92</i>
<i>Figure 3-5: The Chisholm parameter C-value against gas superficial velocity in circular horizontal microchannel with inner diameter of $496 \mu\text{m}$ under different liquid viscosity in the inertia-dominated region at 25°C</i>	<i>94</i>
<i>Figure 3-6: The Chisholm parameter C-value of nitrogen-water (surface tension: 72.0 mN/m at 25°C) and</i>	

nitrogen-ethanol (surface tension: 21.5 mN/m at 25°C) two-phase system as a function of gas velocity in circular horizontal microchannel with diameter of 496 μm in the inertia-dominated region.....95

Figure 3-7: The comparison of measured two-phase pressure drop (in the inertia-dominated region) in horizontal circular microchannels with predictions of the new model.....96

Figure 3-8: The comparison between the measured two-phase pressure drop in circular horizontal microchannels in the inertia-dominated region and the predicted results of the new model: nitrogen-water two-phase system in microchannels with inner diameter of 302, 496 and 916 μm98

Figure 3-9: The comparison between the measured two-phase pressure drop in the circular horizontal microchannel in the inertia-dominated region and the predicted results of the new model: nitrogen-ethanol two-phase flow and three nitrogen-CMC aqueous solutions two-phase flow system with different concentration: 0.0464%, 0.1262% and 0.2446% in the microchannel with inner diameter of 496 μm 99

Figure 3-10: Verification of the modified Lockhart-Martinelli model using presently proposed C correlation with experimental data in literature. (A) data in Fig.3 (a) of Triplett et al., 1999; (B) data in Fig.12 of Kawahara et al., 2002; (C) Yue et al., 2004; (D) Niu et al., 2009..... 101

Figure 4-1: Taylor bubble velocities versus the mean velocities in liquid slug in circular microchannels: (a) with different channel diameter; (b), (c) with different liquid physical properties in microchannel with diameter of 496 μm 110

Figure 4-2: void fraction ϵ_G of Taylor flow in circular microchannels versus homogeneous void fraction β . (a) with different channel diameter; (b), (c) with different liquid physical properties in microchannel with diameter of 496 μm 112

Figure 4-3: L_B / d_i versus U_{GS} / U_{LS} of Taylor flow in squeezing regime in circular microchannels. (a) with different channel diameters: nitrogen-water two-phase flow; (b) with different liquid physical properties in microchannel with diameter of 496 μm : nitrogen-water, ethanol, 0.2446% CMC two-phase flow, respectively 114

Figure 4-4: Unit cell of Taylor flow 116

Figure 4-5: $f \text{Re}_{\text{liquid}}$ versus L_S / d_i of Taylor flow in circular microchannels with different channel diameters and liquid physical properties 119

Figure 4-6: The comparison between experimental results of $f \text{Re}_{\text{liquid}}$ and prediction of Walsh's

<i>correlation</i>	120
<i>Figure 4-7: The comparison between experimental results of $f Re_{liquid}$ in nitrogen-ethanol two-phase system and prediction of Kreutzer's and Walsh's correlations</i>	122
<i>Figure 5-1: Schematic diagram of experimental setup</i>	127
<i>Figure 5-3: The dependence of two-phase pressure drop on the flow patterns in horizontal circular microchannel ($d_i = 900 \mu\text{m}$)</i>	131
<i>Figure 5-4: The comparison of measured two-phase pressure drop (in the inertia-dominated region) in horizontal circular microchannels with predictions of the new model proposed in Chapter 3</i>	132
<i>Figure 5-5: Two-phase flow patterns in micro-channel reactor during experiments. Experimental conditions: Temperature 50°C, operating pressure 0.29 MPa, liquid velocity 0.026 m/s</i>	132
<i>Figure 5-6: The schematic diagram of gas bubbles in Taylor flow</i>	134
<i>Figure 5-7: The effects of temperature on the oxidation. Experimental condition: Pressure 0.29 MPa, liquid velocity 0.026 m/s</i>	135
<i>Figure 5-8: The effects of pressure on the oxidation. Experimental conditions: Temperature 50°C, liquid velocity 0.026 m/s</i>	136
<i>Figure 5-9 The effects of liquid velocity on the oxidation. Experimental conditions: Temperature 50°C, pressure 0.29 MPa</i>	137
<i>Figure 5-10 The effects of liquid velocity on the space-time yield of hydrogen peroxide. Experimental conditions: Temperature 50°C, pressure 0.29 MPa</i>	138

LIST OF TABLES

<i>Table 1-1: Examples of microchemical engineering applications in practice.....</i>	<i>3</i>
<i>Table 1-2: Critical channel diameters for liquid-vapor two-phase flow based on the correlation of Li and Wang (2003).....</i>	<i>7</i>
<i>Table 1-3: Selected literature on the effects of liquid physical properties on gas-liquid flow regimes.....</i>	<i>18</i>
<i>Table 1-4: Specific interfacial area measured by Hessel et al. (2000) under various flow patterns.....</i>	<i>24</i>
<i>Table 2-1: The physical properties of working fluids and rheological parameters of the CMC solutions.....</i>	<i>42</i>
<i>Table 2-2: Range and precision of experimental instruments.....</i>	<i>45</i>
<i>Table 2-3: Experimental conditions.....</i>	<i>46</i>
<i>Table 3-1: Different expressions of the two-phase mixture viscosity for homogeneous-flow model.....</i>	<i>73</i>
<i>Table 3-2: Chisholm parameter C and various expressions of C correlation for two-phase flow in mini or microchannel.....</i>	<i>76</i>
<i>Table 3-3: Mean relative deviation between predicted results of various homogeneous-flow models and the measured two-phase pressure drop (in the inertia-dominated region) in circular horizontal microchannel ($d_i = 496 \mu\text{m}$), and the percentage of points falling within the relative deviation of 30%.....</i>	<i>86</i>
<i>Table 3-4: Mean relative deviation between predicted results of Lockhart-Martinelli model using various C correlations and the measured two-phase pressure drop (in the inertia-dominated region) in circular horizontal microchannels, and the percentage of points falling within the relative deviation of 30%.....</i>	<i>89</i>
<i>Table 5-1: The Physical Properties of Working liquid and oxygen (Poling et al., 2001; Qingdao college of chemical engineering, 2002).....</i>	<i>129</i>

BIOGRAPHY

Tong ZHANG was born in 1983 in Hua county, Henan province (P.R. China). He earned his Bachelor's degree in Chemical engineering in 2005, from China University of Mining and Technology (CUMT; Xuzhou, China). He has been a student in a combined MA/Ph.D program in Dalian Institute of Chemical Physics (DICP; Dalian, China) from 2005, and he has been a doctoral student co-supervised by Savoie University (Le Bourget du Lac, France) and DICP under the guidance of Prof. Yves GONTHIER, Prof. Lingai LUO and Prof. Shudong WANG, from 2009.

Publications

- [1] Tong Zhang, Bin Cao, Yilin Fan, Yves Gonthier, Lingai Luo, Shudong Wang, 2011. Gas-liquid flow in circular microchannel. Part I: Influence of liquid physical properties and channel diameter on flow patterns. *Chemical Engineering Science* 66, 5791-5803.
- [2] Dingsheng Liu, Jianguo Zhang, Defu Li, Qingdan Kong, Tong Zhang, Shudong Wang, 2009. Hydrogenation of 2-Ethylanthraquinone under Taylor flow in single square channel monolith reactors. *AIChE Journal* 55, 726-736.
- [3] Tong Zhang, Bin Cao, Yilin Fan, Yves Gonthier, Lingai Luo, Shudong Wang. Gas-liquid flow in circular microchannel. Part II: Pressure drop in inertia-dominated region. *Chemical Engineering Science*. Submitted.
- [4] Jianguo Zhang, Defu Li, Qingdan Kong, Tong Zhang, Shudong Wang, 2008. Analysis of effect factors on the stability of palladium catalyst for H₂O₂ production. *Science and Technology in Chemical Industry (Chinese)* 16, 22-25.
- [5] Tong Zhang, Hongjiu Su, Bin Cao, Yves Gonthier, Lingai Luo, Shudong Wang, 2012. Oxidation of hydrogenated 2-ethyltetrahydroanthraquinone in horizontal circular micro-channel reactor. *Chemical Reaction Engineering and Technology (Chinese)* 28, 1-7.

Patent

- [1] Shudong Wang, Tong Zhang, Defu Li, Jianguo Zhang, Qingdan Kong. A method for H_2O_2 production using microreaction technology. Application number: 200810229511.5.
- [2] Shudong Wang, Jianguo Zhang, Defu Li, Qingdan Kong, Tong Zhang. A catalyst for H_2O_2 production and its preparation. Application number: 200710158237.2.